2015

Seismic performance of accelerated bridge construction (ABC) precast bulb-tee girder-to-bent cap connection

Zhao Cheng
Iowa State University

Seismic performance of accelerated bridge construction (ABC) precast bulb-tee girder-to-bent cap connection

by

Zhao Cheng

A thesis submitted to the graduate faculty

in partial fulfillment of the requirements for the degree of

MASTER OF SCIENCE

Major: Civil Engineering (Structural Engineering)

Program of Study Committee:
Sri Sritharan, Major Professor
Jon Matthew Rouse
Hyung Seok Jeong

Iowa State University

Ames, Iowa

2015

TABLE OF CONTENTS

TABLE OF FIGURES

TABLE OF TABLES

ACKNOWLEDGEMENTS

I would like to thank my committee chair, Dr. Sri Sritharan, for his guidance and supports throughout the course of this research. I would also like to show my gratitude to my committee members Dr. Jon Matthew Rouse and Dr. Hyung Seok Jeong for their time and comments on this thesis.

This research was supported by the California Department of Transportation (Caltrans). I thank the Project Advisory Panel from Caltrans for their advices and assistances.

I would also like to thank Robert Peggar and Justin Vander Werff for their work, which laid the groundwork for this research. In addition, thanks are due to Doug Wood and Owen Steffens of the ISU Structures Laboratory for all their hard works, assistances, and expertise during the construction and testing of the test unit.

I want to also offer my appreciation to my friends, colleagues, department faculties and staffs for making my time at Iowa State University a wonderful experience.

Finally, thanks to my family for their encouragement and supports and to my girlfriend for her patience, respect and love.

ABSTRACT

With the total number of structurally deficient or functionally obsolete bridges at more than 20% of the nation's 607,380 bridges in 2013, the nation need to work effectively to decrease the total number below to 15% over the next decade. Accelerated Bridge Construction (ABC) techniques using the precast components are beneficial to effectively repair and replace the deficient bridges by reducing the period of onsite construction and improving the construction quality. However, the knowledge gap regarding the seismic performance of connections between the precast components limits the extensive implementation of ABC techniques in the moderate-to-high seismic regions of the country. Current Caltrans Seismic Design Criteria stipulates to degrade the connection between the precast girder and bent cap to a pinned connection under sever seismic event, which results in an inefficient bridge design. To overcome this issue, two innovative details for the precast bulb-tee girder to cast-in-place bent cap connection have been experimentally tested at Iowa State University. These two moment resisting connection details, named as the Extend Strand with a Mechanical Splice (ESMS) connection and the Extended Strand with a Lap Splice (ESLS) connection, consist of deck reinforcement, unstressed strands extended from the precast girder, and dowel bars grouted through the web of the girder as shown in following schematic. The deck reinforcement placed over the connection region provides the negative moment resistance. The strands spliced by mechanical splice chucks and lap splices within the ESMS and ESLS connection respectively develop the tension continuity to resist the positive moment, and the dowel bars are also designed to withstand the applied positive moments. Both connection details exhibited the adequate capacity to develop the moment resisting connection between the girders and the bent cap under target

seismic demands. The testing results of this study reveal that the concrete crushing at the bottom of girder-to-cap interface induced the strength softening of the connection under the negative moments beyond the target value. For the connection behavior in the positive moment direction, the shear friction behavior was developed at the interface between the precast girder and the cast-in-place diaphragm poured around the girder, which provided the positive moment resistance. Meanwhile, the tension force generated by the strands extended from the girder contribute to the positive moment resistance as well. Based on the understanding of the behavior of the ESMS and ESLS connections exhibited within the experimental tests, an accurate but straightforward design methodology was then established to develop a guide to help with field implementation for these innovative connection details. The success in evaluating the seismic performance of the ESMS and ESLS connections confirms that both connections are adequate to develop the moment resisting connection for the precast bulb-tee girders subjected to the vertical and lateral loads and can be used within the routine bridge designs.

CHAPTER 1 INTRODUCTION

1.1 Background

A former Deputy Secretary of the US Department of Transportation stated the missions of highway engineering as follows：

"Change the way we build highways. We need to build them faster, have them last longer, have them be safer and at a lesser cost."

The above statement was in response to traffic congestions, safety issues and increased costs over the past few decades. Traffic congestion is a growing problem because the overall volume of vehicular traffic in many areas continues to grow faster than the overall capacity of the transportation system (Weisbrod et al., 2003). In addition to improving the traffic management, upgrading the highway network is another solution to relieve the traffic congestion. However, the constructions required for upgrading cause additional traffic congestions in the work zones. Consequently, engineers are trying to utilize innovative ways to build highways faster to reduce the traffic congestions resulting from highway constructions. Furthermore, 24.9% of the nation's 607,380 bridges are suggested to be either functionally obsolete or structurally deficient in 2013, and effective solution should be established to decrease the total number of these bridges to below 15% over the next decade (ASCE, 2014).

The Federal Highway Administration (FHWA) has changed the design life of bridges from 50 to 75 years in considerations of safety, cost, and impacts on traffic. Longer service life of bridges greatly reduce the safety concerns by limiting the need for lane closures and work zone restrictions. Lower life-cycle cost is also a consequence of the

longer bridge service life. In addition, a reduced need for bridge rehabilitation and maintenance can result in fewer traffic delays. In response to this change, it is essential to use high-quality materials and structural members for the construction of future bridge projects to meet the 75-year design life.

The tasks of highway safety cannot be defined just preventing crashes and their associated costs, but they should be defined toward preventing losses of human, financial, and environment disruption during both construction and operation periods. During the construction period, safety concerns mainly consist of the injury risk to the construction crews and the motorists moving through the work zones as well as the environment disruptions (i.e., noise, construction debris disposal, etc.). The Bureau of Labor Statistics reports a total 1,322 fatal occupational injuries at road construction sites from 2003 to 2013 (US Department of Labor, 2014). In addition, a synthesis study of a number of traffic accident studies reveals that the total accidents in construction zones increases up to 119 percent during the period of construction (Paulsen et al., 1978). Environmental disruptions also become an issue with the growing number of work zones. Therefore, highway projects shall be completed quickly to minimize the duration when the construction crews and public motorists are exposed to work zones as well as the environmental disruptions so as to improve highway safety.

The constructions of highway create serious traffic disruptions causing inconvenience to the public and adverse effects on the business community due to the temporary detour, which shall be accounted as the cost paid by the public. The cost to maintain traffic control through a work zone can vary anywhere from 10% in rural areas to 40% in urban areas of the total construction cost (Tang, 2013). Additionally, the labor cost

that is directly related with the project duration is also a high percentage of construction costs. Hence, the technologies to complete the project quickly can be intensely attractive and cost-effective.

1.2 Accelerated Bridge Construction

The technologies to minimize the construction time without sacrificing quality is a matter of great importance in response to the missions of highway engineering. Bridges are significant components of the highway network. A rapid bridge construction is certainly beneficial to overcome the aforementioned missions. One of the most effective strategies of **A**ccelerated **B**ridge **C**onstruction (ABC) is to use prefabricated bridge elements and systems (PBES), which consist of innovative design and construction methods utilizing high performance materials. With the suitable technologies for connecting prefabricated components effectively to form a well-integrated bridge system, ABC technologies lead to numerous benefits that are summarized as below (Khan, 2014):

- Reduced construction time on highway projects,
- An improved construction quality,
- An improved work-zone safety,
- Minimized traffic disruption and reduced adverse impacts on the traveling public,
- Minimized environmental disruptions, and
- Lower life-cycle costs.

ABC utilizes the prefabricated components to form an integrated bridge as shown in *Figure 1-1*. The prefabricated components manufactured in controlled environments are higher quality, which can then minimize the life-cycle costs by lengthening the design life

of the bridge. Moreover, utilizing prefabricated components limits the environment disruptions around the work zones. ABC technologies are able to reduce the typical bridge construction duration to a matter of days as opposed to months as this can reduce traffic congestion and injures in work zones. Delivering highway projects quickly also results in the reduced adverse impacts to business communities and lower labor costs.

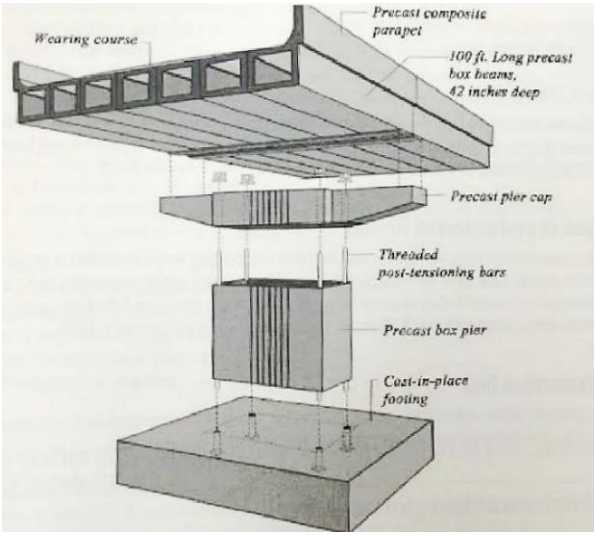

Figure 1-1 *ABC with Prefabricated Components (Khan, 2014)*

Due to its benefits, ABC continues to be advanced around the country and has already been implemented in many states, including Texas, New York, Iowa, Utah, Massachusetts, etc. (Culmo, 2009). However, using the ABC techniques has been limited in moderate-to-high seismic regions of the country. In order to avoid collapse of bridges during earthquakes, reliable seismic connections are necessary as per the formally adopted seismic design philosophy (Priestly et al., 1996). Only limited details are currently available to establish connections between prefabricated components with reliable performance under seismic loadings, which hinders the successful implementation of ABC techniques in seismic regions.

1.3 Seismic Design Philosophy

Earthquakes can pose one of the greatest load demands to the bridges. Also, the bridges are relatively more vulnerable to damage, and can collapse when a single component experiences failure. If basic seismic design principles are ignored, a bridge collapse can occur during earthquake. The converse, however, is also true. In reviewing bridge damages caused by past seismic activities, several design deficiencies have been identified, which are direct consequences of the elastic design philosophy uniformly adopted prior to 1970s (Priestly et al., 1996).

Since the 1970s, the capacity design philosophy has gradually superseded the elastic design approach as the basis for the design of bridges. This design philosophy allows the bridges to behave in an inelastic manner through flexural yielding during earthquakes and helps avoid the collapse of the bridges. The region experiencing flexural yielding, referred as the plastic hinge, is typically preselected within the columns of a bridge to prevent any serious damage occurring in the superstructure and foundation. In order to maintain stable response of a bridge, the plastic hinges are detailed such that the bridge can achieve a certain ductility. The plastic hinges can be located at the top of the column, the bottom of the column, or both if a frame column is established. Hinges at both ends of a column provide more locations for energy dissipation, which also reduce the size of both the column and the footing due to reduced moment demand as illustrated by *Figure 1-2*. The bridge system, in this case, consists of a continuous superstructure and a circular column with a moment resisting connection to the superstructure. Thus, the bridge acts as a simple vertical cantilever under the transverse seismic excitation. Under the longitudinal excitation, the column is subjected to double bending. Only one plastic hinge can be formed

at the base of column in transverse direction, but the column in longitudinal direction can form the plastic hinges at both top and bottom. It can be observed that the moment demand can be reduced due to the additional plastic hinge. Furthermore, the double plastic hinges are beneficial to reduce the displacement at the top of the column as well.

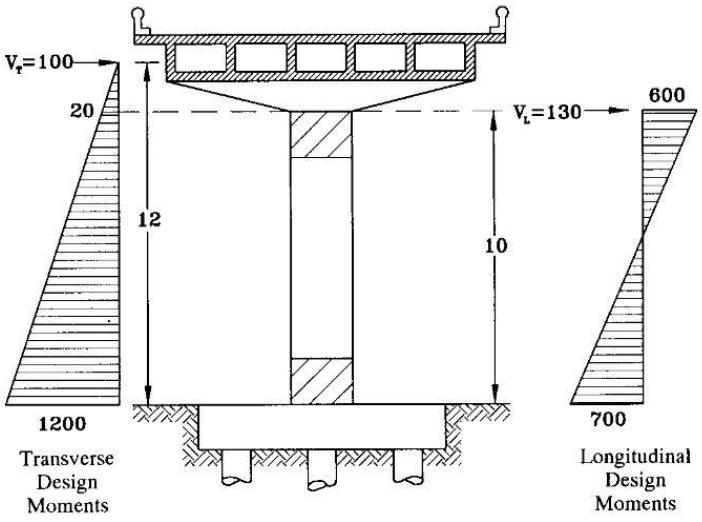

Figure 1-2 *Illustrative Example for Design Moment Demand (Priestley et al., 1996)*

1.4 ABC Connections for Seismic Region

Under seismic conditions, in order to effectively prevent bridge collapse by forming plastic hinges at the column ends, moment resisting connections between column and superstructure and column and foundation are desired. Furthermore, sufficient continuity between the prefabricated members must be developed in order to ensure that the continuous superstructure can remain essentially elastic. Numerous types of moment resisting connections between the column and superstructure and column and foundation, as shown in *Figure 1-3*, have been investigated. Their performances under seismic loads have been investigated (Marsh et al., 2011). However, even though a few concepts have been experimentally tested, ensuring sufficient continuity between precast superstructure members continue to be a challenge from both constructability and performance viewpoints.

One critical connection within the superstructure is the girder-to-bent cap connection as shown in *Figure 1-4*. Precast girders are integrated with a precast or cast-in-place (CIP) bent cap, and the girders can be erected flush with the bottom face of the bent cap, which is a desirable feature adopted by Caltrans. Deck and pier diaphragm are subsequently constructed, forming an integrated superstructure. In accordance with the current Caltrans Seismic Design Criteria (Caltrans, 2013), limited research has confirmed the viability of using precast girders in the superstructure to resist longitudinal seismic loads. This type of system is considered non-standard until connection details are tested adequately and the design procedures are formally adopted. Therefore, a thorough investigation on the performance of precast girder-to-bent cap connections under seismic loads is essential before developing the design methodologies and facilitating the use of ABC in in moderate-to-high seismic regions.

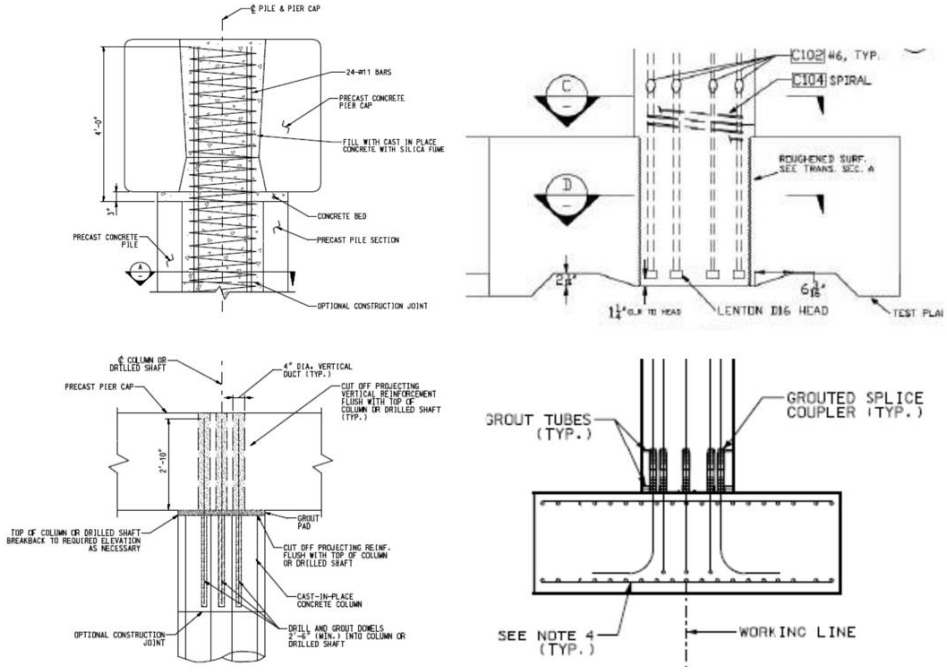

Figure 1-3 *Examples of Moment Resisting Connections between Column and Superstructure/Foundation for ABC Application (Marsh et al., 2011)*

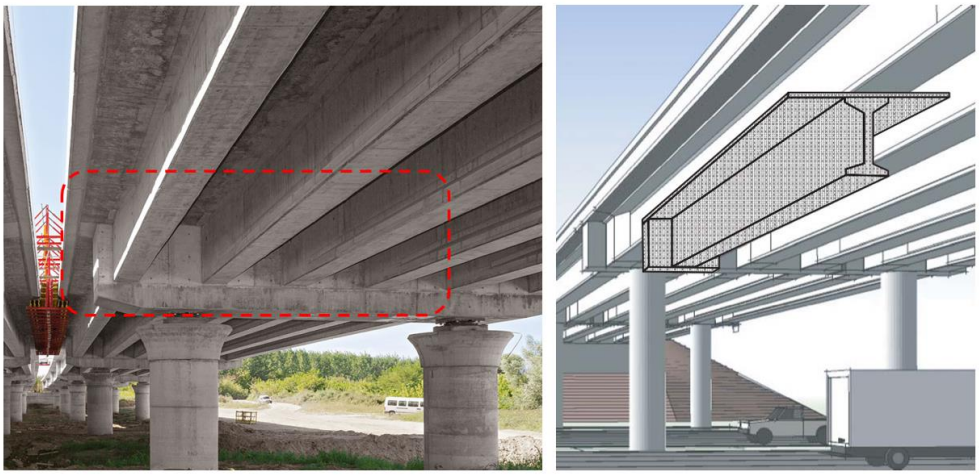

Figure 1-4 *Typical Integral Girder-to-Bent Cap Connection (Restrepo et al. 2011)*

The girder-to-bent cap interface requires continuity to resist the moments and transfer the shears. Moments at the interface typically are negative moments due to gravity loads in continuous bridge. However, time-dependent effects and temperature strain in the decks and girders may induce positive moments on the connection interface (Miller et al., 2004). Furthermore, seismic loads resulting from both the horizontal acceleration and vertical acceleration will induce additional negative moment and positive moment at the girder-to-bent cap connection interface depending on the loading direction. Hence, effective design details with sufficient moment and shear resistance under both the negative and positive moment directions need to be established. It is expected that more than adequate negative moment resistance would be provided due to the participation of reinforcement in the deck over the connection region between the girder and the bent cap (Hanson, 1960, Mattock and Kaar, 1960, Mattock and Kaar, 1961). For positive moment resistance, even though a number of systems involving bent bars, bent strands, embedded girder ends, etc. have been proposed to establish the continuity, the focus of these systems have been primarily on ensuring adequate performance for non-seismic application. Furthermore, the extending these details established for non-seismic condition to seismic

loading likely to create fabrication challenges and performance concerns. Therefore, more research on the girder-to-bent cap connection is required to promote ABC technologies in moderate-to-high seismic regions of the country.

1.5 Research Objectives

To facilitate ABC technologies in moderate-to-high seismic regions, the following two seismic connections for transferring shear and moment between precast girders and cast-in-place bent cap are investigated: the **E**xtended **S**trand with a **M**echanical **S**plice (ESMS) connection (*Figure 1-5*), and the **E**xtended **S**trand with a **L**ap **S**plice (ESLS) connection (*Figure 1-6*). The reinforcement in the deck over the connection region is still relied upon for resisting the negative moments, while the extended strands from the girder ends and dowel bars placed through the girders are used to provide the positive moments. The objectives of this study are to: 1) experimentally quantify the performances and capacities of the ESMS and ESLS connections; and 2) develop suitable design methodologies for these two connections so that they can be used in seismic design practices.

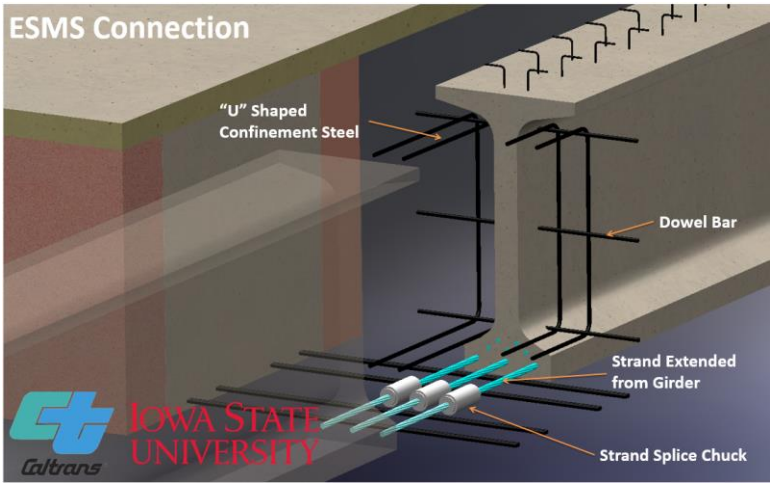

Figure 1-5 *A Schematic View of the Extend Strand with a Mechanical Splice (ESMS) Connection*

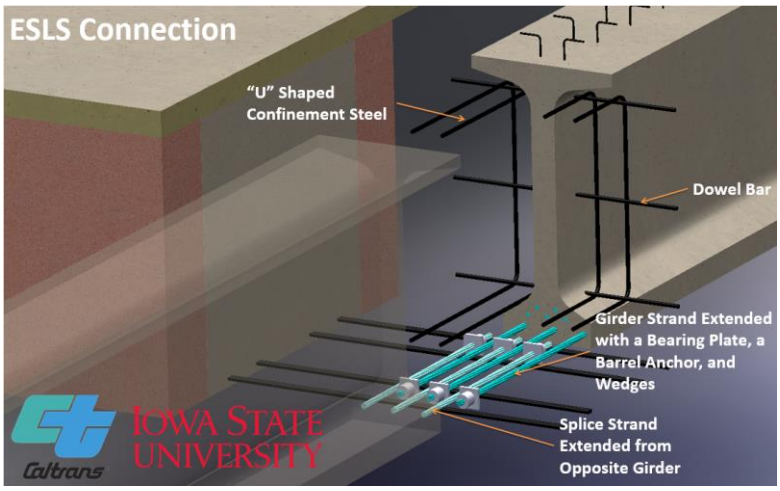

Figure 1-6 *A Schematic View of the Extend Strand with a Lap Splice (ESLS) Connection*

1.6 Thesis Layout

Following the introduction presented in Chapter 1, a literature review regarding previous research on girder-to-bent cap connections is presented in Chapter 2. Chapter 3 provides a summary of the design of the test unit that was used in the experimental part of this study. Chapter 4 presents experimental plan in details, including specimen construction, instrumentation and load protocol. Test results are presented in Chapter 5, while Chapter 6 summaries the design methodologies developed for theses connection as they can be applied to precast bulb-tee girders. Finally, Chapter 7 presents the conclusions of the study and recommendations for further work.

CHAPTER 2 LITERATURE REVIEW

To better understand the knowledge gap in the seismic performance of girder-to-bent cap connections and obtain the background information for the experimental work, an extensive literature review was performed. The findings indicated that several different actions can induce the moment and shear at integral girder-to-bent cap connection, which have to be resisted in an effective manner, especially when using precast girders. Next, the past research that focused on developing moment resistant connections between girder and bent cap were reviewed. In this process, some concerns regarding constructability and seismic performance of precast girder-to-bent cap connection were identified. These concerns limit the implementation of using ABC in moderate-to-high seismic regions. Two innovative connection details were proposed in this study. The expected mechanisms within the proposed connection details are also reviewed. Finally, the similitude theory and experimental techniques are also examined to guide the experimental work.

2.1 Causes of Moment at Girder-to-Bent Cap Connection

Unlike the bridges with simple spans, gravity loads will cause negative moments at the precast girder-to-bent cap connection interface in continuous bridges. Furthermore, extreme events and time-dependent effects will generate additional moments at connection interface of these bridges. Extreme events, like a horizontal earthquake load, can cause positive or negative moments at the connection interface depending on the loading direction. Time-dependent effects due to creep, shrinkage and thermal gradient will induce positive moments at the interface. In order to achieve continuous superstructures, moment resisting connections capable to resisting combination of all of these moments at the precast girder-to-bent cap interface must be developed.

2.1.1 Gravity loads

The connection moments due to gravity loads dependent on the sequence of construction involving the precast girders. For the typical construction sequence shown in *Figure 2-1*, the girders act as simple span members for dead loads of girders and liquid weight of the deck, before the connection continuity is established due to harden of the deck and connection regions. Superimposed dead and live loads act as continuous effects on the composite girder/deck section once the continuity connection is cast.

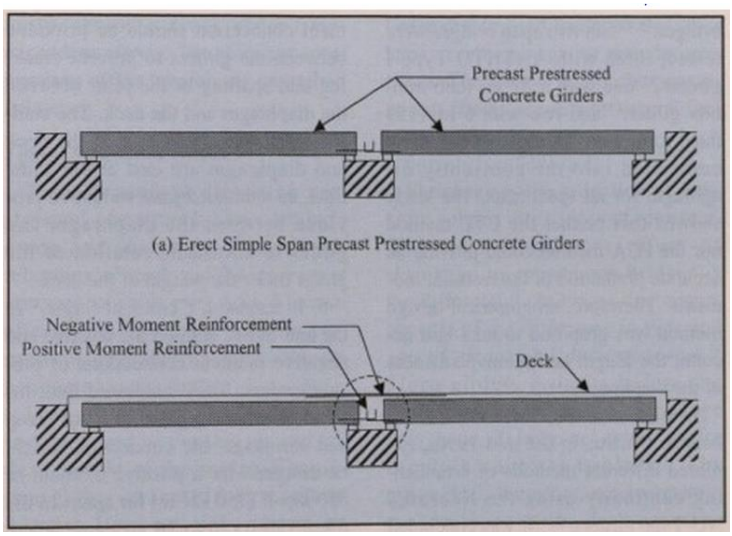

Figure 2-1 *Construction Sequence for Superstructure with Permanent Supports (Mirmiran et al., 2001)*

For bridges with precast girders erected flush with the side face of the bent cap, the temporary supports are erected at abutment and at the bents as shown in *Figure 2-2*. Precast girders, deck and bent cap are supported by temporary supports until the continuity connection is cast. Even though the dead loads of precast girders and deck will act on simple spans with higher midspan positive moments, these dead loads, superimposed dead and live loads are considered to act as continuous effects on the connections between precast girders and cast-in-place bent cap.

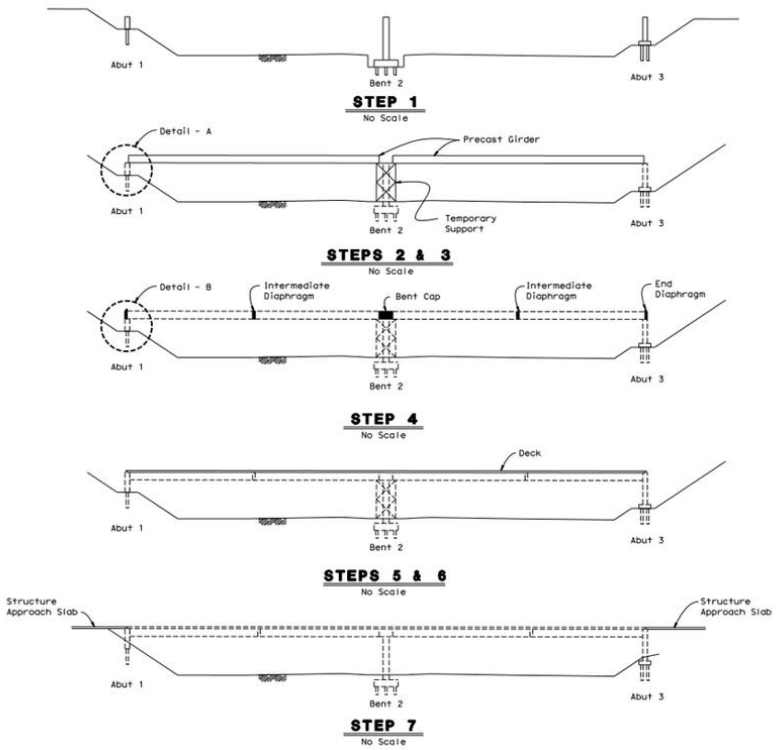

Figure 2-2 *Construction Sequence for Superstructure with Temporary Supports (Caltrans, 2011)*

2.1.2 Time-dependent effects and temperature gradient

Time-dependent effects within the superstructure may introduce additional positive moment at the girder-to-bent cap connection interface. Moreover, the effect of a temperature gradient down the member depth should be included where appropriate (AASHTO, 2012), which causes the girders camber upward and leads to positive moments on the girder-to-bent cap connections. The girder concrete creeps under the prestressing force applied effectively along the bottom of the girder, making the girder to deflect upward. This upward creep will cause positive restraint moments at the pier locations if positive moment connection are provided to the girders at the piers (McDonagh and Hinkley, 2003). Differential shrinkage between the precast girder concrete and CIP deck concrete could also result in a downward deflection of the composite deck-girder system if the shrinkage

of the deck concrete exceeds that remaining in the girder concrete. For the bridges with positive moment connections between precast girders, even though the differential shrinkage may induce a negative restraint moment at pier locations, the combined effects of creep and shrinkage could generate positive moments sufficient to cause cracking at pier locations (Oesterle et al., 1989). Several studies were performed in order to evaluate the time-dependent restraint moments. Around 1960, the studies conducted by the Portland Cement Association (PCA) studied the continuity of precast girders and developed the PCA method, which is typically used for hand calculation for restraint moments (Freyermuth, 1969). CREEP3, a computer program developed in 1970's, is also available to the designer to account for the restraint moments with the considerations of time-dependent effects (Tadros et al., 1977). The analytical studies performed by the Construction Technology Laboratories (CTL) studied the continuous bridge with precast, perstressed girders, and developed a program BRIDGERM to predict time-dependent restraint moments (Oesterle et al., 1989). A spreadsheet program called RESTRAINT, a modernized version of BRIDGERM, was developed by Miller et al. to conduct parametric studies of the continuous system (Miller et al., 2004). RESTRAINT uses flexibility-based analysis and calculate the moments resulting from time-dependent effects including creep of the prestressed girder and differential shrinkage of the girder and deck. Studies at the University of Nebraska, Omaha, in the mid-1990s concluded that the construction sequence has a significant effect on the positive restraint moment (Ma et al., 1998).

For an experimental investigation, two 50-ft-long Type III AASHTO I girders were assembled into a two-span, 100-ft-long, continuous specimen by Miller et al. Based on the findings obtained from the 120 days monitored period, they concluded that the temperature

effects on the system are significant, and daily temperature changes could cause end reactions to very ±20% per day (Miller et al., 2004). Seasonal temperature variations also affect the behavior of the bridge. As an outcome of this experimental study, Miller et al. concluded that temperature gradient can be as significant as the live load effects for continuity connection between concrete girders.

2.1.3 Seismic loads

Past earthquakes have shown the vulnerability of bridges under seismic loading. Extensive research was conducted to evaluate the response of bridges during earthquakes, several design procedures were developed to improve the seismic performance of bridges. Seismic design philosophies for highway bridges based on research findings and lessons learned from past earthquake are continued to be improved. The 1971 San Fernando earthquake was a major turning point in the development of seismic design criteria for bridges in the United States. Prior to 1971, the American Association of State Highway and Transportation Officials (AASHTO) specifications for the seismic design of highway bridges were partially based on a lateral force requirement. The California Department of Transportation (Caltrans) developed the first specialized seismic design criteria in 1973. The Applied Technology Council (ATC) developed guidelines ATC-6 [1] for seismic design of bridges in 1981; AASHTO later incorporated them into the Standard Specifications for Highway Bridges in 1991 (Chen and Duan, 2003). Since the 1989 Loma Prieta earthquake in California, extensive experimental research has been conducted on seismic design and retrofit of bridges in the United States. The capacity design principles were eventually adopted as the basis for all aspects of seismic design. This approach aims to prevent collapse of bridges when they are subjected to severe earthquakes. To achieve

this goal, the seismic lateral displacement demand should not exceed the structural displacement capacity. This is made possible by allowing the structure to deform inelastically without experiencing significant strength loss. In other word, the bridges should be designed with sufficient ductility with little or no significant structural damage (Priestly et al., 1996). The ductile behavior is achieved by allowing inelastic action to take place in preselected regions of selected bridge members such that they can be easily designed, inspected and repaired as needed. In addition, the preselected regions experiencing inelastic action allow the structure to dissipate the seismic input energy. Typically, inelastic regions are selected at the ends of bridge columns. The preselected regions, referred to as plastic hinges, are adequately detailed in order to achieve a specified level of ductility for the bridge. The components not explicitly designed for ductile performance (i.e., superstructure, foundation, etc.) should be designed to remain essentially elastic under the seismic excitation, which is accomplished through the use of overstrength moments of the plastic hinges. Although bridge column can be designed with a plastic hinge at one end and a pinned detail at the other end, designers take advantages of plastic hinges because at both ends of column, because the additional plastic hinge provide more locations for energy dissipation, and reduce the design demands of superstructure and foundation (Snyder et al., 2011). Framed columns fixed at both ends, rather than cantilever columns with fixed base, facilitate to form plastic hinges at both the top and bottom of columns during earthquakes as shown in *Figure 2-3*. Moments will be developed at the connection region between the superstructure and the columns, and the maximum forces will be produced when the columns reached their overstrength flexural moment capacity (Caltrans, 2013). In order to satisfy the equilibrium at the bent cap, additionally negative

and positive moments are induced at the interface between girders and bent cap as shown in *Figure 2-4*, in addition to the moment resulting from the gravity loads.

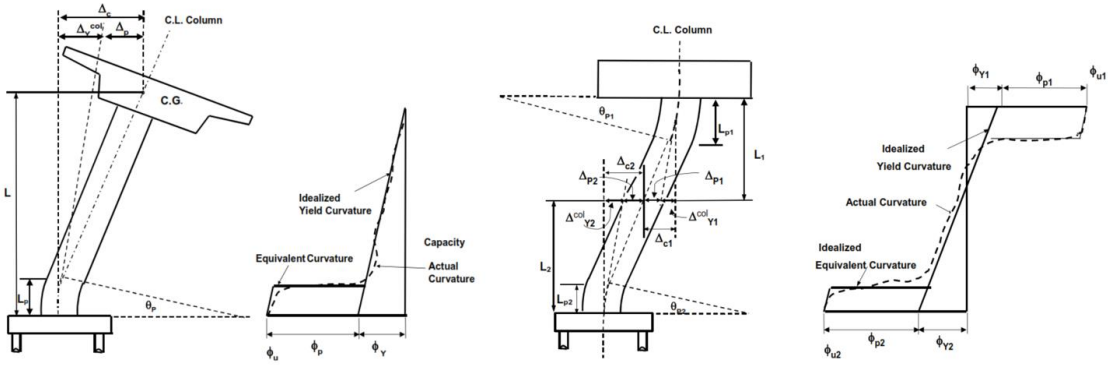

(a) Cantilever Column (b) Frame Column

Figure 2-3 *Cantilever Column vs. Framed Column (Caltrans, 2013)*

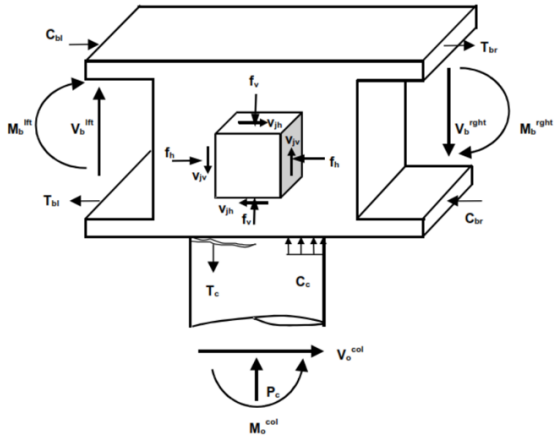

Figure 2-4 *Equilibrium of Forces on Bent Cap under Column Overstrength (Caltrans, 2013)*

Bridges may be vulnerable to vertical ground motions, which should also be given consideration in design. Vertical seismic motion may either increase or decrease the axial load in the plastic hinges and critical shear and moment demands within the superstructure. Like the gravity load effects, the vertical motion of an earthquake contributes to the shear and moment along the girder and the girder-to-bent cap connection as shown in *Figure 2-5*. Recognizing the possible vulnerability of superstructure connections to vertical seismic

motion, Caltrans Seismic Design Criteria (SDC) includes the specific provisions for the design of the superstructure connections. Caltrans SDC stipulates in Section 2.1.3 that "For ordinary standard bridges where the site peak ground acceleration is 0.6g or greater, an equivalent static vertical load shall be applied to the superstructure to estimate the effects of vertical acceleration" (Caltrans, 2013); and "A separate analysis of the superstructure's nominal capacity shall be performance based on a uniformly applied vertical force equal to 25% of the dead load applied upward and downward" in Section 7.2.2.

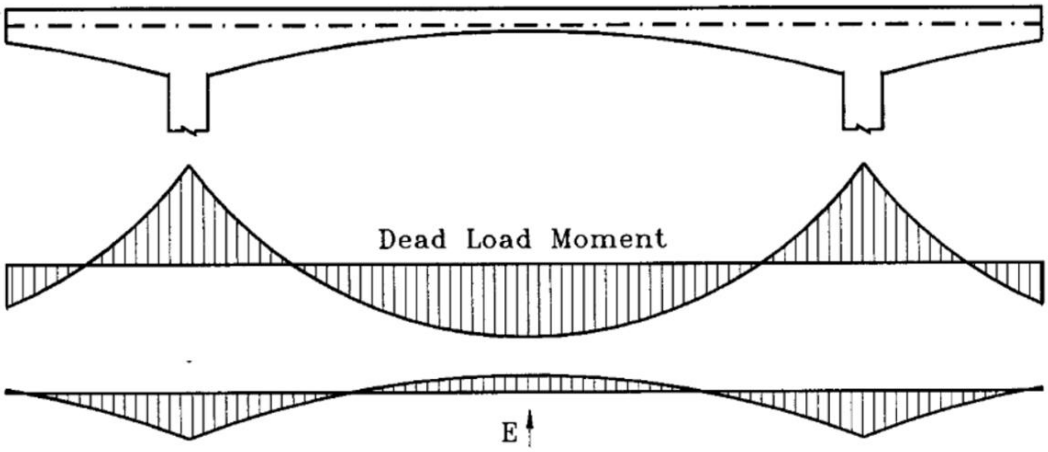

Figure 2-5 *Vertical Acceleration Effects on a Continuous Superstructure (Priestly et al., 1996)*

2.2 Moment Resisting Connection for Precast Girders

Continuous superstructures have several benefits. It results in the preferred structural behavior for overload conditions or extreme events, enhances the riding surface for vehicles, and improves the durability of bridge by eliminating joints at the supports (Mirmiran et al., 2001). As discussed earlier, numerous effects can induce either negative or positive moments at the end of precast girders. Hence, moment resisting connection for precast girders is necessary in order to use them in continuous bridge superstructures. The

required negative moment connection can be achieved by providing continuous reinforcement in the deck over the connection region between the precast girder and bent cap. The studies conducted by the Portland Cement Association (PCA) shows that this type of connection is adequate for resisting negative moments and shear (Hanson, 1960, Mattock and Kaar, 1960, Mattock and Kaar, 1961). For positive moments generated at the precast girder ends, several different continuity connection details were studied to resist restraint moments resulting from gravity loads and time-dependent effect and temperature gradient; however, only limited connection details are currently available to establish continuity connection resisting seismic loads.

2.2.1 Continuity connections designed for restraint moments

In the late 1960s, researchers at the Portland Cement Association (PCA) developed various connection details to resist the positive restraint moments (Freyermuth, 1969). Continuity behavior was evaluated for two two-span specimens, one with no positive moment connection and the other using the hooked bar detail as shown in *Figure 2-6*. The specimen without positive moment connection cracked at diaphragm and lost its continuity for positive restraint moments, and the continuity of specimen with hooked bars was reduce to about 80% of the elastic moment once the cracking showed up. Both specimens showed that the cracking did not affect the ultimate capacity of the negative moment connection. Eventually, the hooked bars fractured in a brittle manner at the knee of the hook under the fatigue testing after about 670,000 applications of the load. These studies recommended the stress in bent bars in the diaphragm shall be limited to 60% of yield stress under live loads and time-dependent effects.

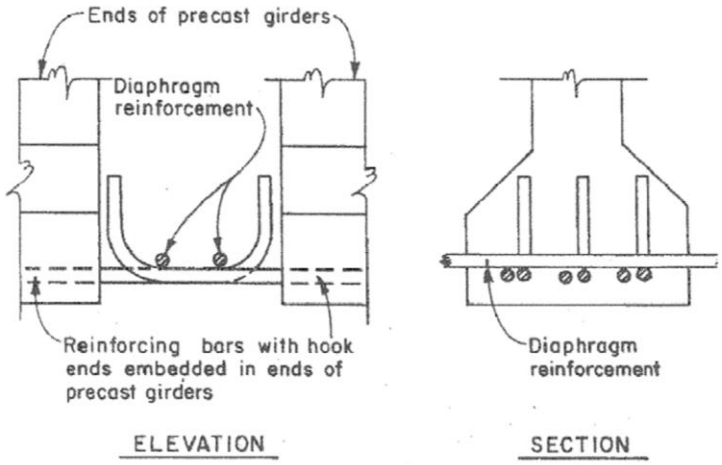

Figure 2-6 *PCA Method Connection (Freyermuth, 1969)*

A study on the feasibility of using extended prestressing strands to develop positive moment continuity of precast I-girder was conducted by the Missouri Cooperative Highway Research Program (Salmon, 1974). First phase of the study investigated the bonding characteristics of untensioned prestressing strand. Sixty nine pull-out tests were completed with three strand end configurations: straight, frayed and a 90 degree bent. It was found that bent strands provided the best anchorage, and straight strands were found to perform better than frayed strands. The stiffness of slip, and equations relating stress to the embedment length were also determined. Six full-scale bent-strand connections were tested in the second phase of the study. Three specimens consisting of two short, 6 ft 3 in. stub girders, a 30 in. diaphragm, and a 6.5 in. slab and three other specimens made only of the girders and diaphragm without slab were constructed. The stub girders were embedded 17.5 in. into the diaphragm and ¾ in. diameter coil tie rods were used to transmit force between the girder and the diaphragm. All specimens were tested for positive continuity with monotonic static loads. From the results of the study, a design method was proposed for continuity connection using bent strand. The required area of extended 90 degree bent strand is given by:

$$A_{ps}(req'd) = \frac{M - A_s f_y\,(jd_{ps} + d - d_{ps})}{f_{ps} jd_{ps}}$$

where

M = designed positive moment;

A_s = area of the diaphragm coil tie rod;

f_y = yield stress of the diaphragm coil tie rod;

d_{ps} = depth from extreme compression fiber to centroid of strand;

jd_{ps} = internal moment arm;

f_{ps} = (L_e - 8.25 in.)/0.228 ≤ 150 ksi; and

L_e = embedment length (in.).

Miller et al. reviewed the existing continuity connection details on precast/prestressed bridges, and tested the restraint moment connections based on the surveys of state DOTs, designers, fabricators and contractors (Miller et al., 2004). In their approach, the analytical studies were firstly performed by using RESTRAINT Program. Based on their analytical studies, using a moment resisting connection with capacity above 1.2M_{cr} did not significantly improve the behavior of the connection subject to restraint moments, where M_{cr} is the positive cracking moment of the girder-deck composite cross section. Thus, the experimental specimens for this study were designed with positive moment capacity of 1.2M_{cr} in order to avoid the reinforcement congestion within diaphragm. The first phase of the experimental research included the tests for the six connections consisted of different combinations of connection type (bent bar or bent strand) and diaphragm widths. *Figure 2-7* shows typical details. Specimens 1 and 2 tested bent-strand and bent-bar connections. Specimens 3 and 4 had the precast stub girders embedded into the diaphragm with extended bent strands and extended bent bars. Specimen 5 consisted the connection with extended bar with the girder ends embedded into diaphragm

6 in. into the diaphragm and additional stirrups in the diaphragm. The continuity connection tested within Specimen 6 consisted extended bars with the girder ends embedded 6 in. into the diaphragm and 3 #5 horizontal bars placed through the web of the girder. The results from first phase of experimental tests indicated that both the extended strand and extended bar connections developed sufficient strength, resisting restraint moments due to time-dependent effects and temperature gradient. Comparing the findings from each specimen, embedded girder ends and placing horizontal bars improve the connection performance, while additional diaphragm stirrups did not improve the strength of connection.

In the next phase of this research, two full-size specimens with designed strength of $1.2M_{cr}$ were conducted of 50 ft Type III AASHTO I girders jointed with a 10 in. diaphragm within second phase of the research. First specimen consisted reinforced concrete deck for negative moment connection and extended bars for positive moment connection as shown in *Figure 2-8*. Second specimen, as shown in *Figure 2-9*, had the same details except the extended strands were used for the positive moment connection. For the first specimen, a part of diaphragm was cast 28 days before the slab was cast in order to pre-compress the diaphragm by slab self-weight. Prior to test for continuity, the first specimen was monitored for 120 days. It was found that differential shrinkage of the deck did not cause additional negative moment; instead, positive moments from creep and shrinkage developed at the connection. Both specimens were loaded with the loading regime representing the worst case resulting from gravity load, creep, shrinkage, and temperature effects. The connection was then experienced fatigue cycles simulating live-load and time-dependent and temperature effects until the connection failed. The experimental tests showed that both connections maintained continuity for the restraint

moments even though positive moment cracks had formed. The additional test conducted on the second specimen for negative moment capacity confirmed that positive moment cracks had no effect on negative continuity of the system.

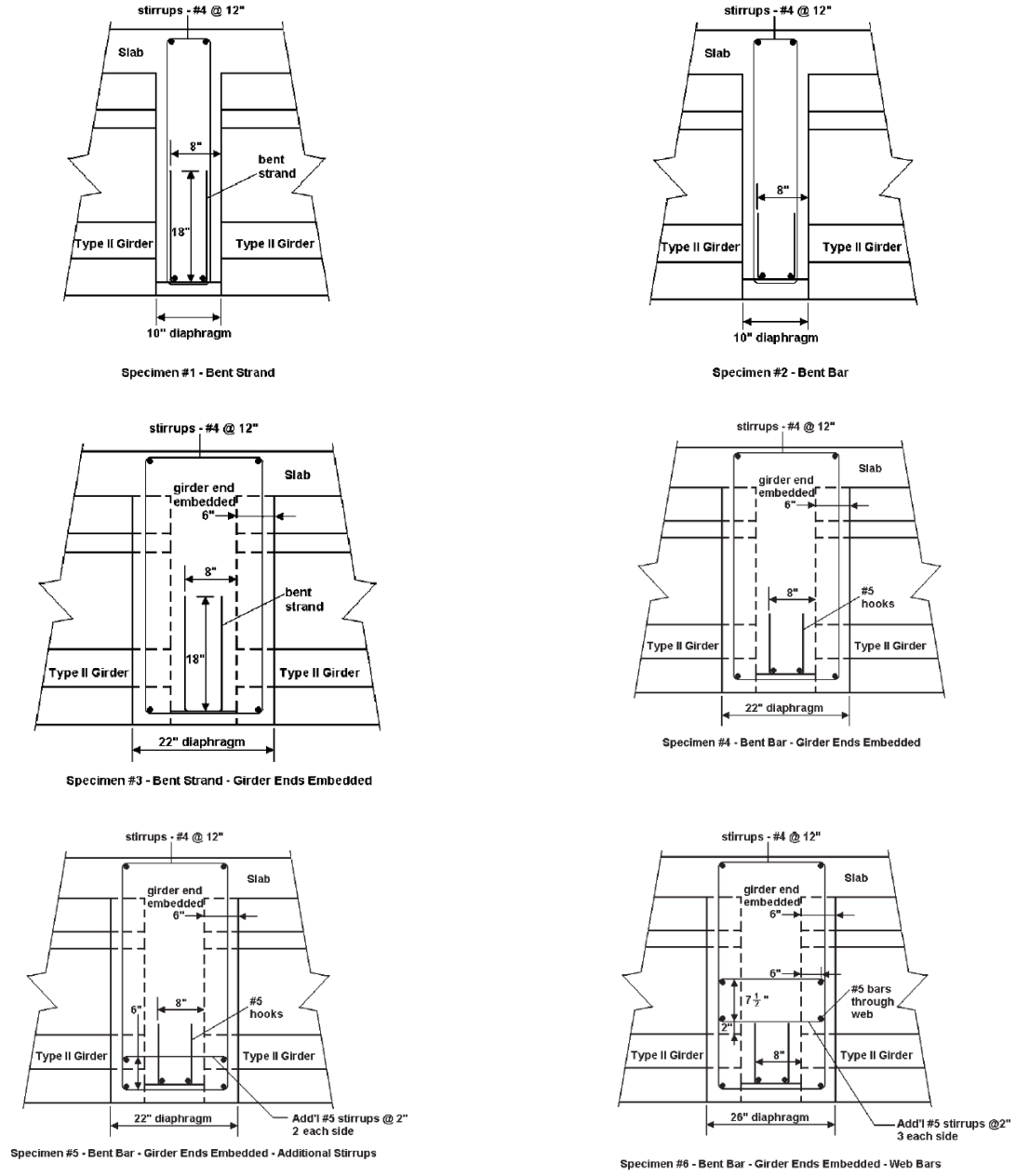

Figure 2-7 *Details of the Connections Used in the Frist Phase of Testing (Miller et al., 2004)*

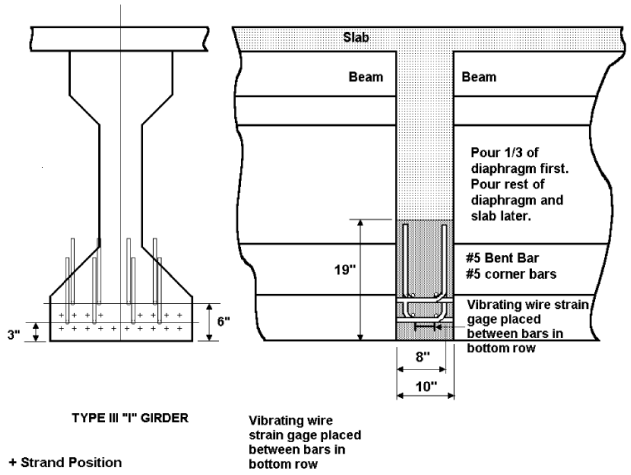

Figure 2-8 *Bent Bar Specimen with Partial Diaphragm Used in the Second Phase of Testing (Miller et al., 2004)*

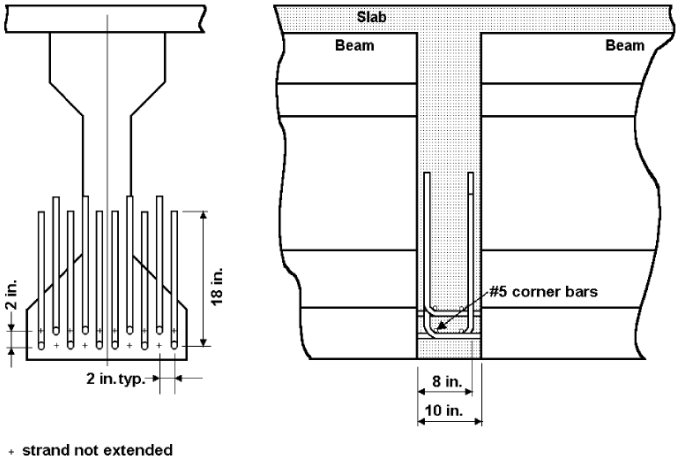

Figure 2-9 *Full-size Specimen with Bent Strand Used in the Second Phase of Testing (Miller et al., 2004)*

2.2.2 Continuity connection designed for seismic loads

Generally, the connections for precast components subjecting to seismic loads can be classified in terms of their performances. If a connection is established within a plastic hinging region, then the connection must be capable of sustaining inelastic deformations and dissipating kinetic energy input to the bridge system by an earthquake. Such connections are termed energy-dissipating (ED) connections. The connections, which are designed using capacity protection principles and not permitted to experience inelastic

action, are termed capacity-protected (CP) connections (Marsh et al., 2011). *Figure 2-10* illustrates the examples of ED connections and CP connections. Continuity connection within superstructure shall be designed as CP connection to keep essentially elastic during seismic activities. In addition, a ductile behavior of connection is also preferred to maintain sustainability of structure for unexpected seismic loads.

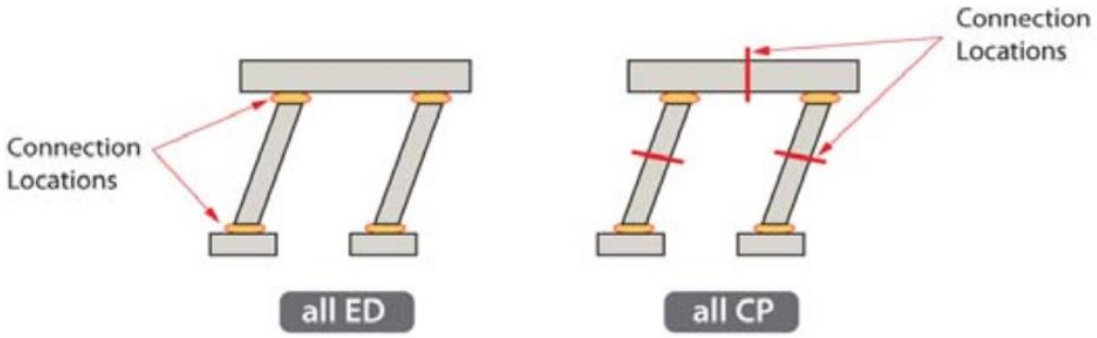

Figure 2-10 *Energy-dissipating (ED) vs. Capacity-protected (CP) Connections (Marsh et al., 2011)*

Research project has been performed by Restrepo et al. for precast/post-tensioning girder-to-cap connections subjecting to seismic loads, and their findings were presented in NCHRP Report 681 (Restrepo et al., 2011). The design of the post-tension was governed by Strength III limit state with seismic demands of 0.6g peak rock acceleration. Also, vertical ground motion with a magnitude of 0.8g of vertical excitation was considered. The test specimen consisted of a girder, deck, and reaction block representing the girder-to-cap connection region of prototype bridge as shown in *Figure 2-11*. The precast girder was placed to maintain an approximate 1 in. closure joint between the reaction block and girder. The Masterflow 928 high-strength, non-shrink grout containing a 0.2% volume fraction of polypropylene fibers was then gravity fed into the closure joint. Prior to the deck casting, the first post-tensioning operation consisted of setting the wedges for bottom tendon with

the stress approximating 5% guaranteed ultimate tensile strength (GUTS). The middle tendon was stressed to the stress of 75% GUSTS. Both the bottom and middle ducts were then grouted using SikaGrout 300PT. The top post-tensioning tendon was stressed to the same stress with middle tendon following the casting and curing of the deck; the duct was then grouted and allowed to cure. Following the application of the simulated dead loading, 100 cycles of essentially elastic loading were imposed primarily in the negative moment direction to investigate the response of the connection under service and ultimate loads, and the connection remained essentially elastic under the dead loading. In the seismic loading cycles, the loading protocol was resulted from a combination of lateral seismic load demands and vertical seismic shear demand held constant during all phases. The distributed flexural cracking was observed within the deck with a large crack width observed at the girder joint in the negative seismic loading cycles. During positive seismic loading cycles, elastic response was observed up to the point of joint opening. As the joint began to open, the concentrated rotations about the end resulted in a reduction in the positive flexural stiffness; however, the increase in the flexural resistance continued. A separation was observed between the top flange of girder and deck leading to a reduction in shear stiffness across the joint during loading cycles past 0.6% joint rotation. It was concluded that the proposed system was capable of satisfying operational and service level demands in accordance with LRFD code provisions. However, Restrepo et al. recommended that the adequate shear reinforcement shall be provided in order to minimize the vertical shear slip between the girder and the bent cap during flexural joint opening.

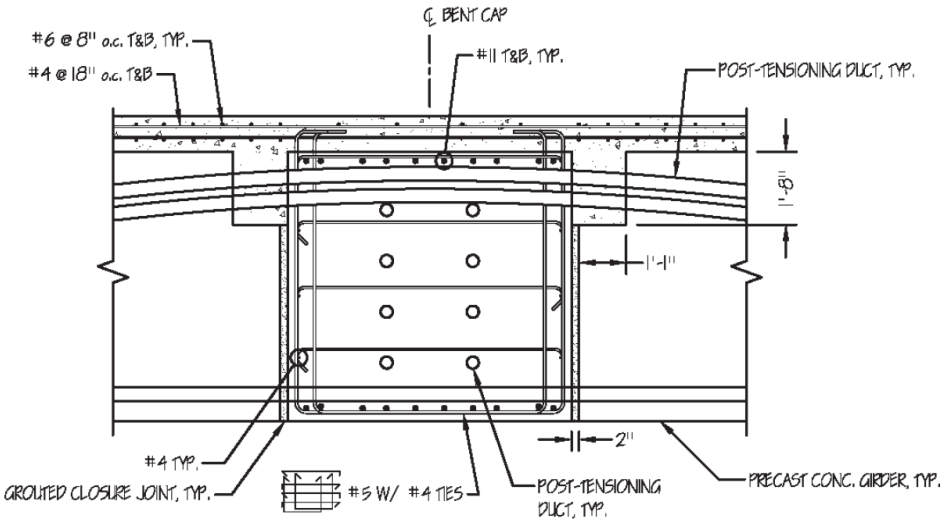

Figure 2-11 *Prototype Girder-to-Bent Cap Connection Details (Restrepo et al., 201)*

California Department of Transportation (Caltrans) has funded a series of investigation regarding the seismic response and overall moment capacity of precast girder-to-bent cap connections for seismic applications. In response to the Caltrans' Seismic Design Criteria degrading the precast girder-to-bent cap connection as pinned connection, Snyder et al. conducted a research consisting the analytical and experimental studies to quantify the behavior and moment resistance of the precast I girder to inverted-T bent cap connection under seismic conditions (Snyder et al., 2011). The inverted-T bent cap, in the shape of an upside-down letter "T", can be placed on top of the column. Precast girder with dapped ends are placed on the ledge of the inverted-T. A prototype bridge was designed with plastic hinges in both the top and bottom of column based on the Caltrans procedures used for incorporating inverted-T bent caps. The analytical study was conducted by finite element analysis (FEA) model and grillage model to better analyze and predict the behavior of the test unit during the experimental study. In the experimental study, a test unit consisting a single column, an inverted-T bent cap and a half span of five girders on each side of the bent cap was then developed based on a 50% scale of the prototype bridge as

shown in *Figure 2-12*. One side of the inverted-T bent cap was constructed using the as-built connection details while the other was constructed using the improved connection details. The as-built connection details consisted diaphragm around the girder and dowel bars placed through the girders in order to establish a continuity connection. The improved connection was similar with as-built connection except the additional untensioned, bonded prestressing strands through the connection as shown in *Figure 2-13*. The test unit was subjected two phases of testing. The first phase involved cyclic lateral loading in the longitudinal direction to simulate the horizontal earthquake effects on the entire bridge. The second phase focused on the connection behaviors and involved cyclic pushing and pulling of the superstructure in the vertical direction, which was performed on both sides of the bent cap to test both as-built and improved connection details. First phase test results indicated that both the as-built and improved connections behaved as fix connection and did not show signs of significant damage when the plastic hinges formed at the top of bottom of column. The flexural cracking observed across the width of the deck showed that the diaphragm action of the deck had engaged all of the girders. In the second phase of test, the test unit experienced a maximum upward displacement of 3 in. and a maximum downward displacement of 6 in.. During the positive moment cycles, a significant gap opening was observed between the bottom of girders and bent cap on the as-built connection side. However, the improved connection did not experience significant damage. Even though the improved connection was not fully tested, the test was terminated due to the strength degradation of the as-built connection causing an unstable structure. Overall, the analytical study results compared well to the measured response of the test unit for both phases of testing. The test results concluded that the as-built connection had a significant

positive and negative moment capacity; and the improved connection detail seemed to perform better than as-built detail. Based on the analytical and experimental studies, it was suggested that the precast girder to inverted T bent cap connection with the similar details with the as-built connection/improved connection details shall be treated as fixed connection in further bridge design.

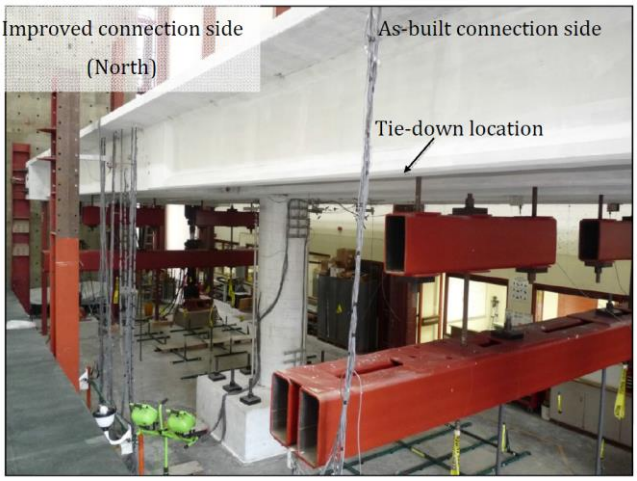

Figure 2-12 *Test Unit with Five Girders on Each Side (Snyder et al., 2011)*

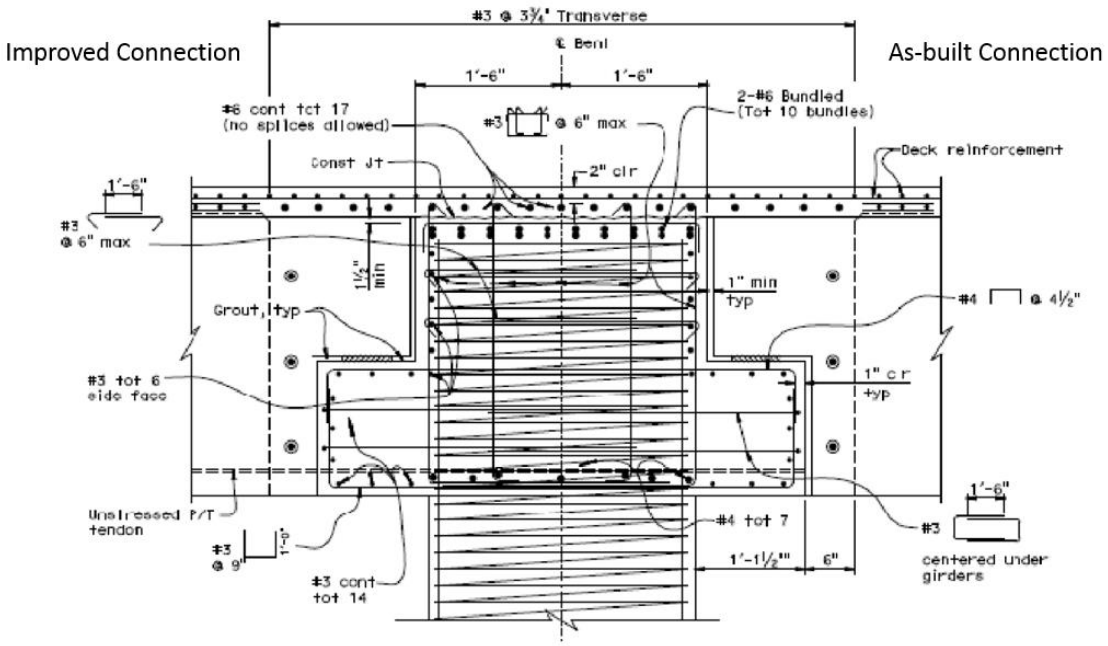

Figure 2-13 *As-built Connection and Improved Connection Details (Snyder et al., 2011)*

Based on the studies performed by Snyder et al., the experimental studies funded by Caltrans were conducted by Vander Werff et al. in order to fully test the capacity of precast girder-to-bent cap connections and evaluate the connection behavior under the seismic condition (Vander Werff et al., 2015). The experimental investigation included the tests on the connections for dapped-end I girder with inverted T bent cap and connections for precast bulb-tee girder with cast-in-place bent cap. Two set of connection details were proposed as shown in *Figure 2-14*. All connections were designed to remain essentially elastic when plastic hinges have been formed at the ends of column with the effects resulting from 0.25g vertical acceleration. In addition, ductile behavior of connections were also preferred to maintain sustainability of structure for unexpected seismic loads. The first set of connections included the GUSC and LUSC connections establishing continuity connection for precast I girders, and the second set of connections can be used for precast bulb-tee girders. All connection details included continuous deck reinforcement for negative moment continuity. Within the GUSC connection, which is same as the improved connection tested by Snyder et al., unstressed strands passed through the girder-to-cap interface in the region of the girder bottom flange to provide positive moment tension continuity, and dowel bars oriented transversely and had been grouted through the girder web into the diaphragm. The LUSC connection utilized four dowel bars confined by looped unstressed strands to develop positive moment continuity connection. Unlike the GUSC and LUSC connections, the ESSP and ESBS connections were developed for precast bulb-tee girders rather than I girders. The ESSP connection utilized unstressed strands anchored with steel plates and strand chucks at the end of the extended strands and lap splicing with the extended strands coming from the opposite girder, and the ESBF connection

incorporated extended strands bent at 90 degrees with a development length of 60 in. for 3/8 in. diameter strand. All four connections experienced the cyclic loads simulating the combined effects resulting from gravity loads, column overstrength moment due to horizontal seismic acceleration, and vertical seismic acceleration effects. All connections did not exhibit significant damage and remained essentially elastic under the design demands. In order to investigate the ductility and inelastic performance, all connections were loaded cyclically with large displacement until failure. During the larger displacement cycles, the damages appearing on all connections were characterized as the gap opening at the girder-to-cap interface, concrete cracking and spalling on the diaphragm adjacent to the girder due to girder pulling out and cracking distributed over the width of deck. The experimental studies confirmed that all connection details are viable, structurally-sufficient ways to establish moment resisting connections in high seismic regions, which could not be degraded as pined connection and resulted in a more efficient bridge designs.

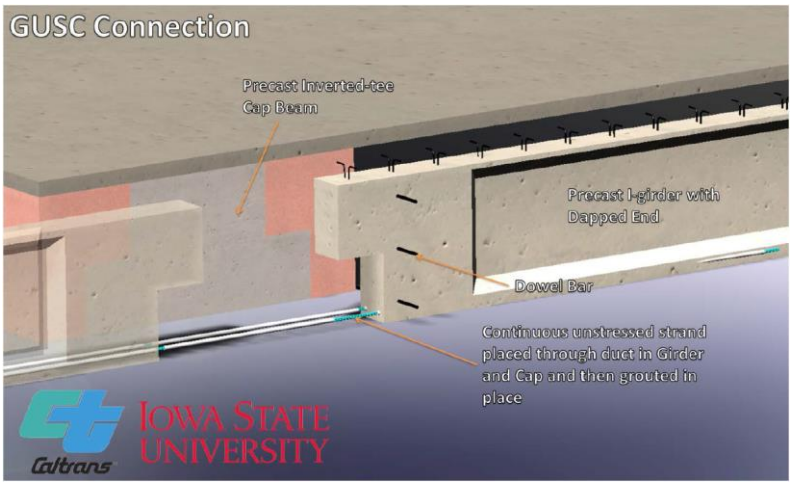

(a) The GUSC Connection Designed for Precast I Girders with Dapped Ends

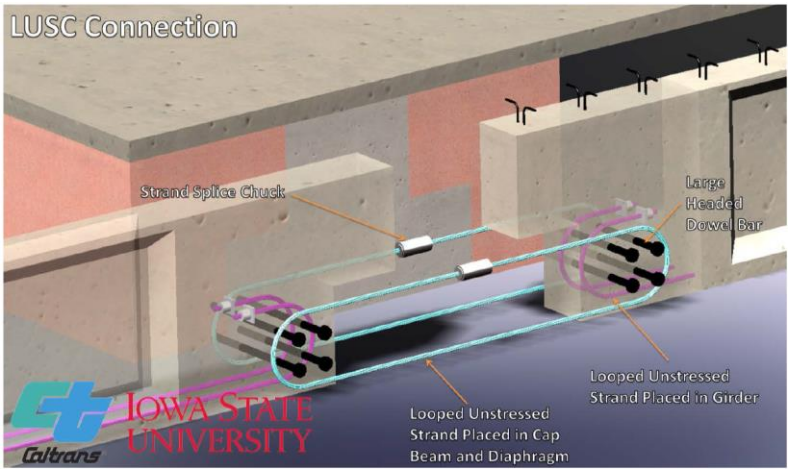

(b) The LUSC Connection Designed for Precast I Girders with Dapped Ends

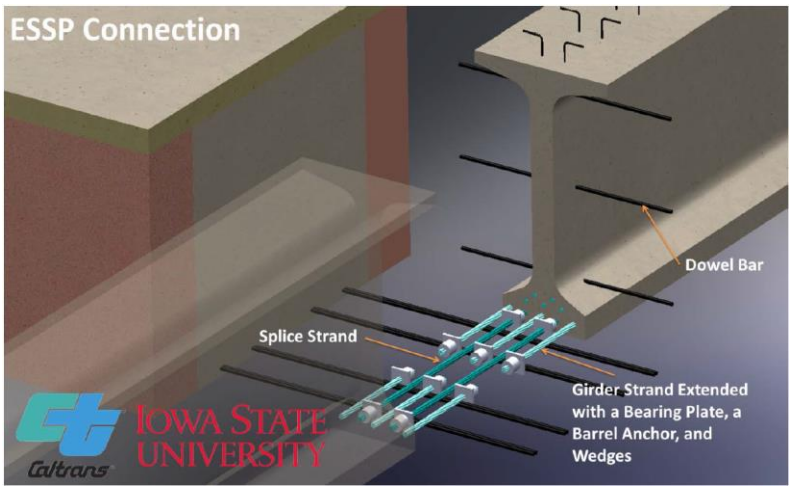

(c) The ESSP Connection Designed for Precast I Girders with Dapped Ends

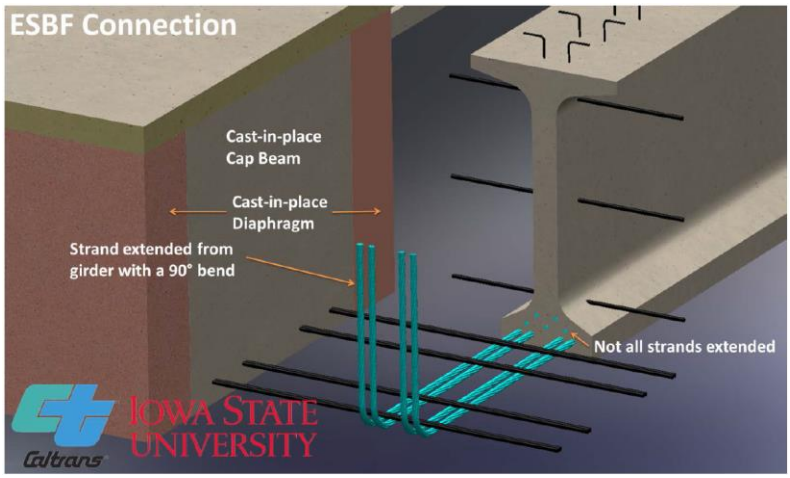

(d) The ESBF Connection Designed for Precast Bulb-tee Girders

Figure 2-14 *Schematics View of Precast Girder-to-Bent Cap Connection Details (Vander Werff et al., 2015)*

2.2.3 Concerns and issues related to moment resisting connections

Even though numerous moment resisting connections developed for precast girder have been tested and implemented, there are still a number of issues mainly concerning fabrication issues, unreliable design methodologies and their applicability under seismic condition.

Additional reinforcement that is required in order to develop the continuity resulting in congestion within the connection region as shown in *Figure 2-15*. The congestion of reinforcement induces the consolidating concerns for connection resulting from the use of small spacing between reinforcement. The honeycombs surrounding reinforcement may cause a weak bonding and result in the reduction of effective strength of reinforcement. The bent bars are difficult to use in construction, labor intensive, and are often asymmetrical, which can lead to uneven stresses and failure in the interface between the precast girders and bent cap (Miller et al., 2004). Also, the extended bars are likely damaged or fractured during fabrication and transportation. In the event of damaged bars, holes must be drilled into the girder ends through which the new bars are embedded and anchored with epoxy.

Figure 2-15 *Congestion within Connection Region due to the Use of Bent Bars (Miller et al., 2004)*

Though Salmons and Miller et al. proposed the design method for continuity connection resisting restraint moments, a design methodologies for establishing a seismic moment resisting connection has not been accepted yet. The analytical study conducted by Miller et al. showed that adding additional reinforcing bars to establish the positive moment connection with a capacity above 1.2 times the cracking moment composite section is not effective, and the additional reinforcement only brings congestion but provide little benefit to the performance of connection (Miller et al., 2004). Moreover, there are no accepted method to design the continuity connection with bent strand, and the effect of embedding the girder cannot be quantified by currently available design methodologies. In addition, it is typically assumed that cracking will occur at the interface between girder and bent cap under positive moments, but the observations from experimental tests and field showed that the cracking will possibly take place in the diaphragm (Miller et al., 2004) (Snyder et al., 2011) (Vander Werff et al., 2015). Under seismic condition, the load path within connection regions will be complex to expect and their integrity can only be investigated using large-scale tests (Marsh et al., 2011). However, very few such test have been

completed on girder-to-bent cap connection for seismic application. Significant knowledge gaps continue to remain for seismic performance and design methodologies of precast girder-to-bent cap connections.

2.3 Expected Connection Mechanisms

The deck reinforcement within the proposed precast bulb-tee girder-to-bent cap connections provides the negative moment resistance, and the unstressed strands extended from the girder as well as the embedding girder end with dowel bars grouted through the web of girder provide the resistance for positive moments. To get better understanding of the related mechanisms, a literature review of the bond-slip behavior of reinforcing bars and unstressed strands was performed. The shear-friction behavior involving embedded girder ends was also reviewed. The key findings are presented below.

2.3.1 Bond-slip behavior

Longitudinal reinforcement slip resulting from strain penetration would induce a member end rotation. For the connection between precast girder and bent cap, bond-slip of deck reinforcement and unstressed strands locating at the interface may affect the girder rotation respecting to the bent cap, which is one of the most meaningful parameters to reflect the connection performance. In order to accurately quantify the performance of precast girder-to-bent cap connection subjecting to flexure, the bond-slip behavior of reinforcements should be understood and accounted.

2.3.1.1 Bond-slip of reinforcing bar

For reinforcing bar embedded in concrete, three mechanisms consisting of chemical adhesion, frictional force and mechanical bearing of ribs transfer forces from reinforcing bar to surrounding concrete as shown in *Figure 2-16* (ACI 408 Committee, 2003). Friction

and bearing will transfer most of the force after initial slip of the bar. When a deformed bar moves with respect to the surrounding concrete, the bearing forces are balanced by compressive stresses on the concrete contact surfaces, which are resolved into tensile stresses resulting in cracking in planes that are both perpendicular and parallel to the reinforcement. The cracking in surrounding concrete is common leading to the splitting cracks (*Figure 2-17a*) and "pullout" failure (*Figure 2-17b*) if anchorage to the concrete is inadequate.

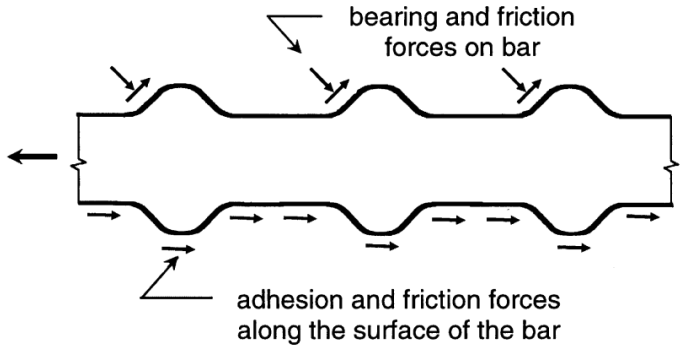

Figure 2-16 *Bond Force Transfer Mechanisms (ACI 408 Committee, 2003)*

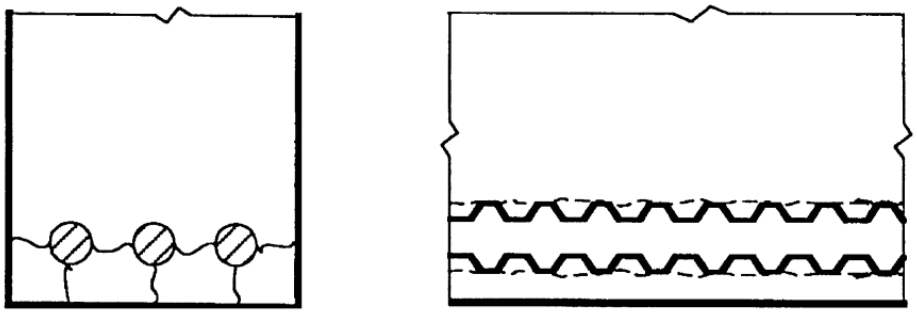

(a) Splitting Cracks (b) "Pullout" Failure

Figure 2-17 *Cracks between Bars and Concrete due to local Concrete Crushing (ACI 408 Committee, 2003)*

The model reflecting bond-slip behavior is commonly showed by the curve of the bar forces/stresses obtained at at the loaded end of the bar versus the external slip of the reinforcing bar, measured with respect to the concrete. Eligehausen et al. developed the

bond-slip model based on the test results from 125 pull-out specimens with short embedment length of five times the bar diameter (Eligehausen et al., 1983). The bond-ship model plots a general ship of local bond-ship relationship as shown in *Figure 2-18.*

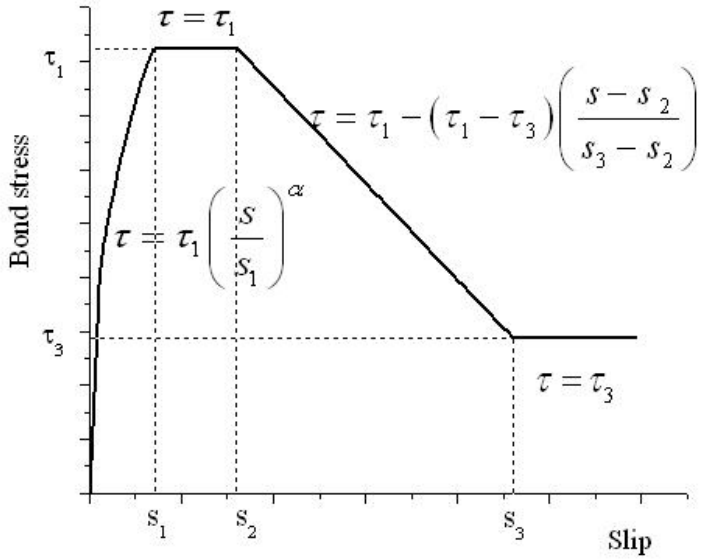

Figure 2-18 *Bond-slip Model Proposed by Eligehausen et al.*

The parameters within this model, which were determined from the experimental pull-out tests, are expressed as following:

The peak bond stress, $\tau_1 = 31\sqrt{f'_c}$ (psi);

The frictional bond resistance, $\tau_3 = 0.35\tau_1$(psi);

$s_1 = 0.15c_0$;

$s_2 = 0.35c_0$; and

$s_3 = c_0$, where c_0 is clear lug distance.

An approach to model the hysteretic reponse of bond-slip behavior was then suggested by Zhao and Sritharan (Zhao and Sritharan, 2007), and this model was confirmed by the experimental studies conducted by Liang and Sritharan (Liang and Sritharan, 2014). For reinforcing bars that are fully anchored into to concrete, the bar slip occurs only along

a portion of the entire embedment length, and the bar can experience much higher strain in comparision to the poor anchored bar. Based on the test data from literatures, Zhao and Sritharan propsed a bond-slip model for fully anchored reinforcing bars, which consists a straight line for the elastic region and a curvlinear portion for the post-yield region as shown in *Figure 2-19*. Within this monotonic bar stress (σ) vs. loaded-end slip (s) relationship, the slope of the straight line was taken as K, and $\tilde{\sigma} = \frac{\sigma - f_y}{f_u - f_y}$ is the normalized bar stess, $\tilde{s} = \frac{s - s_y}{s_y}$ is the normalized bar ship, $\mu = \frac{s_u - s_y}{s_y}$ is the ductility coefficient, b is the stiffiness reduction factor with the suggested value regioning from 0.3 to 0.5, which represents the ratio of the initial shope of the curvilinear portion at the onset of yieding to the slope in the elastic region (K), f_y and f_u are, respectively, the yield and ultimate strength of the steel reinforcing bar, and s_y and s_u are the loaded-end slips when bar stresses are f_y and f_u, respectively. To maintain a zero slope near the ultimate strength of the bar, a value of factor $R_e$should be slightly greater than one and was selected as 1.01 by Zhao and Sritharan.

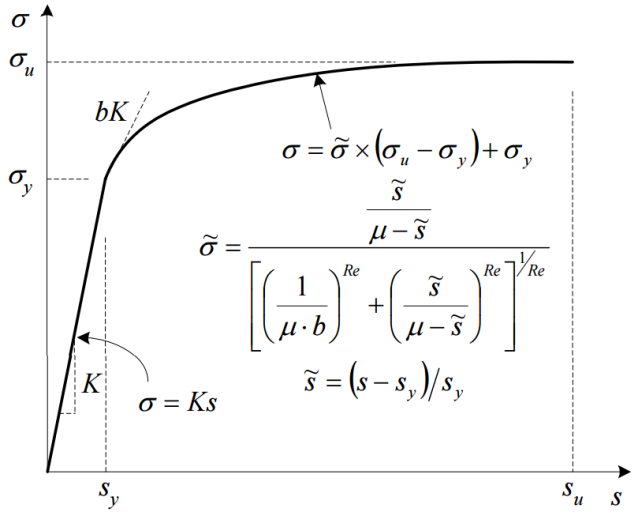

Figure 2-19 *Bond-slip Model Proposed by Zhao and Sritharan*

The model proposed by Zhao and Sritharan was then confirmed by experimental studies conducted by Liang and Sritharan (Liang and Sritharan, 2014), which consisted of the pull-out tests on No.6 and No. 8 reinforcing bars with the embedment length of forty-eight times the bar diameter. The comparisons between the experimental measured bond-slip behavior and theoretical behavior are shown in *Figure 2-20* (a) and *Figure 2-20* (b). The study concluded that the bond-slip model proposed by Zhao and Sritharan captures the strain penetration effects satisfactorily.

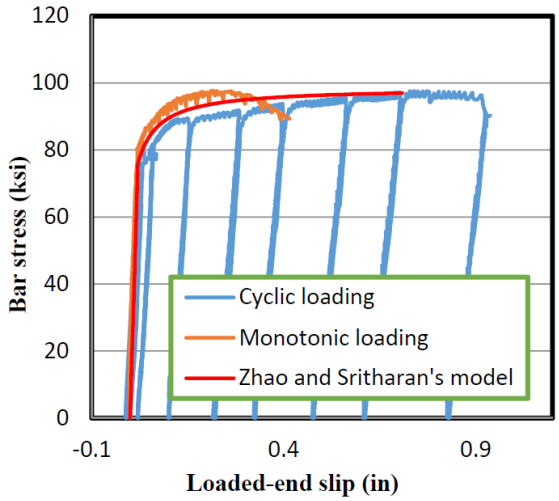

(a) Bar stress vs. load-end slip relationship of the #6 bar

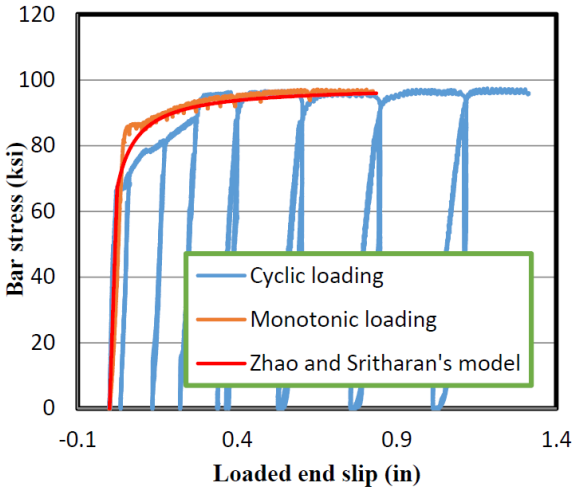

(b) Bar stress vs. load-end slip relationship of the #8 bar

Figure 2-20 *Bar Stress vs. Load-end Slip Relationship (Liang and Sritharan, 2014)*

2.3.1.2 Bond-slip of unstressed strand

The nature of the bond of unstressed strands in concrete differs from that of reinforcing bars and stressed strands. The helical texture of strand does not contribute to the bond since the strand tends to unscrew from the surrounding concrete. However, as a strand subjects to pull-out forces and elongates, the change of the strand pitch respecting to the surrounding concrete increases the normal and frictional forces improving the bond for strand. This effect causes high normal and shearing stresses in the concrete surrounding the strand. Local concrete crushing may occur at the strand-concrete interface as slip progresses (Salmons and McCrate, 1977).

Salmons and McCrate performed a study on the bond behavior of untensioned prestressing strand to evaluate load-deformation characteristics and load-embedment requirements (Salmons and McCrate, 1977). The specimens with three strand configurations including straight, frayed and bent 90 degree over a reinforcing bar were tested. Similar with bond-slip behavior of reinforcing bar, strand stress vs. loaded end slip relationship is commonly used to characterize the bond-slip behavior for strand. Comparing the strand stress vs. loaded end slip relationships for specimens with same strand configuration but four embedment lengths as shown in *Figure 2-21*, Salmons and McCrate verified that the bond-slip behavior appears to be independent of the embedment length. Based on this study, strand diameters has no apparent effect on relationships between slip and steel stress. The study also indicated that the strand configuration with bent 90 degree over a reinforcing bar provide the highest strength and stiffness comparing with other two configurations. Salmons and McCrate finally suggested the strand embedment length used for design as follows:

a. Strand bent 90 degree over reinforcing bar (6 in. per-bend length)

$$L_e = 0.163 f_s + 8.25\ in.$$

b. Straight strand

$$L_e = 0.337 f_s + 8.00\ in.$$

c. Frayed strand without bends

$$L_e = 0.552 f_s + 5.50\ in.$$

where

L_e= embedment length of strand, in.; and

f_s= maximum stress in the strand, ksi.

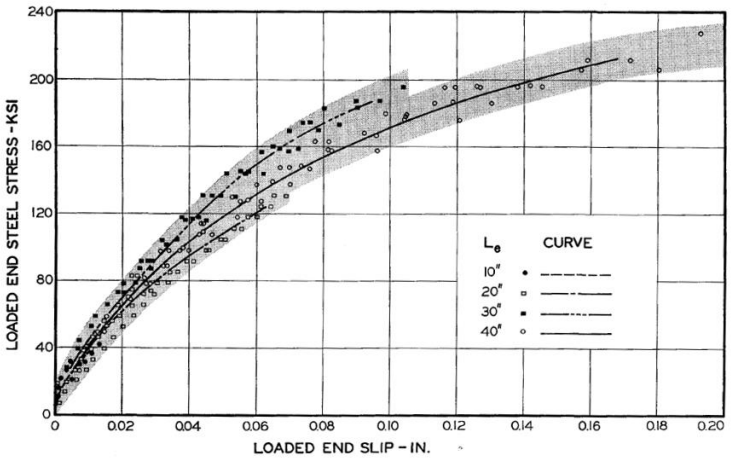

Figure 2-21 *Slip as a function of loaded end steel stress for the four embedment lengths of the bent series (Salmons and McCrate, 1977)*

A series of pull-out tests on strands with three sizes (0.375-in., 0.5-in. and 0.6-in.) and different anchoring configurations (straight, 90-degree bent, bond head and end plate) were performed at Iowa State University to investigate bond-slip behavior and strand anchorage as part of this precast girder-to-bent cap connection study by Liang (Liang and Sritharan, 2015). The experimental tests showed that the anchorage devices including bond

head and end plate were able to significantly short the embedment length. Based on the measured strain data, the strain distribution along the embedment length can be characterized as a linear relationship. The analytical study verified the linear strain distribution by comparing the analytical relationship between strand stresses and loading end displacements with the measured response as shown in *Figure 2-22*. Finally, the average bond stress of 335 psi was concluded for the strand embedded in concrete with normalized compressive strength of 4500 psi.

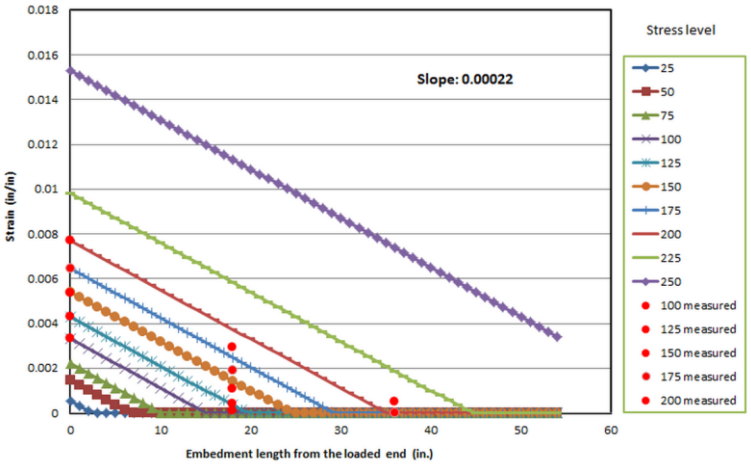

(a) Strain Distribution for 0.375-in. Diameter Strand

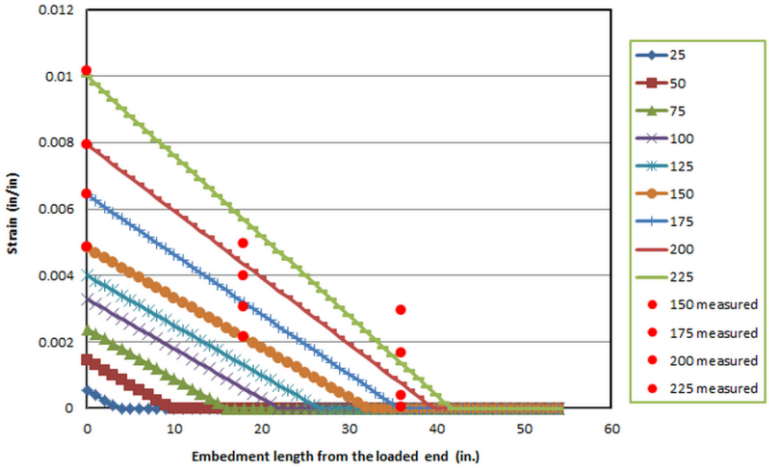

(b) Strain Distribution for 0.6-in. Diameter Strand

Figure 2-22 *Measured and Analytical Strain Distribution Comparisons (Liang and Sritharan, 2015)*

2.3.2 Shear friction behavior

Shear friction behavior includes the cohesion components resulting from shear transferred through the slip plane and dowel action, and friction components due to clamping force in the reinforcement crossing the interface plane. The mechanism of shear friction is considerably more complex than conventional friction. The mechanism of shear friction is considerably more complex than conventional friction. A “wedging action” developed by the roughness of the shear plane forces the crack to open in direction perpendicular to the interface. This cracking opening induces tension in the reinforcement crossing the plane of interface resulting in a “clamping” force. Furthermore, any compressive force resulting from load conditions crossing the interface also result in a clamping force (Harries et al., 2012). The shear resistance is directly proportional to the normal clamping force through a friction coefficient as shown in *Figure 2-23*. Moreover, an additional component of shear friction, evident in the experimental data, from cohesion and/or aggregate interlock is proposed by Mattock (1974). Ali et al. claimed that failure of cohesion at the interface to transmit shear force results from loss of contact, which in turn occurs due to crushing of interlocking aggregates and cement paste (Ali and White, 1999). Hence, concrete strength and joint surface condition also affect the shear friction capacity.

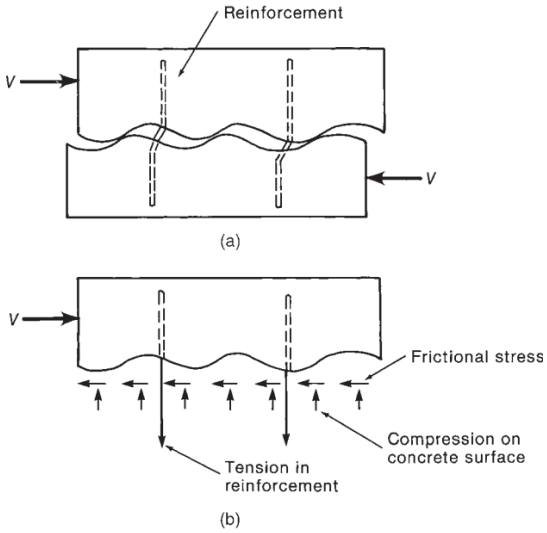

Figure 2-23 *Shear Friction Mechanisms (Macgregor et al., 1997)*

The shear friction behavior can be divided into three stages consisting of precracked behavior, postcracked behavior and post-ultimate behavior (Harries et al., 2012). The behavior during precracked stage is characterized by a relatively linear relationship between the applied load and shear displacement with negligible reinforcement strain. The cohesion component at the shear interface contributes to the shear resistance during this stage. The behavior following the crack appear at the shear interface, referred as postcracked behavior, is characterized by a softening behavior, visible interface crack widths, and low reinforcement strains. The shear displacement continues to have a relatively linear relationship with the applied shear load. Furthermore, the shear friction developed by reinforcement begins to engage in the shear resistance. Following the achievement of the ultimate shear load, the post-ultimate behavior is characterized by an increment in shear displacement and reinforcement strain without any additional increase in applied load. A relatively rapid degradation of shear resistance takes place up to a certain shear displacement (ultimate shear displacement). It is proposed that the failure mechanism

may be attributed to the bond failure of the crossing reinforcement, the aggregate interlock failure, and the concrete failure around reinforcement (Valluvan et al., 1999).

Section 11.6 of the ACI 318-11 and Section 5.8.4 of AASHTO LRFD (2012) specify the nominal shear resistance of shear friction in Table 1. Considering only normal weight concrete and reinforcement oriented perpendicular to the interface, the provisions from AASHTO LRFD (2012) and ACI 318-11 associated with shear-friction are summarized in *Table 2-1*.

Table 2-1 *Shear-friction Provisions in AASHTO LRFD (2012) and ACI 318-11*

<table>
<tr><td></td><td colspan="4">AASHTO LRFD (2012), Section 5.8.4</td><td colspan="2">ACI 318-11, Section 11.6</td></tr>
<tr><td>Nominal shear resistance</td><td colspan="4">$V_{ni} = cA_{cv} + \mu(A_{vf}f_y + P_c)$</td><td colspan="2">$V_n = A_{vf}f_y\mu$</td></tr>
<tr><td>Limitations</td><td colspan="4">$f_y \leq 60{,}000\ psi$
$V_{ni} \leq K_1 f'_c A_{cv}$
$V_{ni} \leq K_2 A_{cv}$</td><td colspan="2">$f_y \leq 60{,}000\ psi$
For concrete either cast monolithically or cast on surface intentionally roughened:
$V_n \leq 0.2f'_c A_c$
$V_n \leq (480 + 0.08f'_c)A_c$
$V_n \leq 1600A_c$
For all other cases:
$V_n \leq 0.2f'_c A_c$
$V_n \leq 800A_c$</td></tr>
<tr><td>Parameter</td><td>c, ksi</td><td>μ</td><td>K_1, ksi</td><td>K_2, ksi</td><td>λ</td><td>μ</td></tr>
<tr><td>Monolithically cast</td><td>0.40</td><td>0.4</td><td>0.25</td><td>0.5</td><td>1.0</td><td>1.4λ</td></tr>
<tr><td>Concrete slab on surface intentionally roughened</td><td>0.28</td><td>1.0</td><td>0.3</td><td>1.8</td><td>1.0</td><td>1.0λ</td></tr>
<tr><td>Other on surface intentionally roughened</td><td>0.24</td><td>1.0</td><td>0.25</td><td>1.5</td><td>1.0</td><td>1.0λ</td></tr>
<tr><td>Cast against surface with no roughening</td><td>0.075</td><td>0.6</td><td>0.2</td><td>0.8</td><td>1.0</td><td>1.0λ</td></tr>
</table>

Notes: $A_{cv}(A_c)$ is area of concrete shear interface; A_{vf} is area of reinforcement crossing shear interface; P_c is net compressive force; f_y is yield strength of reinforcement crossing shear interface; μ is friction factor (ASSHTO 2012) and coefficient of friction (ACI 318-11); c is cohesion factor; K_1 fraction of concrete strength available to resist interface shear; K_2 is limiting interface shear resistance.

The ACI 318-11 provisions specify a more conservative shear resistance by neglecting cohesion component and applied compressive forces at the shear interface. However, ACI 318-11 reports in the commentary that the sum of the resistance to shearing of protrusions on the crack faces and the dowel action of the reinforcement can be represented to establish a closer estimate of shear-transfer strength. ASSHTO (2012) introduces a term accounting for the cohesion at shear interface. For simplicity, the term "cohesion factor" is used to capture the effect of cohesion. The values of parameters presented provide a lower bound of numerous experimental data. It should be noted that all parameters resulting from experimental data are subject to the limitations implied by the data set from which they were obtained.

The slip at shear interface, referred as shear displacement, is a critical behavior affecting shear friction resistance. Shear displacement affects the cohesion component of shear friction in an adverse manner, and the clamping force developed in the interface reinforcement (Harries et al., 2012). The value of shear displacement when the shear load first reaches the ultimate value (yield shear displacement) were determined by experimental tests conducted by Harries et al., which ranges from 0.025 to 0.041 in.. Nevertheless, very limited data for the ultimate shear displacement were reported. Available experimental data exhibited the values ranging from 0.25 to 0.45 in. for the ultimate shear displacement (Valluvan et al., 1999).

2.4 Structural Model and Experimental Techniques

The definition of a structural model is "any physical representation of a structure or portion of a structure. Most commonly, the model will be constructed at a reduced scale", which is defined by ACI Committee 444, Experimental Analysis for Concrete Structures.

Many reduced-size structural components are customarily used in research studies because of the great reduction in loading magnitudes and construction costs. For reinforced and prestressed concrete structures, the prototype behavior can be represented by using a reduced-size model made of materials that are similar to the prototype material. In addition, the load path within a connection between precast concrete members will be complex during inelastic response, which can only be investigated using structural models. The similitude theory and experimental techniques were reviewed to guide the experimental studies.

2.4.1 Similitude theory

Any structural model must be designed and loaded according to a set of similitude requirements that relate the model to the prototype, and the similitude theory was developed to predict prototype performance from model tests. Any physical phenomena are described in term of dimensions such as length, mass, time, temperature, etc. All governing equations of physical problem can be expressed as follow:

$$\mathrm{f}(x_1, x_2, \cdots, x_k) = 0$$

where $x_1, x_2, \cdots, x_k$ are k physical variables.

As a key theorem in dimensional analysis, Buckingham Pi theorem states that physical laws are independent of the form of the units, and any dimensionally homogeneous equation involving physical quantities can be expressed as an equivalent equation involving a set of dimensionless parameters. Therefore above equation can be represented in form of follow:

$$\mathrm{g}(\pi_1, \pi_2, \cdots, \pi_{k-r}) = 0$$

where $\pi_1, \pi_2, \cdots, \pi_{k-r}$ are dimensionless products of k physical variables, and r is the number of fundamental dimensions that are involved in the physical variable.

Similitude requirements for modeling result from forcing the pi terms to be equal in the model and prototype (Harris and Sabnis, 2010). Therefore, the similitude relationship corresponding to the pi terms can be used to solve the scale factors. If the same material is used in the model and the prototype, the model and prototype stresses need to be identical to represent the prototype behavior by using a model. Therefore, the identical strain in the model and the prototype will be used as the similitude relationship to solve the scale factors.

2.4.2 Experimental techniques

An appropriately reduced-size model can be constructed by using the similitude theory. However, meaningful interpretation of such model tests is not possible unless proper instrumentation and loading techniques are used. The forces and deformations reflecting the structural behavior are measured through instrumentations. In general, strain, deflection, cracks, force, etc. need to be measured during a test of the reinforced or prestressed concrete structural model. For strain measurement, electrical resistance strain gage is the most commonly used because the output can be easily amplified, recorded, and displayed as well as the cost is relatively low (Harris and Sabnis, 2010). However, instability of the mounting cement and environmental conditions may cause the reduction of its sensitivity. The linear variable differential transformer (LVDT) is a reasonably compact electrical device that can be used for the precise measurement of displacement (Herceg, 1976). A similar device, the direct current differential transformer (DCDT), is also widely used in experimental work for displacement measurements. The loads and reactions can be measured with load cells. In order to record the large amount of data, the

data acquisition systems that digitally record data continuously are used in structural testing laboratories.

The quasi-static tests with slow loading rates are carried out to study structural performance regarding cracks, hierarchy of collapse and associated levels of damage. Quasi-static tests are performed by imposing predefined force or displacement histories on the test specimen. The slow loading rate provides a detailed insight regarding the elastic and inelastic behavior of a structure. However, the effect of acceleration and velocity cannot be reflected with a slow loading rate. Therefore, the test needs to be adequately designed to account for these effects in the predefined force or displacement histories when the dynamic effects are important.

CHAPTER 3 DESIGN OF TEST UNIT

3.1 Prototype Bridge

The large-scale tests were developed to further understand and quantify the seismic performance of the proposed precast bulb-tee girder-to-bent cap connections. Prior to the experimental tests of the ESMS and ESLS connections, two sets of connection tests were conducted to investigate the seismic performance of the girder-to-bent cap connections designed for precast I-girders and precast bulb-tee girders at Iowa State University. The first set of the connection tests investigated two configurations established for the precast I-girder-to-precast inverted-T bent cap connections (the GUSC connection and the LUSC connection). The following set of connection tests investigated two details designed for the precast bulb-tee girder to cast-in-place bent cap connections (the ESSP connection and the ESBF connection). The test results from the aforementioned connection tests demonstrated that all four connections behaved as the moment resisting connections under the target seismic demands resulting from gravity load, horizontal seismic excitation, and vertical acceleration over 0.5g, as opposed to degrading to a pin condition under positive moment.

Following the completion of two sets of connection tests noted above, the possibility of optimizing the connection details was examined in this study through the experimental tests of ESMS and ESLS connections. The prototype bridge that was used for the second set of connection tests was used in this study. As shown in *Figure 3-1*, this was a continuous precast bulb-tee girder bridge with four spans of 124 ft - 150 ft - 150 ft - 124 ft. Bulb-tee girders, which can reach a span length up to 150 ft (Caltrans, 2012), were chosen to be used in the prototype bridge in order to investigate the connection behavior of the bridge with long spans. The single column bents along with the maximum

superstructure width corresponding to five girders were used for the prototype bridge to generate the maximum possible moment at the girder-to-bent cap connection interface.

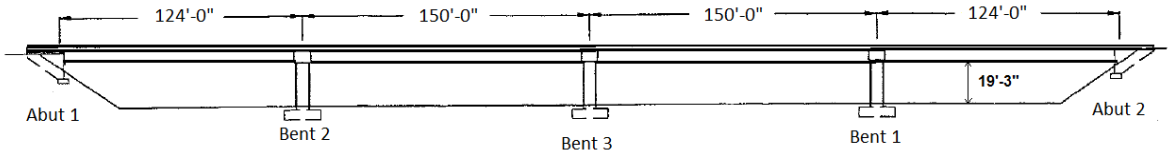

Figure 3-1 *Prototype Bridge for Third Test Unit*

3.1.1 Column design

Snyder et al. conducted a research to quantify the behavior of the precast I-girder to inverted-T bent cap connection under seismic conditions in the system level (Snyder et al., 2011). In this system test, a circular column was designed with plastic hinges located at the ends of the column with a corresponding column overstrength moment of 17,622 k-ft (Thiemann, 2010). The overstrength moment developed in the column plastic hinges of the prototype bridge used for the second set of connection tests was found to be 42,565 k-ft by scaling the column of the system test. It should be noted that the column height was not necessary to scale in order to keep the constant clearance height of 19 ft 3 in.. A specific column detail was not necessary for this study since an overdesigned column would be used for the test unit.

3.1.2 Girder and deck design

The CA-BT85 girders listed in Caltrans Bridge Design Aids were selected in order to reach the longest possible span length of 150 ft. A set of reference drawings from a proposed widening project of interstate I-215/I10 in California provided by Caltrans detailed the girder reinforcements for CA-BT73 girders. Combine with reinforcement details provided by the first two sets of connection tests and the reference drawings, the

reinforcements were detailed for the CA-BT85 girders. A typical reinforcing concrete deck with a thickness of 8 in. was used for the prototype bridge used in this study according to current Caltrans design standards.

3.1.3 Bent cap design

The prototype bridge for this study was designed with the cast-in-place, rectangular bent caps and the girders without dapped ends. The rectangular bent caps eliminated the ledges, or corbels, provided by the inverted-tee bent cap, while the tests for the ESBF and ESSP connections showed that the rectangular bent cap with the appropriate connection details was able to develop the adequate shear resistance. A set of reference drawings provided by Caltrans were used to determine the bent cap reinforcement details for the prototype bridge. By scaling the bent cap shown in the reference drawings, the dimensions of the bent cap were determined. The depth of the bent cap was 7 ft 0-5/8 in. to correspond with the CA-BT85 girders, and length was set to 34 ft 5 in. to accommodate five girders with 8 ft center-to-center spacing. The ends of the bulb-tee girders were embedded into the pier diaphragm with a length of 1 ft 10-1/2 in..

3.1.4 Girder-to-bent cap connection design

The design of the precast bulb-tee girder to cast-in-place bent cap connections was completed based on the combination of current field practices and research results. Each connection, which would be subject to both positive and negative moments equivalent to the summation of gravity load, column overstrength moment, and 0.5g vertical acceleration effect, needed to be accordingly designed. The magnitudes of the positive and negative design moments were normally calculated based on the distribution of moment generated at the girder ends. In the report by Snyder et al., the percentages of the column overstrength

moment were used with 45% corresponding to the positive moment and 55% to the negative moment (Snyder et al., 2011). It was found afterwards that these percentages, however, would be changed to 30% for positive moment and 70% for negative moment if the vertical acceleration was considered. The shift in percentage of moment can be attributed to the vertical acceleration in the positive moment direction being counteracted by the moment generated from the gravity of the superstructure. However, it is important to note that the column overstrength design moment increases if vertical acceleration is considered. *Equation (3-1)* and *Equation (3-2)* were used to calculate the positive and negative design moments at the girder-to-bent cap connection of the prototype bridge.

$$M_{pos} = pos\% \times M_o \tag{3-1}$$

$$M_{neg} = neg\% \times M_o \tag{3-2}$$

where:

M_{pos} = positive design moment,

M_{neg} = negative design moment,

M_o = column overstrength moment,

$pos\%$ = percentage of overstrength moment applied in positive direction, and

$neg\%$ = percentage of overstrength moment applied in negative direction.

Therefore, the positive and negative design moments at the girder-to-bent cap connection were:

$$M_{pos} = 0.3 \times 42565 = 12770\ k-ft$$

$$M_{neg} = 0.7 \times 42565 = 29796\ k-ft$$

In order to determine the negative moment subjected by a single girder, the total negative design moment was multiplied by a distribution factor of 0.24 based on the results from previous research regarding the topic of load distribution (Vender Werff and Sritharan, 2015), which resulted in a single girder negative design moment of 7150 k-ft An equivalent stress block approach was then used to calculate the appropriate deck reinforcement over the connection region, which provided the tension resistance for the negative moment demands. The deck and girder act as a composite section and therefore are assumed to be similar to a T-beam. *Equation (3-3)* and *Equation (3-4)* were used in order to determine the area of deck reinforcing steel and the compression block depth.

$$M_{neg} = A_s f_y (d - \frac{a}{2}) \tag{3-3}$$

$$A_s f_y = 0.85 f'_c a b_f \tag{3-4}$$

where:

M_{neg}= negative design moment,

A_s = area of steel,

f_y = yield strength of steel,

d = depth from center of deck steel to bottom of girder,

a = depth of compressive block,

f'_c= compressive strength of concrete, and

b_f = width of lower flange.

Solving *Equation (3-3)* and *Equation (3-4)* resulted in a deck reinforcing steel area of 15.56 in.^{2} per girder and an equivalent compression block depth of 10.24 in..

Both the unstressed strands extended from the girder ends and the dowel bars grouted through the web of girder were implemented in the connection region to resist the applied positive moments. The positive moment demand for the single girder was calculated by multiplying the aforementioned positive design moment (M_{pos}) by the distribution factor of 0.24 and was found to be 3065 k-ft Test results from the second set of connection tests showed that the dowel bars provided a significant positive moment resistance and therefore would reduce the required number of extended strands. By examining the data from the previous connection tests, it was determined that the dowel bars would provide the positive moment resistance of approximately 1280 k-ft per girder within the prototype bridge. *Equation (3-5)* and *Equation (3-6)* were then formulated using an equivalent stress block approach with the assumptions that the girder and deck would act as a composite section and the compressive area of the section would be limited to the deck.

$$N_s = \frac{M_{pos} - M_{DA}}{f_{sy} A_{strand} (d_s - {}^{a}/_{2})} \tag{3-5}$$

$$a = \frac{A_{strand} f_{sy} N_s}{0.85 f'_c b_d} \tag{3-6}$$

where:

N_s = number of strands,

M_{DA} = dowel action moment resistance,

f_{sy} = yield strength of strand,

A_{strand} = area of single prestressing strand,

d_s = depth from top of deck to centroid of strands,

a = depth of compression block, and

b_d = effective width of bridge deck for a single girder.

Solving *Equation (3-5)* and *Equation (3-6)* resulted in five 0.6 in. diameter strands need to be extended per girder with a compressive block depth of 0.71 in.. However, by examining the performance of the ESSP and ESBF connections, this design approach resulted in the overdesigned details. Therefore, in order to optimize the design for the moment demands resulting from gravity, horizontal seismic exactions, and vertical acceleration effective of 0.5g, the number of extended 0.6 in. diameter strands was reduced to four rather than five from the aforementioned preliminary calculation.

3.1.4.1 ESMS connection

The ESMS (Extended Strand with a Mechanical Splice) connection was designed to be an integral connection providing the negative and positive moment continuities between the precast bulb-tee girder and the bent cap. As shown in *Figure 3-2*, the deck reinforcing steel was provided over the girder-to-bent cap connection region. Unstressed strands were extended from the end of the precast girder and spliced with the strands extended from the opposite girder using mechanical splice chucks. The mechanical splice chucks were selected to fully develop the strength of strands and to reduce the congestion in the connection region due to its compact size.

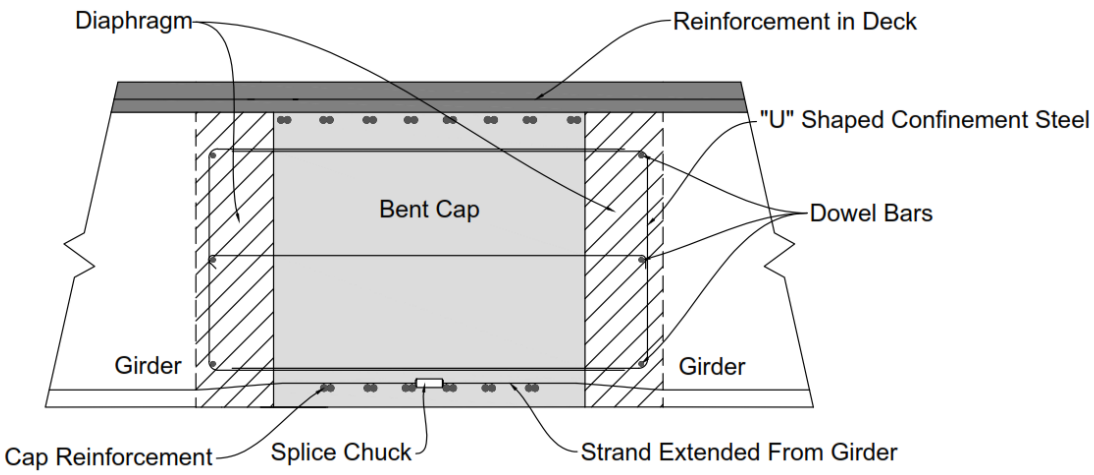

Figure 3-2 *ESMS Connection Schematic*

3.1.4.2 ESLS connection

Another precast bulb-tee girder-to-bent cap connection was the ESLS (Extend Strand with a Lap Splice) connection as shown in *Figure 3-3*. The ESLS connection was also designed to provide continuity such that the precast bulb-tee girder and cast-in-place bent cap can form an integral superstructure. The reinforcement in the deck was placed as that used in the ESMS connection to establish the negative moments continuity. Unstressed strands extended from the precast bulb-tee girder were anchored with the strand chucks consisting of bearing plates, barrel anchors, and wedges. The extended girder strands with strand chucks were then lap spliced with the strands extended from the opposite girder with a minimum lap length of 20 in. as per the suggestion for Caltrans Project Advisory Panel. The expected force transfer mechanism between the extended girder strands is shown in *Figure 3-4*. The tension acted on the strand is resisted by the anchor of the bearing plate and the bonding stress along the strand. Within this expected model, the tension from the strand would be transferred to the strand extended from opposite girder by struts along the lap splice length.

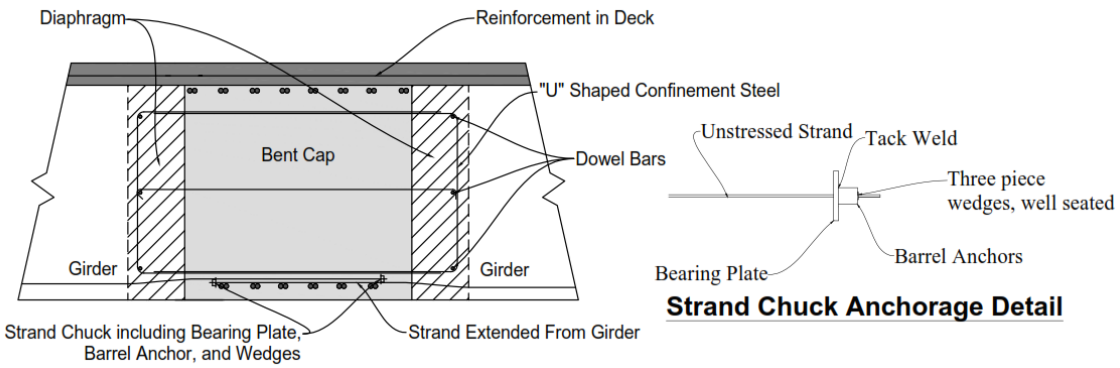

Figure 3-3 *ESLS Connection Schematic*

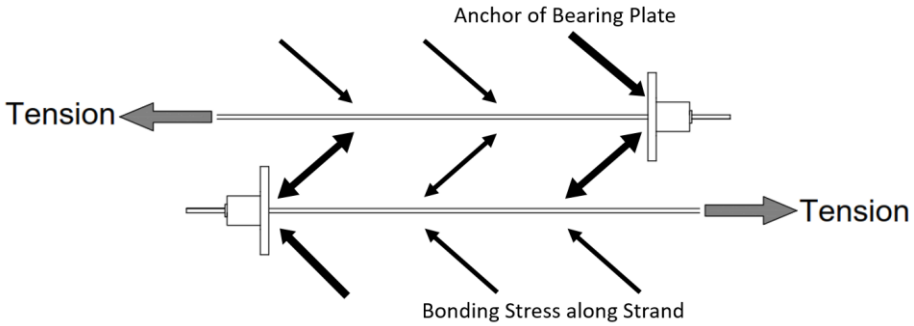

Figure 3-4 *Expected Anchorage Mechanism for Strands in the ESLS Connection*

3.2 Test Unit Design

The test unit was designed to investigate the seismic performance of the ESMS and ESLS connections. Based on the prototype bridge presented in the previous section, a 40% scale test unit was designed. The test unit represented the region of the prototype bridge where the girder-to-bent cap connection moment would be highest during the seismic activities. This region was determined to be located at Bent 3 as indicated in *Figure 3-5*.

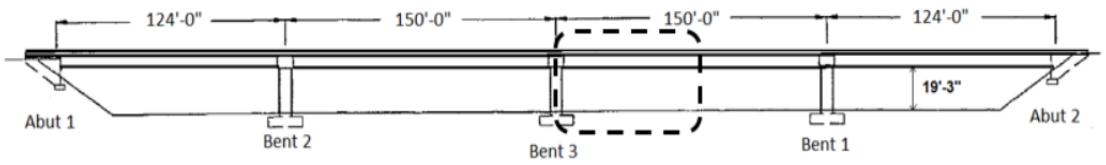

Figure 3-5 *Region of Highest Moment during Seismic Activities*

The girders were placed on only one side of the bent cap to simplify the experimental test, because the simultaneous test resulted in the issue of moment distribution if the girders were placed on both sides of the bent cap. The test unit was designed with two girders with an individual deck in order to test the ESMS and ESLS connections respectively. The factors shown in *Table 3-1* were used to design the test unit by appropriately scaling the prototype bridge. Details regarding the design of the girders, the bent cap, the girder-to-bent cap connections, and the column with a footing are discussed in the following sections.

Table 3-1 *Test Unit Scale Factor*

Parameter	Scale Factor
Length	0.4
Area	0.16
Stress	1
Force	0.16
Moment	0.064
Uniform Load	0.4
Displacement	0.4

3.2.1 Girder design

The precast bulb-tee girders for the test unit were firstly designed by scaling the girders of the prototype bridge. The scale factors listed in *Table 3-1* were used and resulted in the girder section shown in *Figure 3-6*. Only half of the 150 ft prototype span was scaled for the test unit since, due to symmetry, the moment behavior of the girder-to-bent cap connection could be represented without considering the entire span length. Scaling half the 150 ft span resulted in a 30 ft girder for the test unit. Furthermore, the prestressing force

from the prototype girder was scaled for the test unit as well. It should be noted that the scaled prestressing force within the bottom flange of the girder was reduced by approximately 23% in order to prevent cracking at transfer stage. The final design of the girders resulted in 10 3/8 in. diameter strands within the bottom flange. Moreover, scaling of the girder reinforcement resulted in the use of wire mesh since standard rebar sizes were too large. In addition, 1 in. diameter holes were placed at one end of each girder to allow for the insertion of dowel bars. Detailed design drawings are provided in Appendix A.

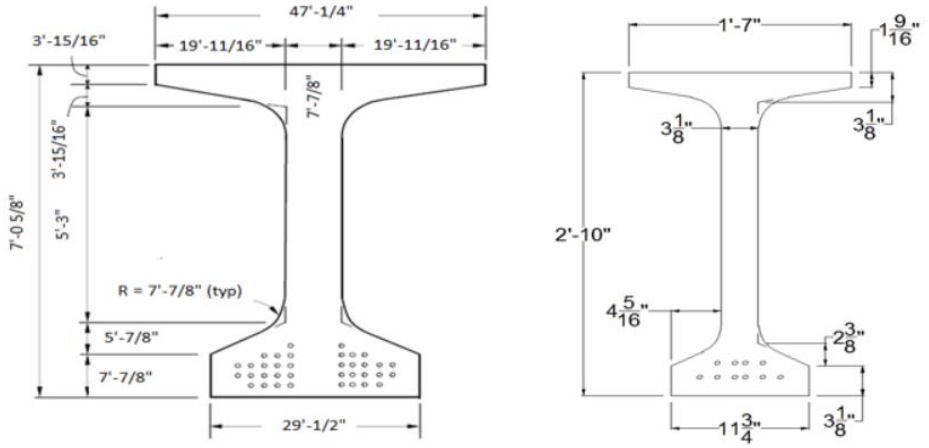

Figure 3-6 *Cross-section of Prototype Girder (left) and Test Unit Girder*

3.2.2 Bent cap design

The bent cap for the test unit was designed to accommodate two girders which were attached 4 ft on either side of the column centerline to allow the construction of each girder with its own deck. The bent cap had a design width of 54 in., height of 34 in., and length of 12 ft 4 in., which are the same dimensions as the bent cap used in the second set of connection tests.

The bent cap used in the second set of connection tests showed an adequate capacity to prevent permanent deformation during the entire test. Therefore, the bent cap used for

this study was reinforced as the same as the cap for the second set of connection tests. The bent cap also need to be detailed to remain relatively rigid under the torsion, which is roughly equivalent to the moment at the connections since the girders only attached to one side of the bent cap. The longitudinal post-tensioning force was applied by six post-tensioning bars to increase the torsional resistance of the bent cap.

3.2.3 Connection design

Both the ESMS and ESLS connections were designed by scaling the prototype bridge. The required deck reinforcing steel was determined in the same manner as the prototype bridge. Eventually the area of the deck reinforcement was calculated to be 5.26 $in.^2$, which was distributed across the width of the deck. The connection details for the positive moment resistance also scaled from the prototype bridge using 3/8 in. diameter strands, which required four girder strands extended from the precast girder. The "U" shaped confinement steel was added to fit alongside the girder web and between the top and bottom girder flanges as shown in *Figure 3-7*, which was respected to confine the diaphragm concrete surrounding the dowel bars and prevent spalling on the front face of the pier diaphragm. In addition, BASF M100 micro fiber added at 0.5 lbs. per cubic yard and BASF MAC MATRIX macro fibers added at 3.0 lbs. per cubic yard were added to the concrete mix design for the bent cap, diaphragm, and deck in order to help prevent cracking and spalling at the deck and the girder-to-cap interface region. The connection details for the test unit were provided in Appendix A.

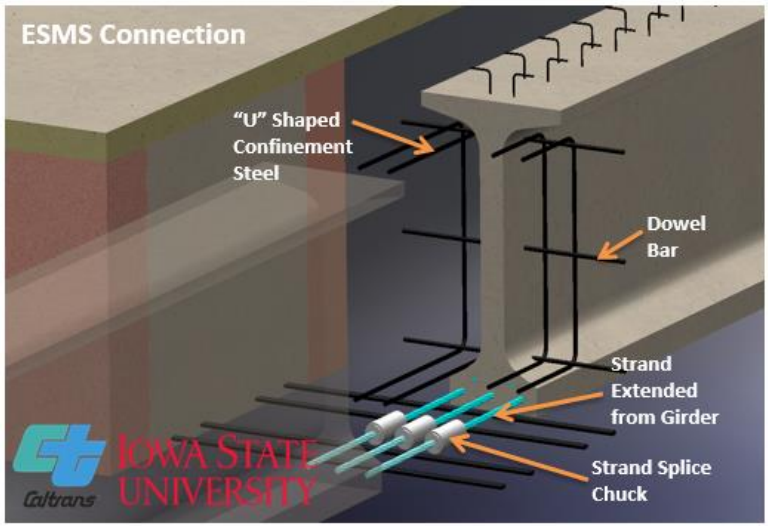

Figure 3-7 *Addition of "U"-shaped confinement steel*

3.2.4 Column and footing design

The column and footing used for the second set of connection tests were reused for the test unit with the ESMS and ESLS connections. The column was designed to remain essentially elastic throughout the test, and the footing was then designed to resist the overstrength moment of the column. In order to secure the bent cap with the column, the post-tensioning ducts were inserted in the column and footing for the placement of 2 in. diameter post-tensioning bars with the yield stress of 150 ksi. As shown in *Figure 3-8*, the post-tensioning bars would be anchored in a pocket underneath the footing, run through the column, and be extended through the top of ducts. The bars would be post-tensioned to secure the bent cap to the column and also increase column moment resistance by applying an axil force. A 3 ft by 3 ft square column with the height of 3 ft was designed, and the footing was designed as an 8 ft × 8 ft × 2 ft square.

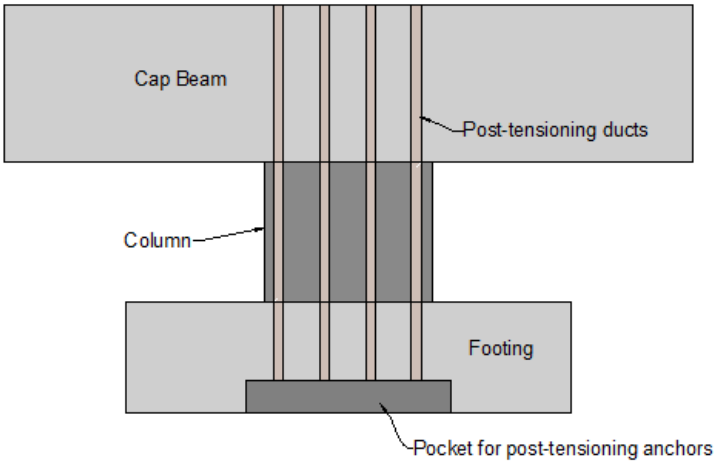

Figure 3-8 *Post-tensioning Bars Schematic*

CHAPTER 4 EXPERIMENTAL WORK

4.1 Test Unit Construction

4.1.1 Construction sequence

The construction of the test unit took place in the Iowa State University structural laboratory. The footing and column were reused from the test unit constructed for the second set of connection tests. The falsework was initially placed surrounding the column to support the bent cap throughout the construction process. Two bulb-tee girders precast at Cretex Concrete Products in Iowa Falls, IA were then placed on the bent cap falsework and temporary support throughout the construction of the test unit as shown in *Figure 4-1*.

Figure 4-1 *Place the Girder on Temporary Falsework*

The precast girders arrived at ISU laboratory with six of the ten girder strands extending 8 ft from each girder. Since only four strands were required to be embedded into the bent cap, the strands in the upper row were cut. Before the fabrication of the bent cap, the dowel bars were inserted through the holes blocked out transversely through the web of the girders, and grouted in place as shown in *Figure 4-2*. The reinforcement cage for the bent cap and the pier diaphragm were tied on the falsework, and the extended girder strands

were spliced according to each connection details. The mechanical splice chucks were used in the ESMS connection to splice the strands extended from the precast girder with the strands added on the back of the bent cap as shown in *Figure 4-3*. The strands located at the back of the bent cap with the external anchorage were added in order to simulate the strands extended from an opposite girder. For the ESLS connection, the strands with strand chucks were also lap spliced with strands at the back side of the bent cap as shown in *Figure 4-3*. The post-tensioning ducts were inserted longitudinally though the bent cap for the cap post-tensioning. At the same time with the fabrication of the bent cap, the deck reinforcing steel was placed over the girder on the formwork constructed by bridge hangars, brackets, and plywood as shown in *Figure 4-4*. The formwork for bent cap was fabricated and set into place. The bent cap and deck concrete with BASF M100 micro fiber added at 0.5 lbs. per cubic yard and BASF MAC MATRIX macro fibers added at 3.0 lbs. per cubic yard was then placed in one continuous pour and allowed to cure. The finished test unit is showed in *Figure 4-5*.

Figure 4-2 *Dowel Bars Inserted through the Web of Girder*

Figure 4-3 *Extended Girder Strands in the ESMS and ESLS Connections*

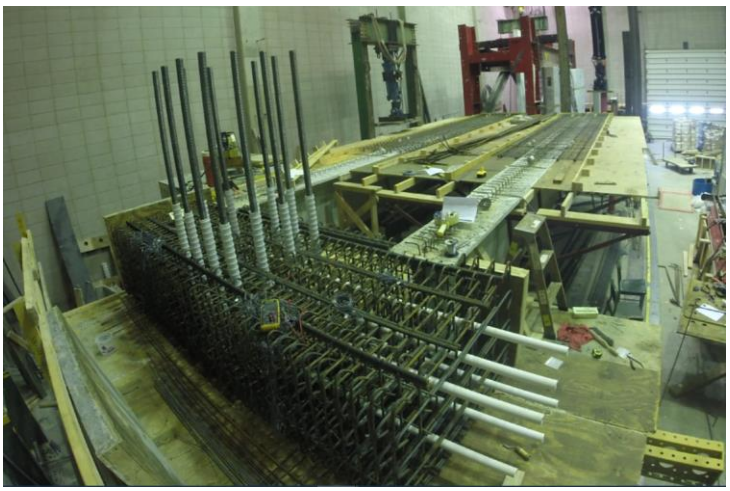

Figure 4-4 *Reinforcement Cage for Bent Cap and Deck Reinforcing Steel*

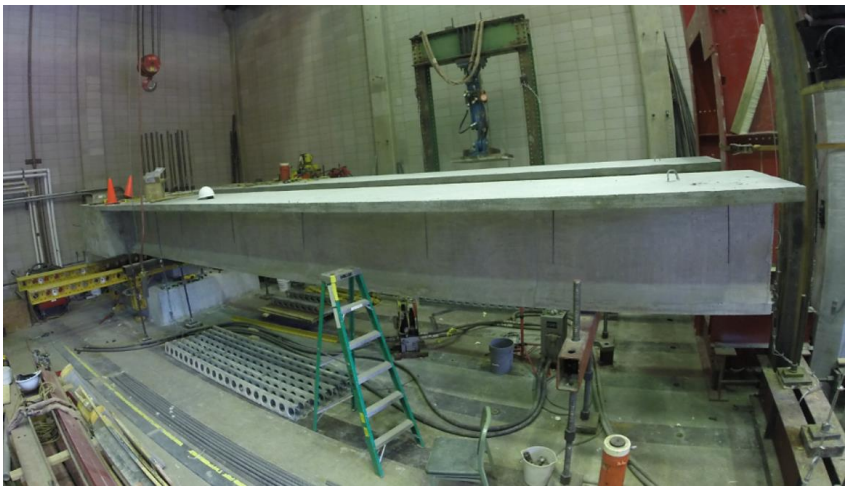

Figure 4-5 *Test Unit with the ESMS and ESLS Connections*

4.1.2 Construction challenges

4.1.2.1 Unraveling **of** unstressed strand

For the precast bulb-tee girder, concrete was poured around the prestressed strands. The strands were cut loose from the bulkheads of the stressing bed, and the prestressing force was transferred to the concrete when the concrete was harden. The unraveling of the unstressed strand was caused by a sudden release of prestressing force as shown in *Figure 4-6*. The strain gauges were mounted within the unraveling regions of the strands to capture the behavior when the strands were stressed. The effect of unraveling is discussed in the following chapter.

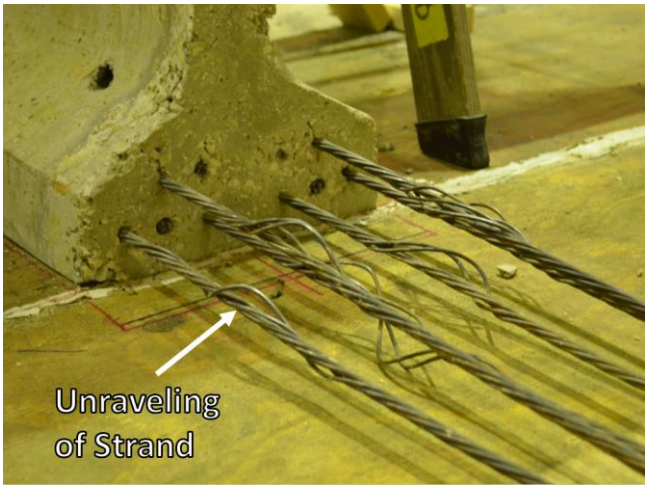

Figure 4-6 *Unraveling of Unstressed Strand*

4.1.2.2 Pour of the bent cap

Before the pouring of the bent cap and deck, a trial batch of concrete with BASF M100 micro fiber added at 0.5 lbs. per cubic yard and BASF MAC MATRIX macro fibers added at 3.0 lbs. per cubic yard was mixed to determine the effect of fiber on the flowability of concrete. This trial batch showed that the additional micro and macro synthetic fibers significantly reduced the slump of concrete, which induced the issue for the consolidation

of concrete. In addition, the heavy reinforced bent cap made the pouring work more challenging. In order to avoid the honeycombs within the bent cap, aggregate chips were used in the mix design. Plasticizer and retarding admixtures were also used to improve the flowability of the concrete. Subsequent tests for compressive strength of cylindrical concrete specimens demonstrated that the concrete used in the test unit satisfied the design requirements.

4.2 Instrumentation

In order to capture the response of the test unit, a significant number of both internal and external sensors was used on the critical regions of the specimen. Uniaxial steel strain gauges were the primary internal sensors, and their locations are illustrated in the following sections. The external instrumentations consisted of string potentiometer (string pot), linear variable differential transformer (LVDT) and Optotrak Certus® motion capture system (Optotrak). The following sections presents the instrumentation plan including both internal and external instrumentation. Note that the red "×" in the figures indicated the location of strain gauge herein.

4.2.1 Internal instrumentation

4.2.1.1 Bent cap

Both top and bottom longitudinal reinforcing bars of the bent cap were instrumented with a total of twelve strain gauges. The instrumented reinforcing bars were located at 6.5 in. from the center line of the bent cap as shown in *Figure 4-7*. The strain gauges were lined up with the center of bent cap and the center lines of girders as detailed in *Figure 4-7*. Note that the strain gauges were labeled using the following format: BCT(B)# (**B**ent **C**ap strain gauge at **T**op/**B**ottom longitudinal reinforcing bars in Location

#). For example, BCTB2 corresponds to bent cap strain gauge at bottom longitudinal reinforcing bar at location 2 noted in *Figure 4-7 (b)*.

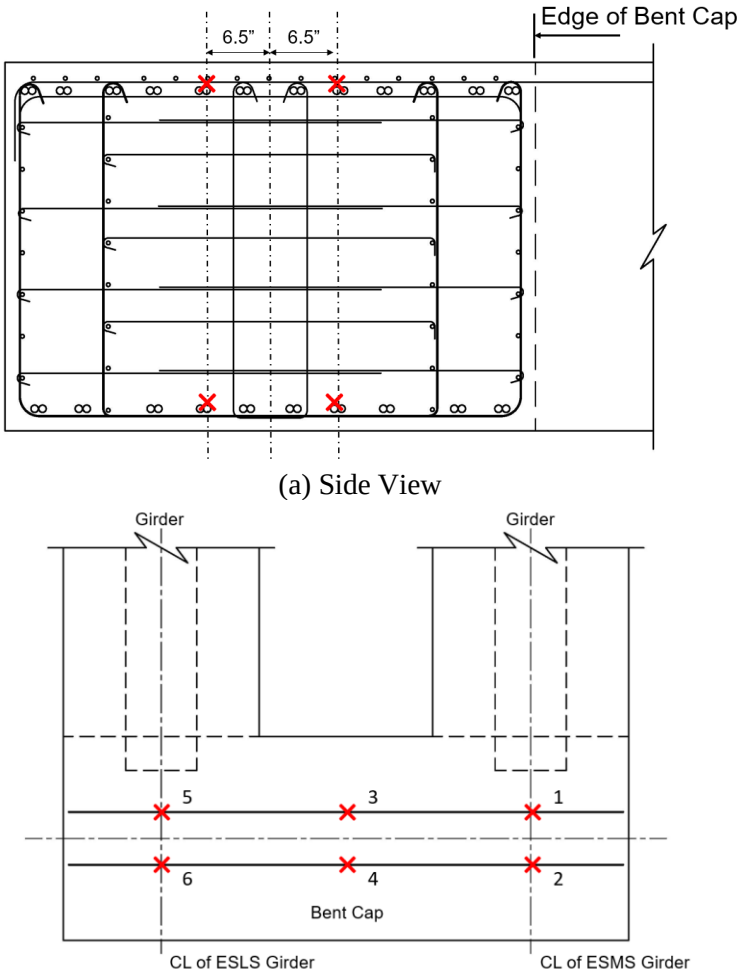

Figure 4-7 *Strain Gauge Location for the Bent Cap Longitudinal Reinforcing Bars*

In addition, both the inner stirrups behind the girder and the outer stirrups next to the girder were instrumented with a total of eight strain gauges in each connection. In the configuration shown as *Figure 4-8*, three inner stirrups were instrumented with six strain gauges, which were located 11.5 in. and 25.5 in. from the base of the bent cap. Moreover, a total of two strain gauges were mounted on the outer stirrups at locations of 17 in. from the base of cap. Note that, for the inner stirrups, the strain gauges were labeled as

CS#I(C/O)T(B) (**C**ap **S**tirrup strain gauge for connection **1/2** on **O**utside/**C**entral/**I**nside stirrup at **T**op/**B**ottom), whereas the strain gauges for the outer stirrups were labeled as CS#OO(I) (**C**ap **S**tirrup strain gauge for connection **1/2** on **O**uter stirrup at **O**utside/**I**nside location). In addition, the ESMS connection was referred as Connection 1 and the ESLS connection was referred as Connection 2, herein. For example, CS2OI corresponded to the cap stirrup strain gauge for the ESLS connection on outer stirrups at the inside location.

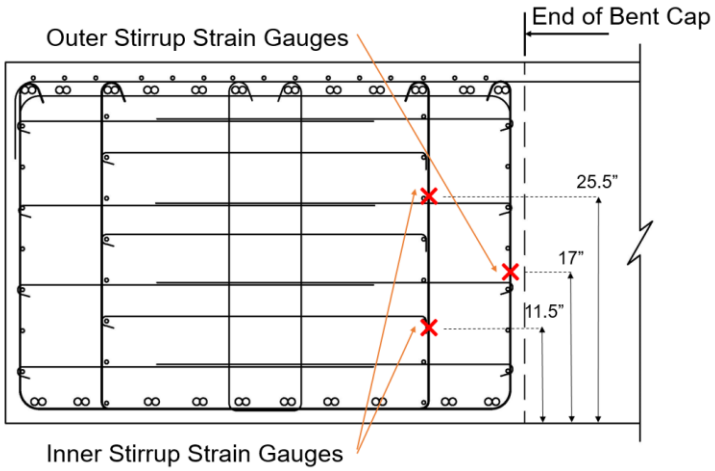

(a) Side View

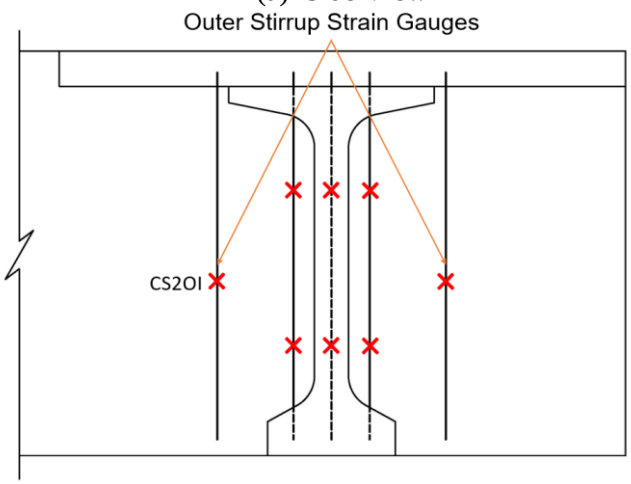

(b) Front View

Figure 4-8 *Strain Gauge Location for Cap Stirrups*

4.2.1.2 Precast Bulb-Tee girder

One of ten prestressing strands at the bottom of each precast girder was gaged as identified in *Figure 4-9*. A total of four strain gauges were placed 12 in., 24 in., 48 in., and 15 ft from the end of girder. It should be noted that the strain gauges were installed after the prestressing strands had been tensioned. Consequently, the recorded initial strain readings did not include the initial pre-strain and subsequent pre-strain losses.

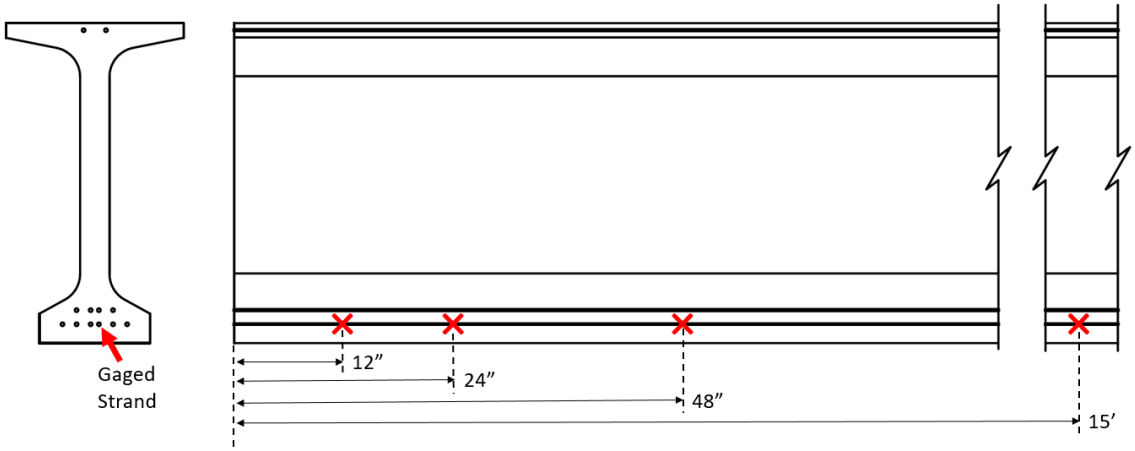

Figure 4-9 *Location of Strain Gauges in a Prestressed Strand of Each Bulb-tee Girder*

4.2.1.3 Precast Bulb-Tee girder-to-bent cap connection

The precast bulb-tee girder-to-bent cap connection was the most critical regions of specimens, which was instrumented extensively with thirty-four strain gauges. These gauges were placed on the dowel bars, the "U" shaped confinement steel (dowel confinement), and the strands extended from the girder. Furthermore, the deck reinforcement over the connection region was also instrumented. The following subsections present all of these gauge locations in detail.

4.2.1.3.1 Dowel bars

A total of three #4 reinforcing bars with lengths of 2.5 ft were used as the dowel bars within the test unit. As shown in *Figure 4-10*, only one strain gauge was placed on the top dowel bar, and located 1 in. from the inside face of the precast girder. The middle dowel bar was instrumented with two strain gauges on both sides of the precast girder. As the most critical dowel bar, the bottom dowel bar was instrumented with a total of four strain gauges, which were placed 1 in. from both the inside and outside face of girder, and 6.25 in. from the inside face. Note that the strain gauges were installed on both the front and the back of bottom dowel bar at inside as shown in *Figure 4-10 (b)*. Similarly, the strain gauges on the dowel bars were labeled in a logical format. DB#T(M)I(O) were used to label the strain gauges on the top and middle dowel bars (**D**owel **B**ar strain gauge for connection **1/2** on **T**op/**M**iddle dowel bar at **I**nside/**O**utside location), and the strain gauges on the bottom dowel bar were labeled as *Figure 4-10*. For example, DB1MO represented the dowel bar strain gage for the ESMS connection on middle dowel bar at outside location.

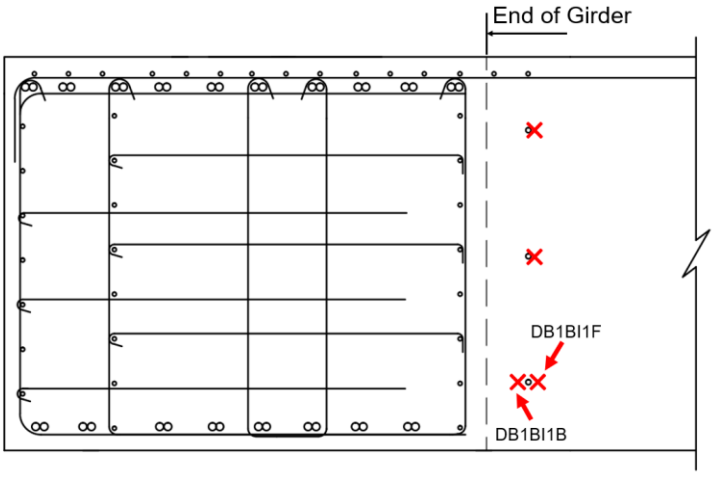

(a) Side View

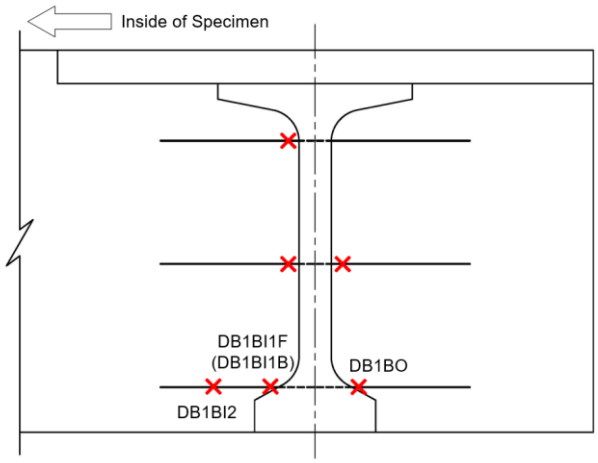

(b) Front View

Figure 4-10 *Location of Strain Gauge Mounted to the Dowel Bars*

4.2.1.3.2 "U" shaped confinement steel

As previous noted, the "U" shaped confinement steel (dowel confinement) was placed on both sides of the precast girder to reinforce the concrete where the dowel bars embedded. In order to evaluate the performance of the dowel confinement, eight strain gauges were installed as the configuration shown in *Figure 4-11*. Two dowel confinements located at the inside of the specimen was monitored. For each of them, the strain gauges were placed on the horizontal legs of the U-shaped confinement. Additionally, the midpoint between the bottom and middle dowel bars was instrumented with a strain gauge. Note that the labels of strain gauges were named as DC#I(O)T(M/B/S) (**D**owel **C**onfinement strain gauge for connection **1/2** on **I**nner/**O**uter confinement at the **T**op/**M**iddle/**B**ottom/**S**ide). Accordingly, DC2OS corresponded to the dowel confinement strain gage for the ESLS connection on the outer confinement at the side location.

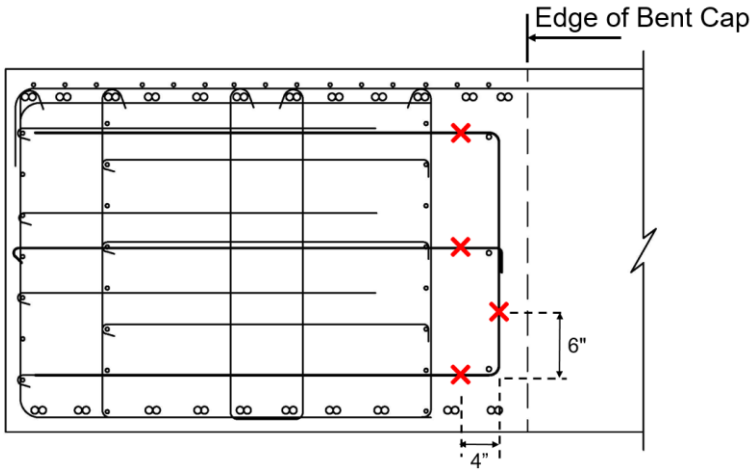

(a) Side View

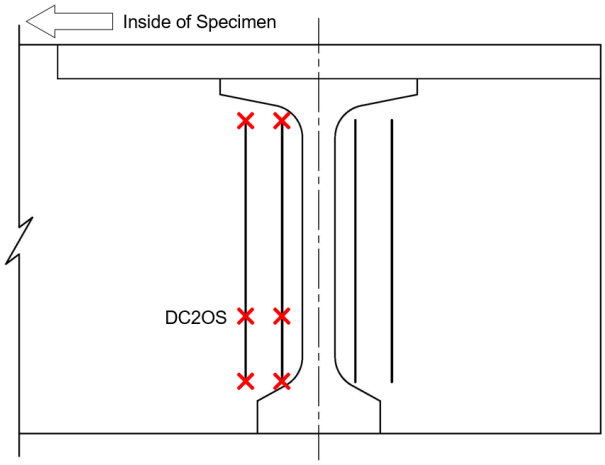

(b) Front View

Figure 4-11 *Location of Strain Gages on the Dowel Confinement Reinforcing Bars*

4.2.1.3.3 Strands extended from girder

The strands extended from the girder were spliced with strands on the other side of the bent cap by the splice chucks in the ESMS connection. For the ESLS connection, the strands were anchored with bearing plates, barrel anchors, and wedges. Several strands extended from the girder and were instrumented extensively with strain gauges shown in *Figure 4-12* and *Figure 4-13* for the ESMS connection and the ESLS connection, respectively.

Two of four strands extended from the girder were instrumented in the ESMS connection, and the strain gauges were placed 2 in. from the girder-to-cap interface and 1 in. from the ends of the splice chuck. Two additional strain gauges were placed at the midpoint between the girder-to-cap interface and the splice chuck. Moreover, in order to verify the continuity developed by the spliced strands, two strain gauges were installed on the spliced strands at 9.25 in. and 19.25 in. from the end of splice chuck. The unraveled region was instrumented with an additional strain gage to investigate the effect of unraveling on the strand behavior as shown in *Figure 4-14*.

Similarly, two of four strands extended from the girder were gauged in the ESLS connection. Besides the strain gauges located at 2 in. from the girder cap interface, a total of eight strain gauges were placed near the ends of the lap spliced region. Note that the strain gauges were labeled as GS#I(O)# (**G**irder **S**trand strain gauge for connection **1/2** on **I**nside/**O**utside strand located **#** in. from the girder-to-cap interface), or GS#I(O)S# (**G**irder **S**trand strain gauge for connection **1/2** on **I**nside/**O**utside **S**plicing strand located **#** in. from the anchorage). For example, GS2O2 corresponded to the girder strand strain gage for the ESLS connection on outside strand located 2 in. from the girder-to-cap interface.

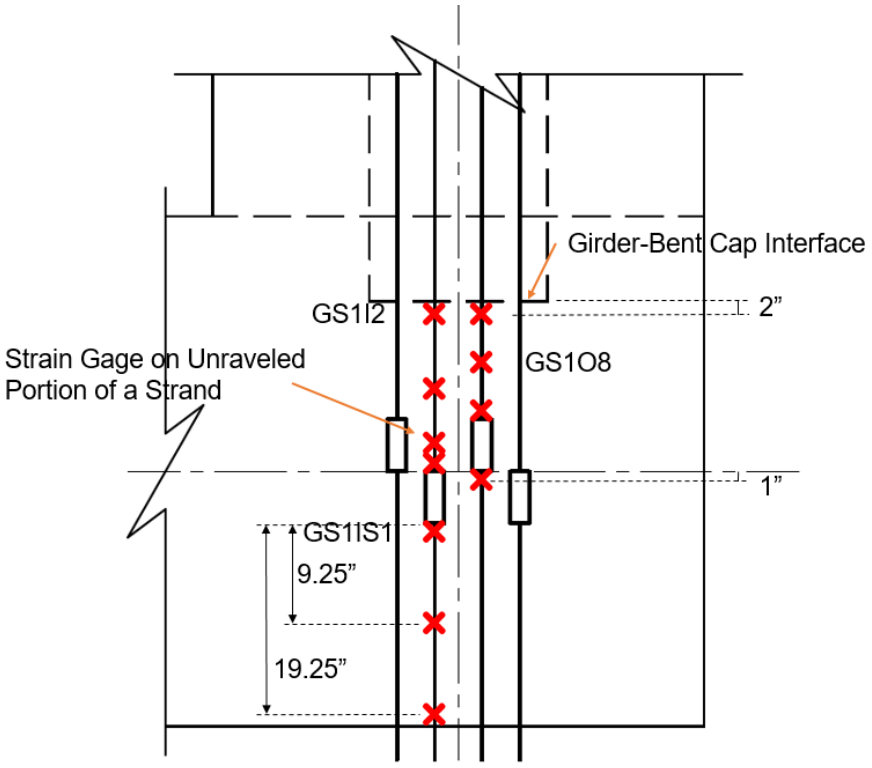

Figure 4-12 *Location of Strain Gauges on the Extended Strands in the ESMS Connection*

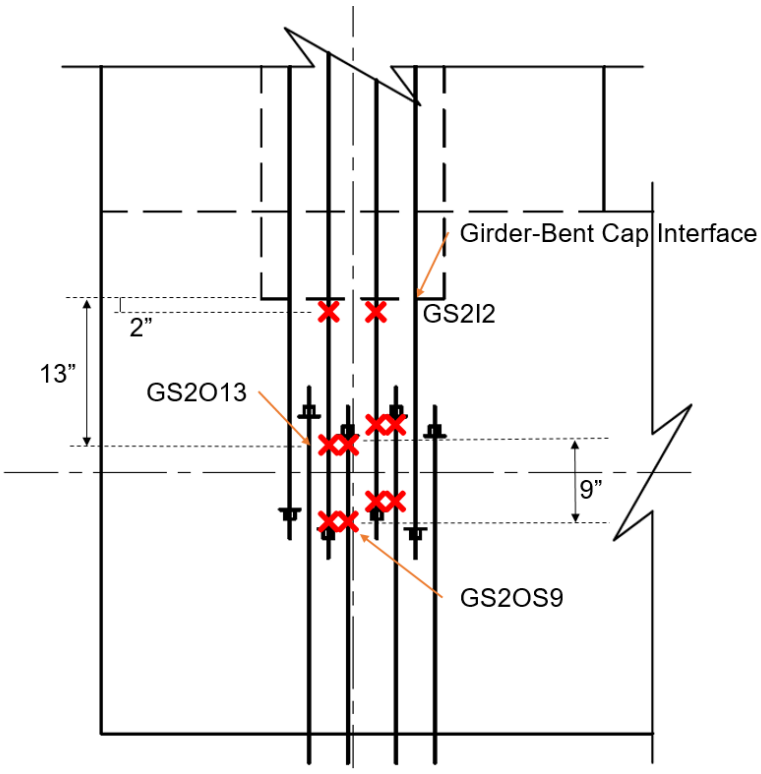

Figure 4-13 *Location of Strain Gauges on the Strands in the ESLS connection*

Figure 4-14 *Placement of Strain Gauge on Unraveled Portion of a Strand in the ESMS Connection*

4.2.1.3.4 Deck reinforcement

Deck reinforcement provided the ability for the girder-to-bent cap connection to resist the negative moment. A total of nine strain gauges were placed as shown in *Figure 4-15*. The first set of strain gauges were lined up with the girder-to-cap interface, and other two set of strain gauges were placed 18 in. from the first set of gauges. The side strain gauges were installed on top of the longitudinal deck reinforcement at 17 in. in transverse direction from the girder center line. Note that the "center" gauges were placed 2 in. from the girder center line. Furthermore, the strain gauges were labeled as DR#I(M/O)G(I/C) (**D**eck **R**einforcement strain gauge for connection **1/2** on **I**nside(**M**iddle/**O**utsider) reinforcement at **G**irder side(**I**nterface/**Bent cap** side). For example, DR1OG identified the deck reinforcement strain gage for the ESMS connection on outside reinforcing bar at the girder side.

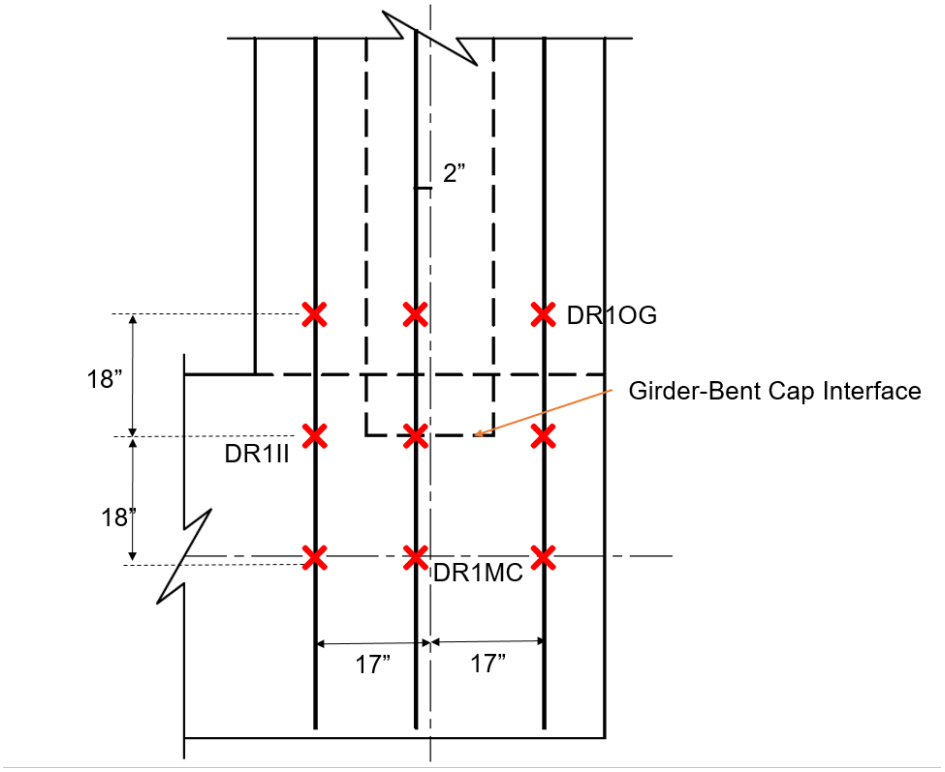

Figure 4-15 *Location of Strain Gauges on the Deck Reinforcement*

4.2.2 External instrumentation

4.2.2.1 Bent cap

A number of external sensors was mounted to monitor the displacement and rotation of the bent cap. As shown in *Figure 4-16*, a total of four string pots were mounted horizontally, and two vertical string pots were placed 32 in. from both ends of the bent cap. Moreover, a total of four LVDTs were mounted to instrument the relative displacement of the bent cap to the column.

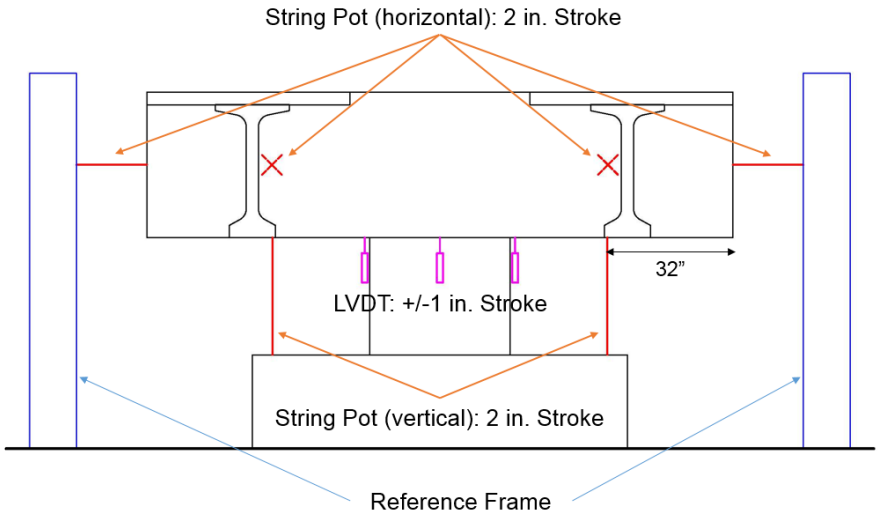

Figure 4-16 *Location of External Sensors for Bent cap*

4.2.2.2 Precast Bulb-Tee girder

The displacement of the girder was instrumented at the loading points with a total of four string pots. Two actuators were attached on the girder at 13.5 ft and 28.5 ft from the girder-to-cap interface. At each loading point, one horizontal and one vertical string pots were placed as shown in *Figure 4-17*.

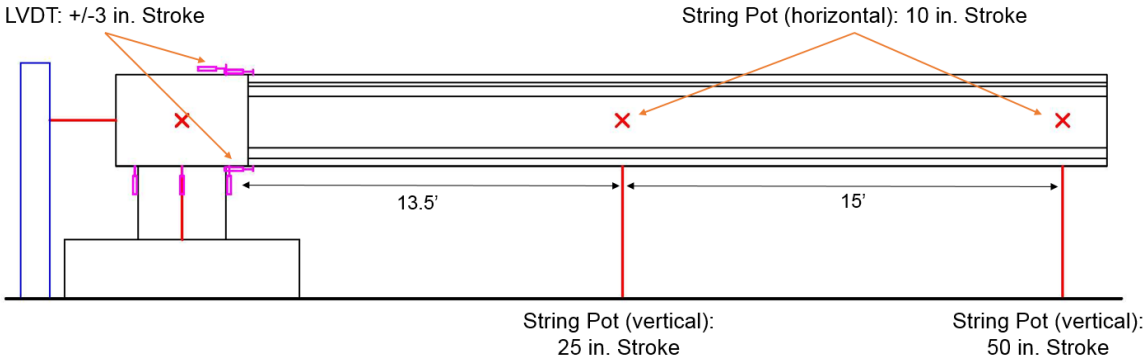

Figure 4-17 *Location of External Sensors for Precast Girder*

4.2.2.3 Precast Bulb-Tee girder-to-Bent Cap Connection

As the interest of this research, it is important to capture the response of the precast bulb-tee girder-to-bent cap connection. A number of external instrumentations were

mounted on the connection region. The following subsections present the location of all instrumentations consisting of the LVDT and Optotrak.

4.2.2.3.1 Linear variable differential transformer (LVDT)

It is important to instrument the opening between the precast girder and the bent cap. In addition, the deformation of the deck over the connection region was essential to investigate the performance of the precast bulb-tee girder-to-bent cap connection. Therefore, LVDTs were mounted on both the deck and girder-to-cap interface as shown in *Figure 4-18* and *Figure 4-19*. Note that the deck deformation was instrumented at the edge of the diaphragm and the girder-to-cap interface.

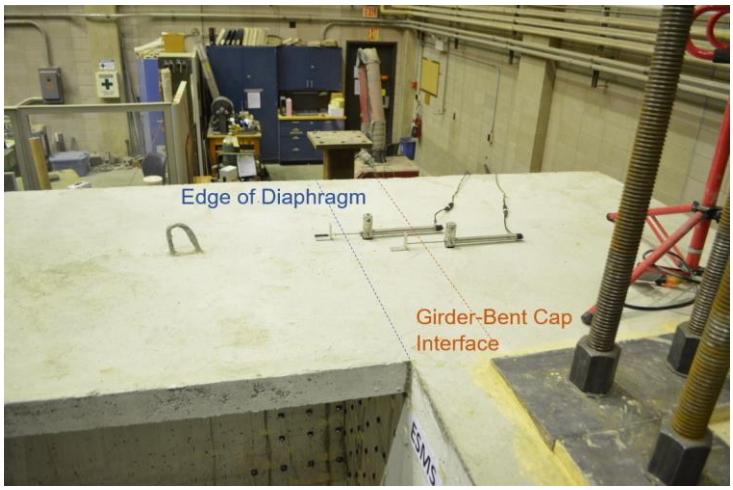

Figure 4-18 *Location of LVDTs on Deck*

Figure 4-19 *Location of LVDT on Girder-to-cap interface*

4.2.2.3.2 Optotrak Certus® motion capture (Optotrak) system

The Optotrak system provided a reliable and convenient motion capture solution with an accuracy of up to 0.04 in. (0.1 mm). With a space digitization camera, the location of each marker can be tracked and recorded. A total of 86 markers were mounted as the 4 in. by 4 in. grid on the connection region consisting of the diaphragm, precast girder, and deck. As the marker layout shown in *Figure 4-20*, the deformation of the connection region and the relative displacement between each of the components were captured by a number of markers.

Figure 4-20 *Optotrak System Marker Layout*

4.3 Load Protocol

In order to qualify the behavior and capacity of connections, both the ESMS and ESLS connection was individually tested by pushing and pulling the girder with a pair of actuators as shown in *Figure 4-21*. The actuator forces corresponding to target shear and moment values were determined by the load protocol. Prototype loads resulting from gravity, horizontal seismic load, and vertical acceleration effects were determined and then properly scaled for the test unit. Each type of load is discussed in the following sections.

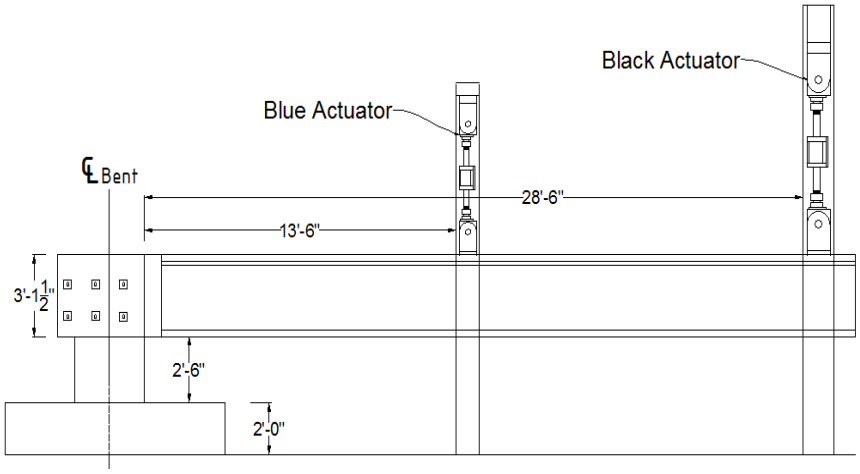

Figure 4-21 *Test Unit Setup*

4.3.1 Gravity load

The connection moment and shear resulting from gravity is dependent on the type of bent cap and the construction sequence. For the ESMS and ESLS connection, the cast-in-place bent cap is used and the precast girders are erected flush with the side face of the bent cap. The construction loading process is explained in order to establish the properly gravity loads at connection region.

For a cast-in-place bent cap, the columns and abutments are initially erected and then the falsework is placed at the location of the bent cap to support the girders throughout the construction process. Formwork is set for the bent cap, diaphragm, and deck. The bent cap and diaphragm can be poured prior to or simultaneously with the deck. The girders are simply supported by the falsework throughout the construction process until the bent cap and deck are poured. After hardening of the bent cap and deck concrete, the falsework and formwork are remove as shown in *Figure 4-22*. The moment will be induced at the girder-to-bent cap interface by the weight of the girder and deck, further wearing surface, and barriers rails. The weight of the superstructure components transfer to the column as a shear force at the connection. Therefore, the gravity moment at the connection interface results from the self-weight of girder, deck, further wearing surface, and barriers.

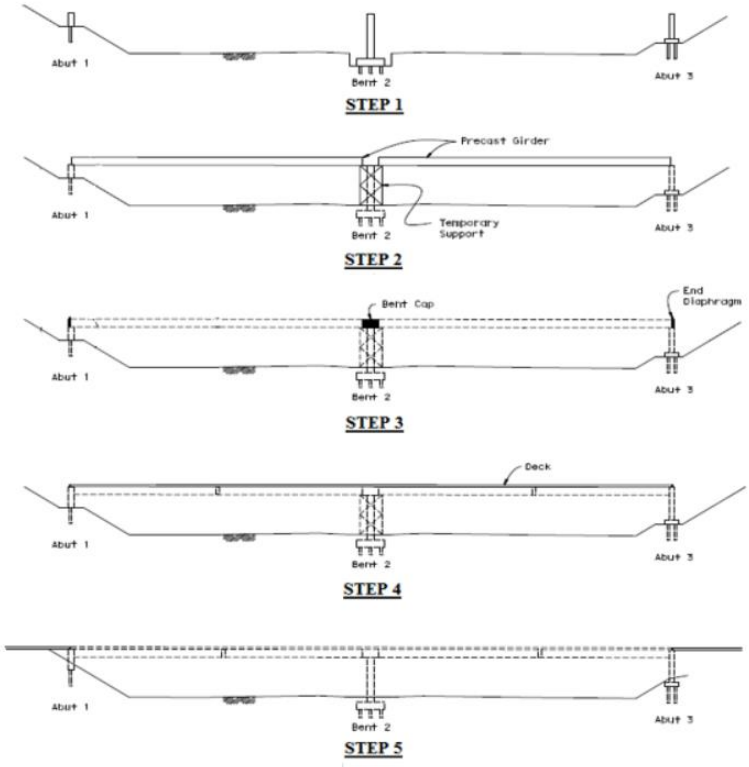

Figure 4-22 *Construction Sequence (Caltrans, 2011)*

4.3.2 Horizontal seismic load

The aforementioned system test was used to determine the moment and shear at connection caused by horizontal seismic exaction. It was assumed that plastic hinges would form at both the top and bottom of the column. Results of the system test gave the overstrength moment of the column. This moment was then scaled for the test unit by multiplying the appropriate scale factors. The resulting moment was multiplied by the factor of 0.45 for the positive direction and 0.55 for the negative direction in order to distribute the overstrength moment resulting from horizontal seismic exaction to girder-to-bent cap connections as shown in *Figure 4-23*.

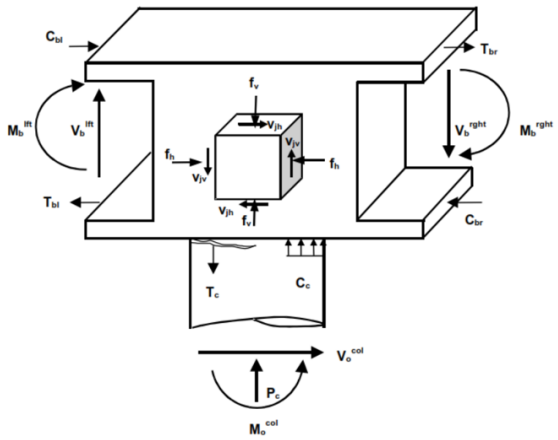

Figure 4-23 *Moment at Girder-to-Bent Cap Resulting from Horizontal Seismic Exaction*

4.3.3 Vertical acceleration effects

An equivalent static vertical uniform load was applied upward and downward to the superstructure to estimate the effects of vertical acceleration. The entire self-weight of the prototype girder and slab was multiplied by ±0.5, ±1.0, and ±1.5 respectively to determine the vertical acceleration effects. The resulting loads were then properly scaled and used to calculate moment and shear values at the connection interface of the test unit.

4.3.4 Load combination of the load protocol

Upon determining the moment and shear values resulting from gravity, horizontal seismic load, and vertical acceleration effects, a loading protocol was developed by combining each load. The tests were conducted to quantify the positive moment capacity of each connection. In order to establish the worst case in positive moment direction, only self-weights of the further wearing surface and barrier were used to produce the gravity moment and shear values for the loading protocol. This resulted in a constant load protocol with the first two sets of connection tests. A test unit moment diagram showing the difference in gravity moment for actual case and load protocol is plotted in *Figure 4-24* with the girder-to-bent cap connection occurring at 30 ft

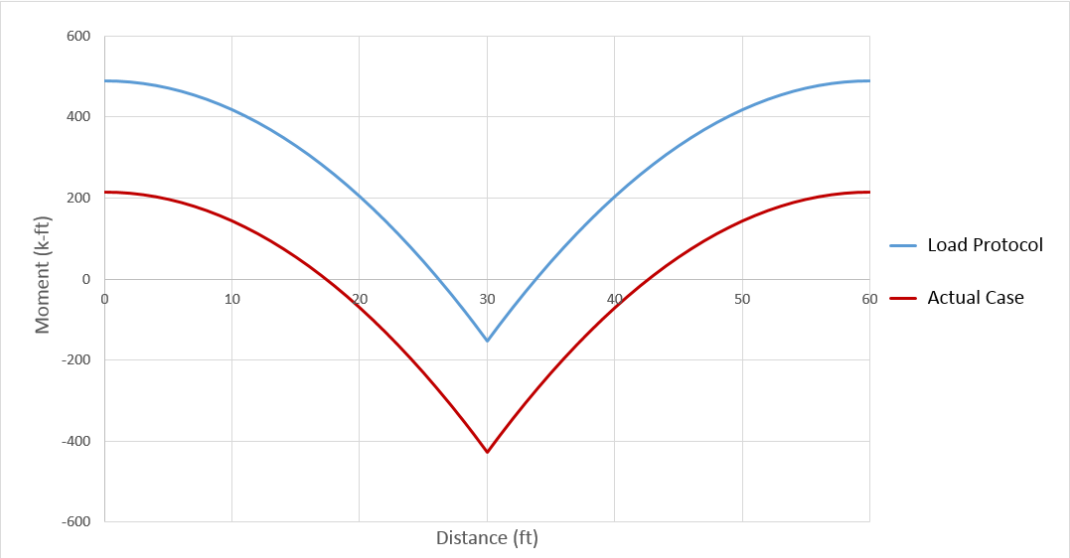

Figure 4-24 *Difference in Gravity Moment for Actual Case and Load Protocol*

The target moment and shear values were determined by cumulating the effects of each load. The target values, with the exception of the gravity load, each contained values for positive moment and shear as well as negative moment and shear to accurately simulate the reversal of forces that the prototype bridge would experience. The horizontal seismic exaction and vertical acceleration were assumed to produce the negative or positive loads simultaneously in order to establish the worst load case. It should be noted that the loads applied to the test unit only represent the scaled prototype loads at the connection interface to simplify the testing as shown in *Figure 4-25*.

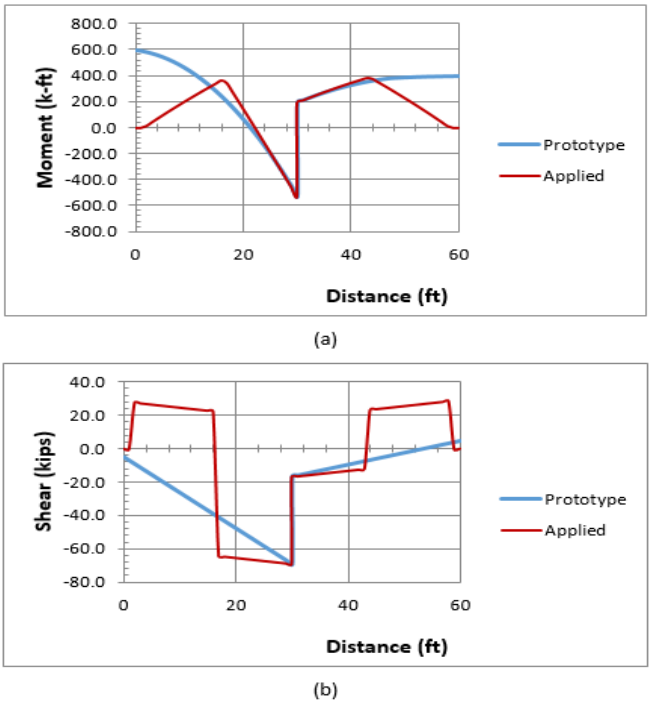

Figure 4-25 *(a) Moment and (b) Shear applied at Test Unit and Prototype Loads*

For the test unit, each girder was attached to two actuators and cantilevered from the bent cap. The actuators were labeled by color and located along the length of the girder. The blue actuator was located 13.5 ft from the connection interface while the black actuator was located 28.5 ft from the interface, and the connection interface was set at the end of the girder embedded in the diaphragm. A load protocol for actuators was established to match the shears and moments applied to the test unit with the scaled prototype loads. A series of load steps were exercised as the load was gradually increased. Each load step contained both a positive and negative moment and shear values which the girder was cycled three times. In order to fully quantify the performance of each connection, a displacement controlled load protocol was added when the connections exhibited inelastic behavior. Each connection would be exercised to failure. The load protocol including force controlled and displacement controlled sequences is shown in *Figure 4-26*, and fully load protocol for entire testing sequence is listed in Appendix B.

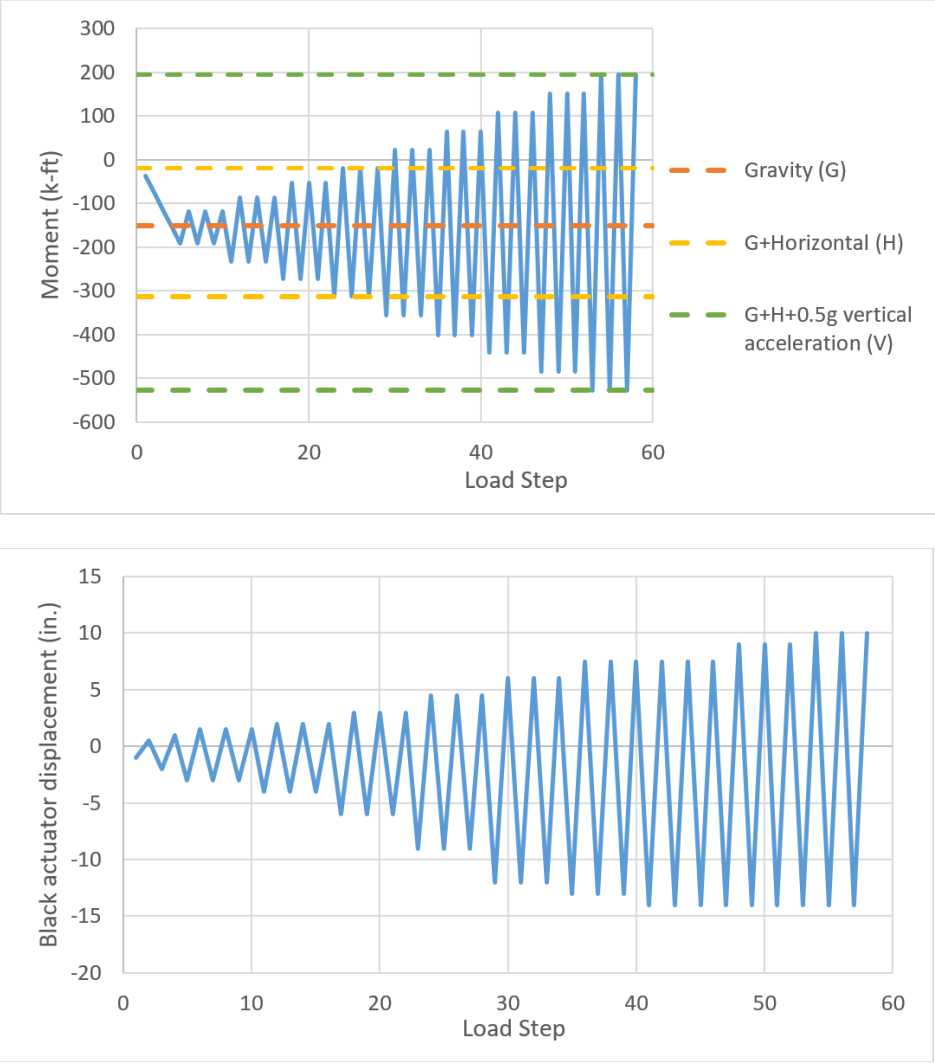

Figure 4-26 *Loading Sequence for Test Unit*

CHAPTER 5 TEST RESULTS

5.1 Overall Performance

In order to form the double plastic hinges at the ends of the column, the adequate continuity between the precast girders and the bent cap need to be developed such that the superstructure would remain elastic when the column overstrength moment was reached. Moreover, vertical acceleration will induce additional negative moment and positive moment at the girder-to-bent cap connection interface depending on the loading direction. The ESMS connection and the ESLS connection were designed to provide the adequate continuity between the precast bulb-tee girder and the bent cap in both negative and positive moment directions such that an integrated superstructure can be formed and exhibit elastic behavior under the seismic loading. During the experimental tests, both the ESMS and ESLS connections performed extremely well and remained essentially elastic under the target seismic demand including gravity load, column overstrength moment, and 0.5g vertical acceleration effects. When subjected to vertical displacement cycles, both of them exhibited sufficient ductility. Detailed testing results were illustrated in the following sections.

5.1.1 The ESMS connection

Testing of the ESMS connection was conducted from September 25, 2014 to September 26, 2014 in the Iowa State University Structures Laboratory. The ESMS connection was subjected to gravity, gravity plus column overstrength moment (horizontal seismic load), and gravity plus horizontal seismic load plus vertical acceleration effects to failure. *Figure 5-1* show the connection moment resistance versus vertical displacement measured at the black actuator location 28.5 ft from the girder-to-cap interface. The

moment magnitudes corresponding to gravity, horizontal seismic load, and vertical load effects relating to of 0.5g, 0.7g, 1.0g, and 1.75g accelerations are also shown in this figure. The connection remained essentially elastic for negative moment up to -914 k-ft, which corresponded to the summation of gravity load, horizontal seismic load, and 1.4g vertical acceleration effects. The connection also remained essentially elastic for positive moment demands up to 159 k-ft, which corresponded to a demand equal to that expected for the combined load due to gravity, horizontal seismic load, and the effects of 0.4g vertical acceleration. Moreover, the ESMS connection reached a maximum negative moment of -1124 k-ft (which is equivalent to demand beyond 1.75g of vertical acceleration in addition to the gravity and horizontal seismic effects) and a maximum positive moment of 300 k-ft (which is equivalent to demand representing the gravity load, horizontal seismic load and 0.7g vertical acceleration). Thus, the ESMS connection exhibited moment resistance well beyond the target seismic effects including the 0.5g vertical acceleration. The connection also exhibited considerable ductility in both negative and positive moment directions.

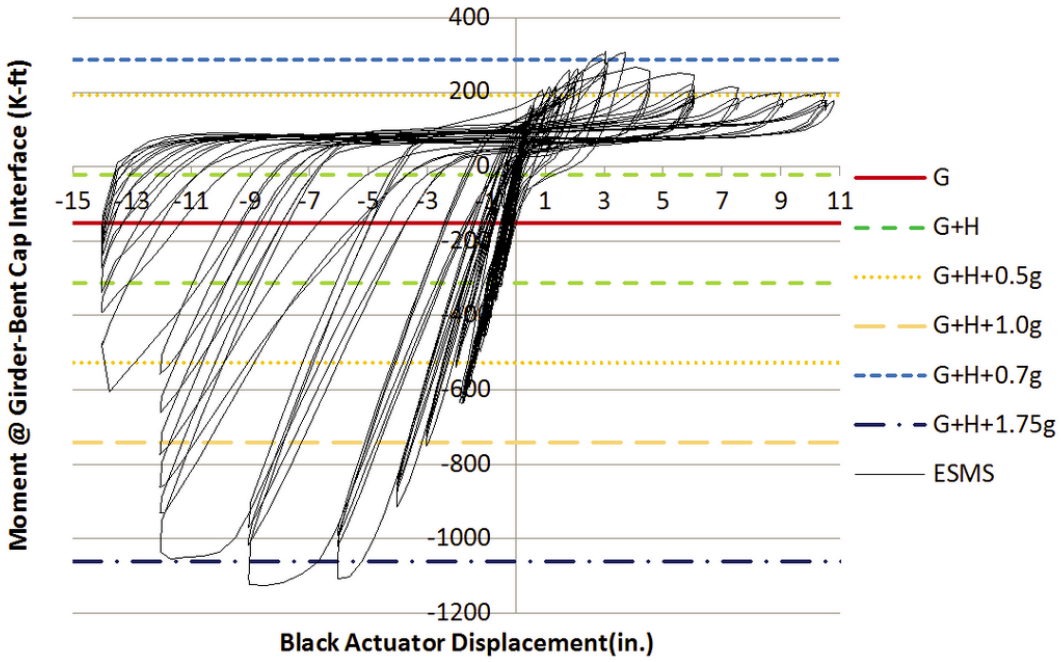

Figure 5-1 *the Measured Moment Resistance versus Black Actuator Displacement*

The negative moment resistance of the connection, as previously noted, relied on the reinforcement in deck to resist tension while the bottom of the girder was compressed against the bent cap. A few flexural cracks on the deck were the only observable damage under the target negative moment corresponding to the summation of gravity load, horizontal seismic load and 0.5g vertical acceleration effects. In order to achieve a better understanding of the failure mechanism, the load was increased to produce larger negative moment. A significant number of cracks in the deck had extended the entire width and penetrated the full depth of the deck during the large displacement cycles as shown in *Figure 5-2*. The cracks were well distributed over the connection region, and the crack width was relatively small. Furthermore, no spalling was observed on the deck during the entire test.

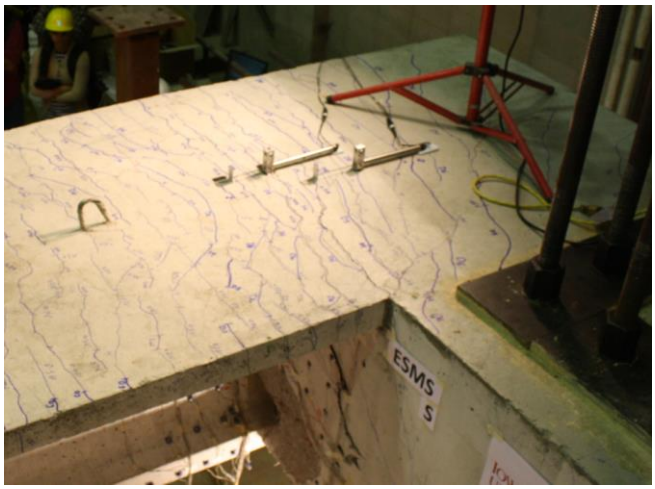

Figure 5-2 *Flexural Cracks on Deck of the ESMS Connection*

Under the target seismic effects including 0.5g vertical acceleration, no visual damage was observed on the bent cap and girder. The bottom cover concrete at the end of the girder began to visually separate with the girder strands as shown in *Figure 5-3* (a), when the applied load equivalent to gravity load, horizontal seismic load, and 1.0g vertical acceleration effects was reached. As the test continued, this portion of cover concrete spalled off. The bent cap cover concrete behind the girder spalled significantly at -6 in. vertical displacement. Meanwhile, the unstressed strands were compressed, resulting in the mushrooming of the strands and the pushing out of the bent cap cover concrete as shown in *Figure 5-3* (b). The damage at the interface between the bottom of the girder and the bent cap continued to grow with the incrementally increased vertical displacement. Eventually the concrete surrounding the bottom region of girder-to-cap interface crushed and spalled off resulting in a void between the girder and bent cap as shown in *Figure 5-3* (c).

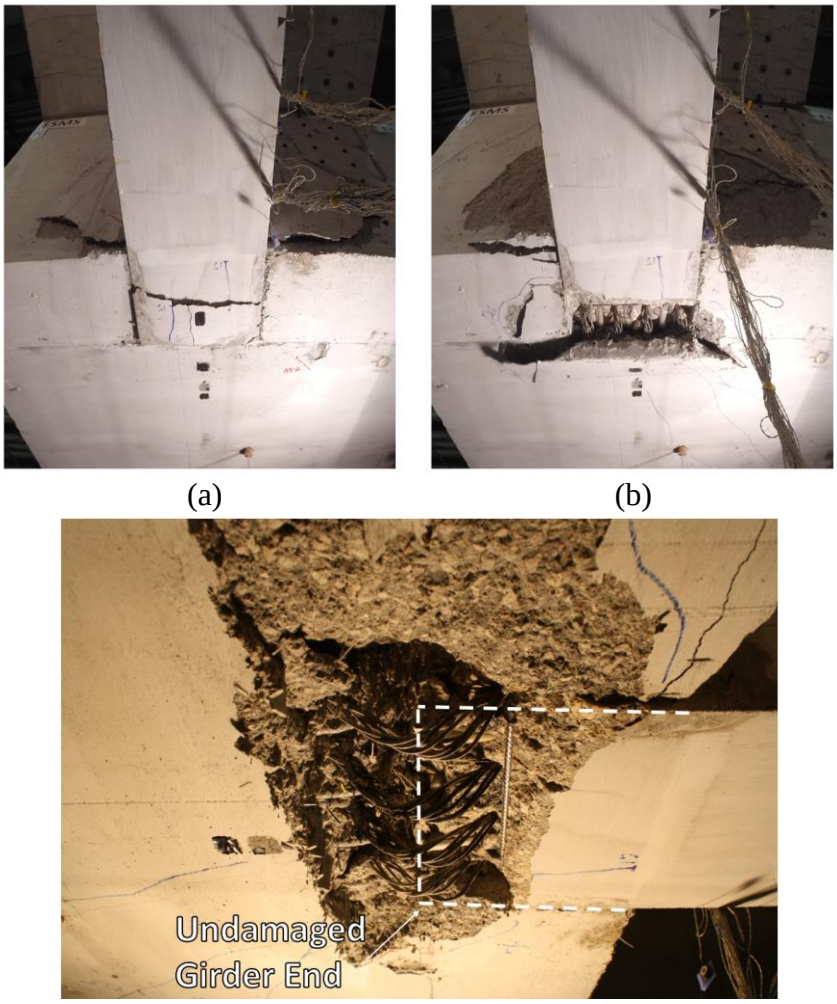

(a) (b)

(c)

Figure 5-3 *(a) Visual Separation of Girder Cover Concrete with Girder Strands; (b) Spalling of Concrete at Bent Cap behind Girder; (c) the Void formed between the girder and Bent Cap*

For the connection behavior in positive moment direction, only hairline cracks were observed on the deck and the girder up to the positive moment from gravity, horizontal seismic load, and 0.4g vertical acceleration effects. When the test continued beyond 0.4g vertical acceleration effects, the girder and the bent cap began to separate at the interface (*Figure 5-4* (a)). A 0.1 in. gap between the bottom of girder and the bent cap was the only damage when the connection was subjected to the target seismic effect. Damage due to the

girder pulling out subsequently appeared on the diaphragm next to the girder at the load equivalent to the summation of gravity, horizontal seismic load, and 0.7g vertical acceleration effects as shown in *Figure 5-4* (b). At 4.5 in. of vertical displacement measured at the black actuator location 28.5 ft from the girder-to-cap interface, the concrete adjacent to the girder on the front diaphragm surface began to spall. As shown in *Figure 5-4* (c), a large portion of the diaphragm next to girder spalled off and separated from the girder after the vertical displacement reached 7.5 in.. The compressed strands at negative moments were stretched and straightened when the positive moments were applied on the connection, but the extended strands did not fracture during the entire test.

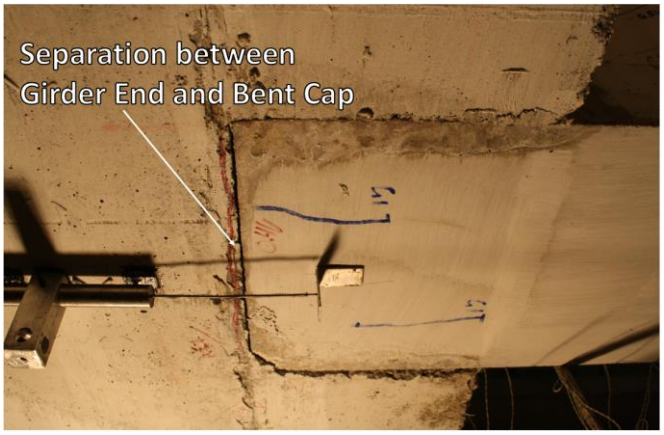

(a)

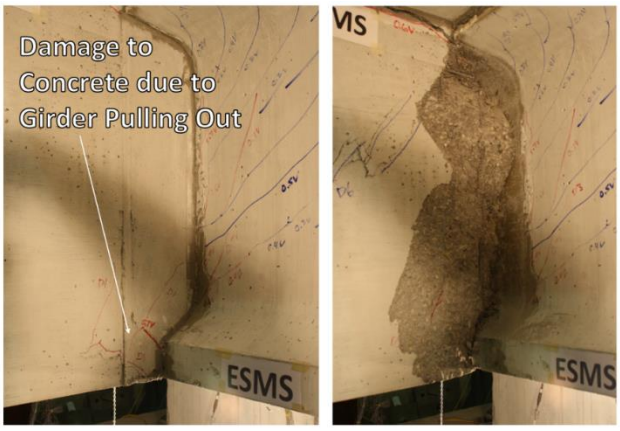

(b) (c)

Figure 5-4 *(a) Separation between Girder End and Bent Cap; (b) Penetration Cracks on Diaphragm; (c) Diaphragm Region where the Spalling of Concrete Was Observed*

5.1.2 The ESLS connection

The ESLS connection was tested from October 7, 2014 to October 8, 2014 at Iowa State University. As with the ESMS connection, the ESLS connection was subjected to equivalent loads up to gravity plus horizontal seismic load corresponding to the column overstrength moment plus vertical acceleration effects. Vertical displacement cycles of increasing moment magnitude were then utilized until failure of the connection was reached. *Figure 5-5* shows the connection moment resistance versus the vertical displacement measured at the black actuator location (28.5 ft from the girder-to-cap interface). The moment magnitudes corresponding to gravity, horizontal seismic load, and seismic effects relating to 0.5g, 1.0g, and 1.75g vertical acceleration were shown as well. The connection remained essentially elastic for negative moment up to -800 k-ft which corresponded to the summation of gravity, horizontal seismic load, and 1.14g vertical acceleration effects. The connection also remained essentially elastic up to a positive moment magnitude of 206 k-ft which corresponded to the combined load due to gravity, column overstrength moment under horizontal seismic acceleration and the effect of 0.5g vertical acceleration. The ESLS connection reached a maximum negative moment of -1158 k-ft (which is equivalent to a demand beyond 1.75g of vertical acceleration in addition to the gravity and horizontal seismic load) and a maximum positive moment of 387 k-ft (which is equivalent to a demand representing the gravity load, horizontal seismic load, and 0.95g vertical acceleration). In addition, the ESLS connection exhibited significant ductility in both negative and positive moment directions. An unexpected positive moment as large as 387 k-ft was applied after the load cycle of gravity plus horizontal seismic load

plus 0.5g vertical acceleration effects. The performance of the connection during the overloading period was monitored and is illustrated in the following sections.

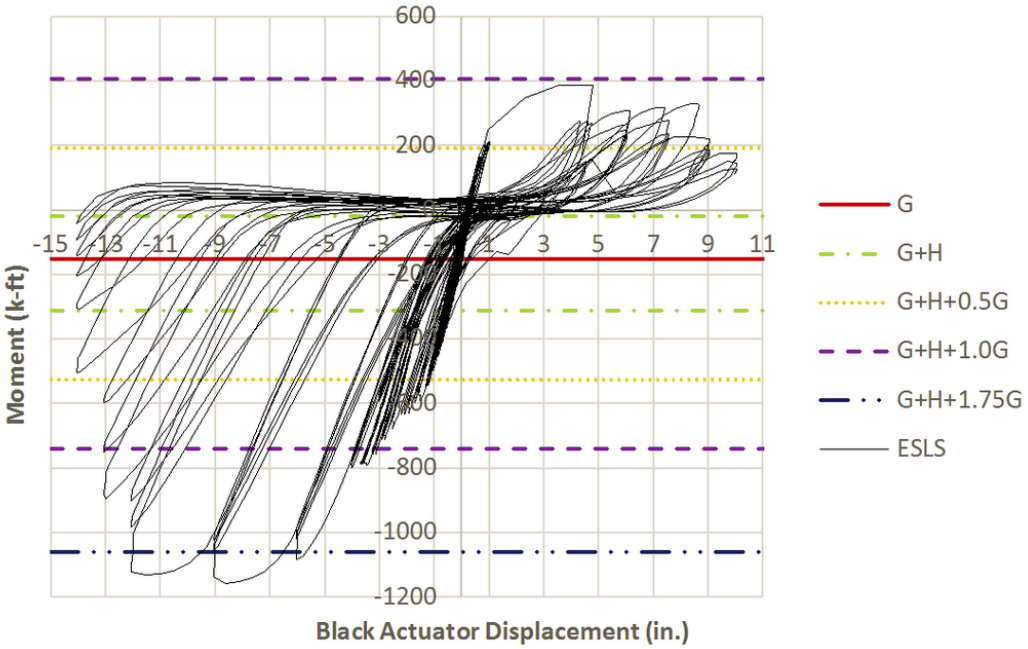

Figure 5-5 *the Measured Moment Resistance versus the Black Actuator Displacement*

The testing observations of the ESLS connection were similar to those noted during the test of the ESMS connection. When the target seismic effects were applied on the ESLS connection, no severe damage occurred except a few flexural cracks on the deck. Related to connection performance in negative moment direction, the only cracks that were observed throughout the entirety of the test had limited width and formed on deck over the connection region as shown in *Figure 5-6*. The cover concrete at the bottom of the girder end and a portion of the cover concrete on the bent cap spalled off after the overloading process as shown in *Figure 5-7* (a). However, the crushing and spalling off of concrete surrounding the girder-to-cap interface did not significantly increase until the vertical displacement of the black actuator reached -6 in. (*Figure 5-7* (b)). As the test continued, the concrete at the girder-to-cap interface gradually crushed and spalled at higher

displacements, eventually forming a void at the bottom region of girder-to-cap interface as shown in *Figure 5-7* (c).

Figure 5-6 *Cracks on Deck of the ESLS Connection*

(a)

(b)

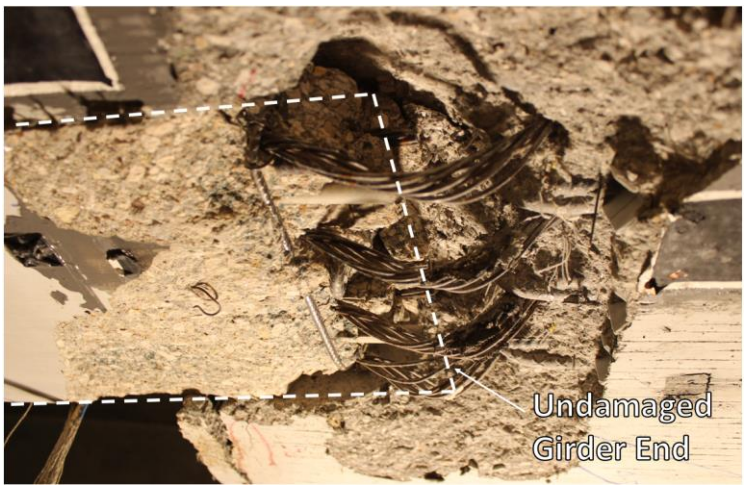

(c)

Figure 5-7 *(a) Spalling of Cover Concrete at Girder End; (b) Spalling of Concrete at Bent Cap behind Girder; (c) the Void Formed Between the Girder and Bent Cap*

Under the target positive moment due to gravity, horizontal seismic load, and 0.5g vertical acceleration effects, no visual damage was noticed within the ESLS connection. In comparison, the girder end was separated with the bent cap under the same target seismic effects within the test of the ESMS connection. During the application of the next load step, one of the actuators shut off, causing a large unexpected positive moment to be applied to the connection. The unexpected positive moment caused the penetration cracks on the diaphragm next to the girder shown in *Figure 5-8* (a). No further damage was observed at the connection region when the test was resumed to the next step in the loading protocol. As the displacement of the black actuator increased to 6 in. within the displacement controlled cycles, the diaphragm next to the girder spalled as shown in *Figure 5-8* (b). One of four strands extended from the girder fractured when the displacement reached 9 in. which caused a reduction in moment resistance. When cycled at a displacement of 10 in., another strand fractured as shown in *Figure 5-8* (c), but the rest of the strands remained effective through the end of test.

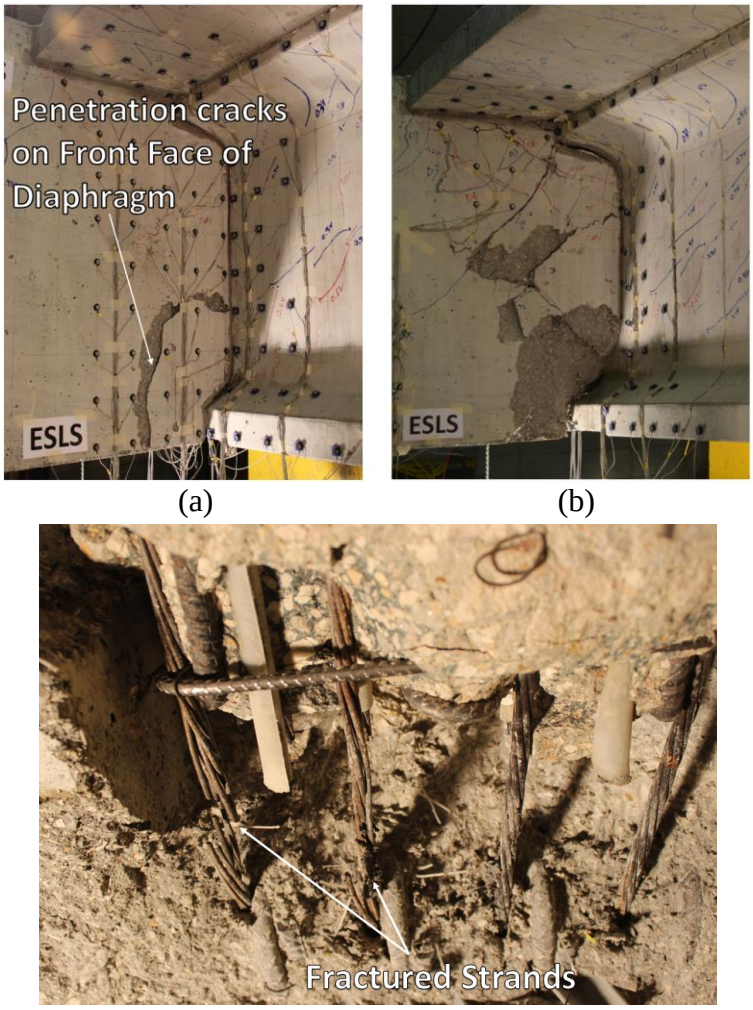

(a) (b)

(c)

Figure 5-8 *(a) Penetration Cracks on the Diaphragm after Overloading Process; (b) Concrete Next to Girder Spalled off; (c) Fracture of the Strands within the ESLS Connection*

5.2 Girder-to-Cap Interface Performance

In addition to the overall performance, a detailed investigation for the girder-to-cap interface performance was beneficial to gain a better understanding of connection behavior. The comparable performances were observed at the girder-to-cap interface for both the ESMS and ESLS connections. When the applied moment reached the target seismic effects corresponding the summation of gravity load, horizontal seismic load, and 0.5g vertical

acceleration effects, no severe damage was observed at the girder-to-cap interface, and the connection exhibited a response in an elastic manner. Under the negative moments, the bottom region of the girder end and the bent cap behind the girder were compressed. This local compression caused the strands to mushroom out. The expanding diameter of mushroomed strands pushed the cover concrete out at the bottom of the girder between the girder end and first girder stirrup, thus causing spalling of concrete in this region as shown in *Figure 5-9* (a). However, test data indicated that this spalling did not significantly change the elastic response of the connections. The continued increase of the strand mushrooming eventually caused the cap concrete to spall on the bottom surface as shown in *Figure 5-9* (b). Consequently, softening of the connection strength occurred, because this significant loss of concrete induced a gap between the girder and the bent cap. This gap allowed the girder to rotate more prior to compressing against the bent cap in the negative moment cycles. As the cyclic load continued to be applied, the concrete immediately adjacent to the girder-to-cap interface began to crush and spall off, as shown in *Figure 5-9* (c). The crushing of concrete allowed the girder to rotate even more and eventually it formed a void between the girder end and the bent cap as shown in *Figure 5-9* (d). The void decreased the depth of girder-to-cap interface and reduced the lever arm for negative moment resistance, which resulted in a significant degradation in negative moment resistance.

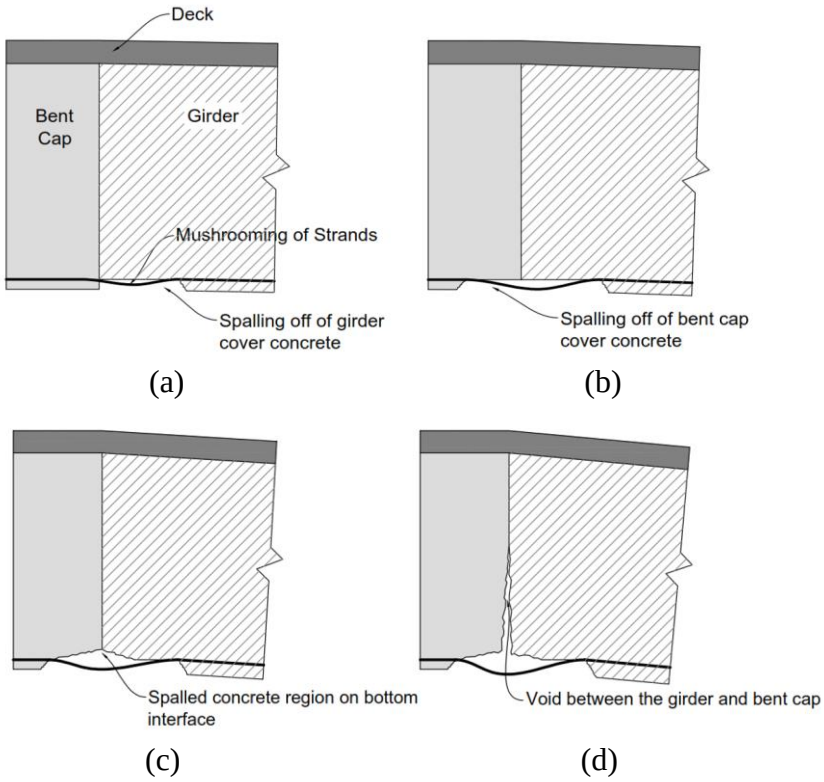

Figure 5-9 *Illustration of Girder-to-Cap Interface Performance*

5.3 Unstressed Strands and Dowel Bars Performance

The performance of unstressed strands and dowel bars were critical for the positive moment resistance. For the unstressed strands, the mushroomed strands under negative moment loading were observed to straighten under positive moment loading, and the tension resistance of strands was not reduced by this behavior. For the ESMS connection, the continuity provided by mechanical splicing of the extended girder strands was initially assumed to transfer the tension to the opposite girder. However, the test data indicated that the splice chucks provided sufficient anchorage for the unstressed strands and that tension forces were not transferred through the splice chuck to the other side. The unraveled portion of the strands caused by a sudden release of prestressing force during the transfer, as mentioned previously, did contribute to a drop in the tensile strength of the strands

extended from the girder. Test data indicated the strands to be only 78% effective in providing tension resistance. To account for this loss of effectiveness, 0.067 in^2 was used as the effective area for a single strand used in the ESMS connection.

As loads were applied to the extended girder strands, strain penetration occurred along the strands causing extension of the strands and a gap opening at the girder-to-cap interface. The unstressed strands used in the ESMS exhibited the comparable performance with observations from the previously described, pull-out tests. The pull-out testing results indicated that strain distribution can be approximated linearly along the embedded strand length. As the tension force resisted by the strands increased, the strain penetration occurred into both the girder side and the bent cap side. When the strain penetration reached the splice chuck, fully anchored behavior was exhibited. The strain distribution along the strand prior to yield is illustrated in *Figure 5-10*.

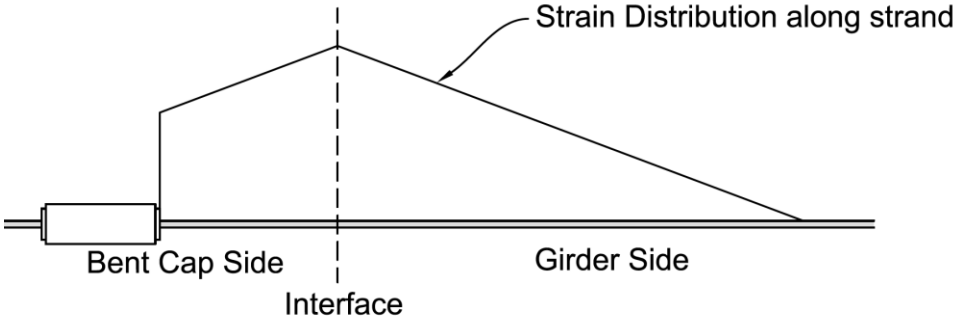

Figure 5-10 *Strain Distribution along Strand in the ESMS Connection*

Similar to the splice chucks used in the ESMS connection, the extended strands within the ESLS connection did not transfer the tension force through the lap splices. The strand chucks including bearing plates, barrel anchors, and wedges, developed the sufficient anchorage to fully develop the strand strength. As the connection was subjected to increasing rotations under positive moment, strands slips at the connection interface

resulted in an opening between the girder end and the bent cap. The strain distribution along the strands in the ESLS connection before the yielding of the strands is illustrated in *Figure 5-11*, demonstrating fully anchored behavior at the strand chuck.

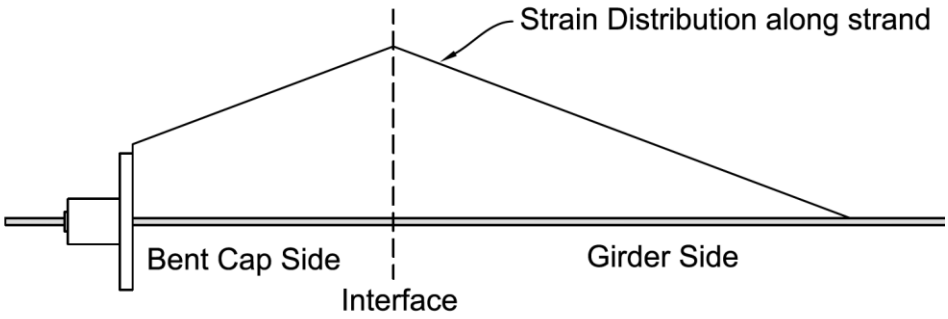

Figure 5-11 *Strain Distribution along Strand in the ESLS Connection*

The dowel bars embedded in the diaphragm adjacent to the girder resulted in the shear friction behavior providing the positive moment resistance. The previous investigation regarding the shear friction behavior was reviewed and summarized in Chapter 2. A general illustration of the dowel mechanism within the ESMS and ESLS connections could be described as follows: the shear friction behavior developed between the precast girder and the cast-in-place diaphragm poured surround girder end and provided resistance against pulling out of the girder under positive moment loading. The relative displacement between the girder and the surrounding diaphragm was resisted by cohesion at the interface between the girder and the diaphragm as well as shear-friction resulting from the clamping force developed by the dowel bars. The first yield condition appeared when the bottom of the girder separated with the bent cap, which indicated that the cohesion began to degrade. The shear-friction resulting from clamping force provided further moment resistance until damage to the concrete due to the girder pullout appeared on the front face of diaphragm at the bottom dowel bar location. The damage to the concrete due

to the girder pullout led to the further spalling of the cap cover concrete. At this point, the shear-friction began to degrade because the decreased clamping force due to the loss of bond strength of concrete surrounding the dowel bars, which resulted in a significant reduction of the moment resistance resulting from shear friction behavior.

5.4 Failure Mechanism

5.4.1 Negative moment behavior

The test unit of the ESMS connection was subjected to a maximum negative vertical displacement of 14 in. and a maximum positive displacement of 10.5 in. measured at the black actuator location 28.5 ft from the girder-to-cap interface. Similarly, the specimen of the ESLS connection underwent a negative displacement up to 14 in. and the positive displacement up to 10 in.. The performance of the ESMS and ESLS connections in both the positive and negative moment directions showed a sufficient moment resistance and considerable ductility. *Figure 5-13* and *Figure 5-14* depicts the measured moment resistance versus rotation response for the negative moment direction for the ESMS connection. The negative moment resistance of the connection relied on the deck steel to resist tension as the bottom region of the girder was compressed against the bent cap. *Figure 5-13* provides the strain data of the deck reinforcements at the interface between the girder and the bent cap. As mentioned previously, the cracks that distributed over the connection region did not cause spalling of the deck concrete. Significant concrete crushing and spalling did occur at the bottom girder-to-bent cap interface during the high displacement cycles. The relative distance between the bottom girder and the bent cap (*Figure 5-12*), which indicated the amount of crushing and spalling that occurred at the interface, is plotted in *Figure 5-14*. It was observed that the first yield condition of the

ESMS connection occurred when the applied moment reached -914 k-ft, but distinct softening behavior did not take place until the applied moment increased beyond -1101 k-ft The ESMS connection then behaved in a ductile manner, and a significant strength degradation was observed as the rotation grew beyond 0.0225 radians in the negative direction. When the ESMS connection subjected to the negative moment corresponding to yield limit state, the strain of deck reinforcement reached the yield value as shown in *Figure 5-13*. As the applied moments increased beyond the yield moment, the deck reinforcement underwent the strain hardening, but the strain of reinforcement were less than 5500 με for negative rotations beyond 0.0136 radians. Severe crushing and spalling of concrete at the bottom girder-to-cap interface occurred simultaneously with the strength softening of the connection at the rotation of 0.0063 radians as can be seen in *Figure 5-14*. The damage at the interface between the bottom of girder and the bent cap continued to grow with the increased rotations beyond 0.0063 radians. The formation of a void resulting from crushing of concrete at the bottom girder-to-cap interface reduced the lever arm for negative moment resistance, which resulted in a significant degradation of moment resistance as the rotations beyond 0.0225 radians were in the negative direction.

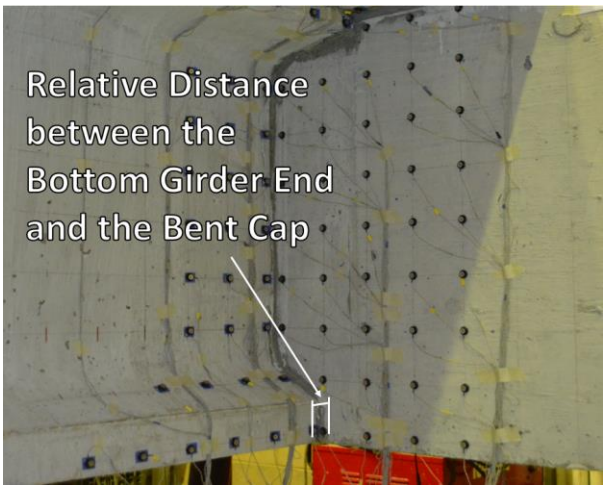

Figure 5-12 *Relative Distance between the Bottom of Girder and the Bent Cap*

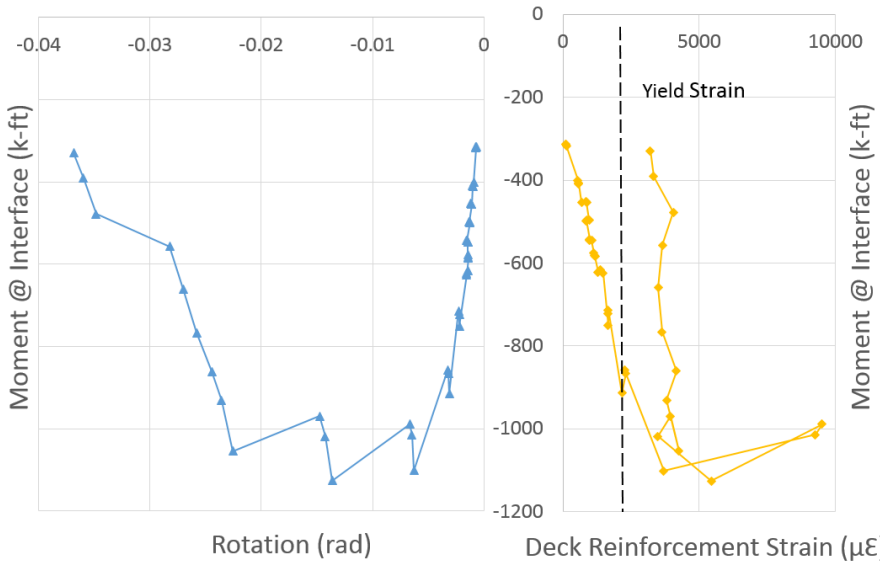

Figure 5-13 *Negative Moment versus Rotation and Negative Moment versus Deck Reinforcement Strain for the ESMS Connection*

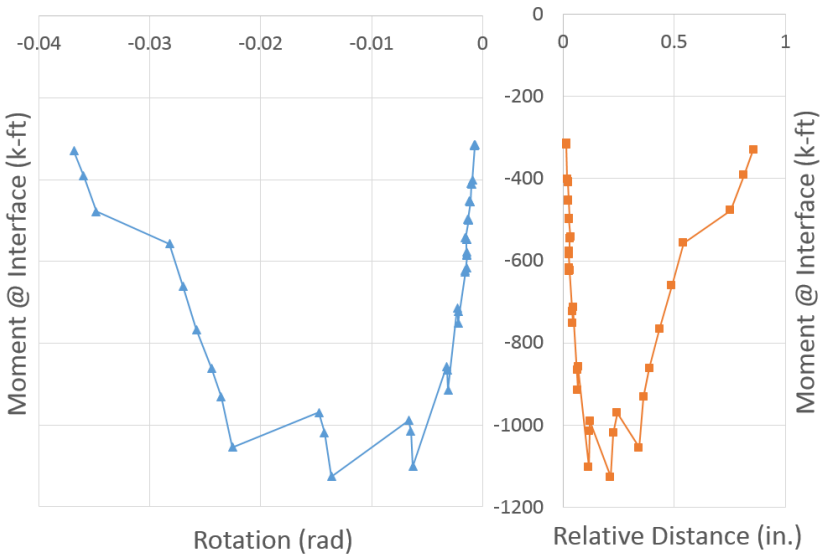

Figure 5-14 *Negative Moment versus Rotation and Negative Moment versus Relative Distance of Girder End and Bent Cap for the ESMS Connection*

For the ESLS connection, the negative moment resistance at the girder-to-cap interface is plotted versus the rotation measured at the girder end as shown in *Figure 5-15*. The deck reinforcement strain data at the girder-to-cap interface was not available for the ESLS connection due to the damage of the strain gauges during the construction process. However, the deck steel strain gauges located 18 in. from the interface indicated that the strain of the reinforcement was mostly limited less than 5500 με for the entire test. Therefore, it was fair to assume that the deck reinforcement at the interface of the ESLS connection performed similarly with the reinforcement in the ESMS connection under negative moment. The relative distances are plotted versus the negative moment resistance for the ESLS connection in *Figure 5-15*. Strength softening was observed as the crushing and spalling increased when the interface moment resistance exceeded -630 k-ft due to the damage caused by the overloading. However, the relationship between rotations and moment resistances remained linear until the applied moment reached -1072 k-ft. At the applied moment of -1158 k-ft, the significant increase in relative displacement indicated

that severe crushing and spalling occurred, resulting in a reduced negative moment lever arm and subsequent strength degradation as shown in *Figure 5-15*. The connection continued to resist stable moment until the rotation reached 0.0194 radians in the negative moment direction. Eventually, strength degradation took place because the crushing and spalling of concrete at the girder-to-cap interface reduced the lever arm for negative moment resistance.

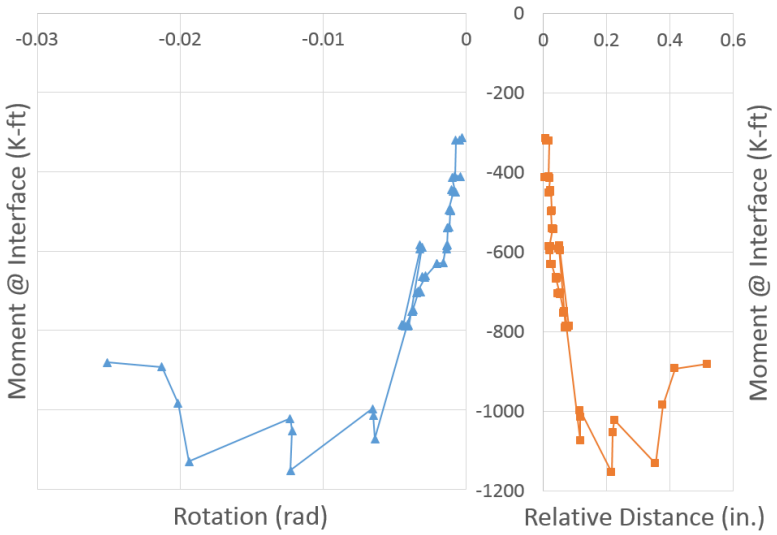

Figure 5-15 *Negative Moment versus Rotation and Negative Moment versus Relative Distance of Girder End to the Bent Cap for the ESLS Connection*

In summary, the ESMS and ESLS connections exhibited the comparable failure mechanism in the negative moment direction. The yield of deck reinforcement caused the first connection yield. The significant increments of concrete crushing and spalling at the girder-to-cap interface resulted in the strength softening of the connections. The formation of a void between the bottom of the girder and the bent cap reduced lever arm for negative moment resistance, which led to the further degradation of moment resistance for the ESMS and ESLS connections.

5.4.2 Positive moment behavior

The positive moment resistance of the connection is dependent on the unstressed strands extended from the girder for tension continuity while the deck and the top region of the girder compressed against the bent cap. The shear-friction developed by the dowel bars through the web of the girder, as well as, the cohesion between the embedded girder end and adjacent cap concrete also contribute to positive moment resistance.

For the ESMS connection, the positive connection moment resistance is plotted versus the girder rotation in *Figure 5-16*. The shear friction behavior is complicated and any direct measurement of this behavior was not possible. Therefore, the moment resistance due to shear friction behavior is approximated by subtracting the moment resistance of the strands from the overall connection resistance. A series of pull-out tests on strands with different sizes and configurations were performed to investigate the strain penetration behavior of unstressed strands. The tests provided the strain distribution along the strands as a function of the applied forces, which was then used to estimate the strand behavior in the ESMS connections. In *Figure 5-16*, the moment resistance of the strands is plotted as a function of the connection rotation; the moment resistance provided by the shear friction behavior is also shown. The data graphed in *Figure 5-16* was consistent with aforementioned test observations. Generally, the connection exhibited an elastic behavior under the applied positive moments corresponding to the target seismic effects including 0.5g vertical acceleration. The yielding of the shear friction behavior was indicated by the separation between the bottom of the girder and the bent cap, and caused the yield condition for the connection. Therefore the increase in overall moment resistance relied on tension in the extended girder strands, which continued to grow with the increasing of girder

rotation. Also, no significant strength degradation occurred for the moment resistance resulting from shear friction behavior until the damage to concrete due to girder pulling out appeared on the front surface of the diaphragm next to the girder. The connection reached its ultimate moment capacity close to 0.01 radians which corresponded to drop in shear friction moment. When the positive rotation reached 0.0254 radians, the cover concrete next to the girder spalled off and caused a significant reduction in shear-friction. The strands extended from the girder experienced high strains simultaneously with the inelastic behavior of the connection and provided residual moment resistance at a rotation beyond 0.0254 radians in positive moment direction.

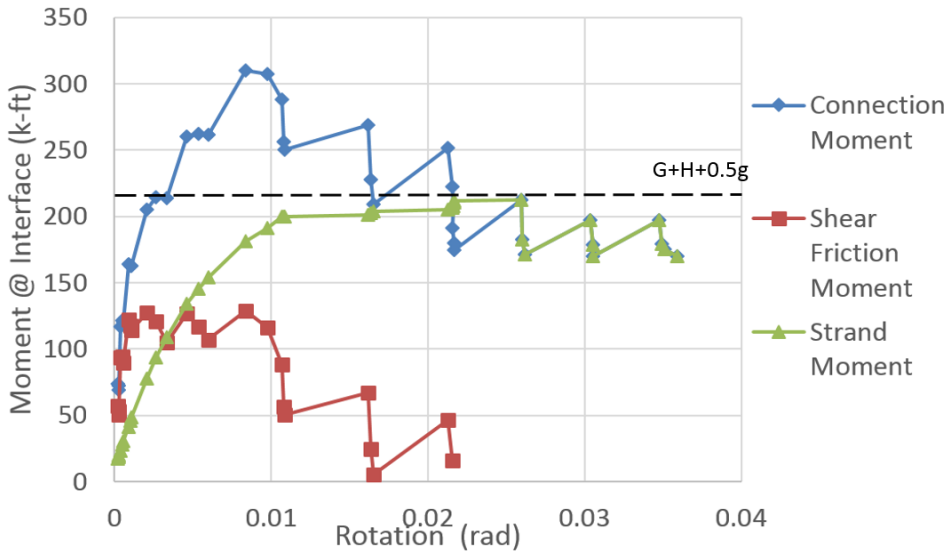

Figure 5-16 *Estimating the Contribution of the Positive Moment Resistance in the ESMS Connection*

The positive moment resistance at the girder-to-cap interface for the ESLS connection is shown in *Figure 5-17*, plotted versus the girder rotation. Similarly, the moment resistance generated by the shear friction behavior and the moment resistance produced by extended girder strands are also shown in *Figure 5-17*. The behavior of the ESLS connection is comparable with that of the ESMS connection in the positive moment

direction. The yield of the shear friction behavior took place simultaneously with the first yield of the connection. Subsequently the connection reached its ultimate moment capacity when the unexpected positive moment was applied. Under the ultimate moment, the damage to the cap concrete due to girder pullout appeared on the diaphragm adjacent to the girder, indicating a potential loss in shear friction behavior. As the connection was subjected to higher displacement cycles, the positive moment resistance decreased due to continued degradation of the shear friction behavior. Although the moment resistance of the shear friction behavior was reduced, the extended strands remained effective to provide resistance until fracture occurred at a rotation slightly above 0.0268 radians. A significant reduction in moment resistance of the ESLS connection occurred at the rotation beyond 0.0268 radians due to the fracture of the strands.

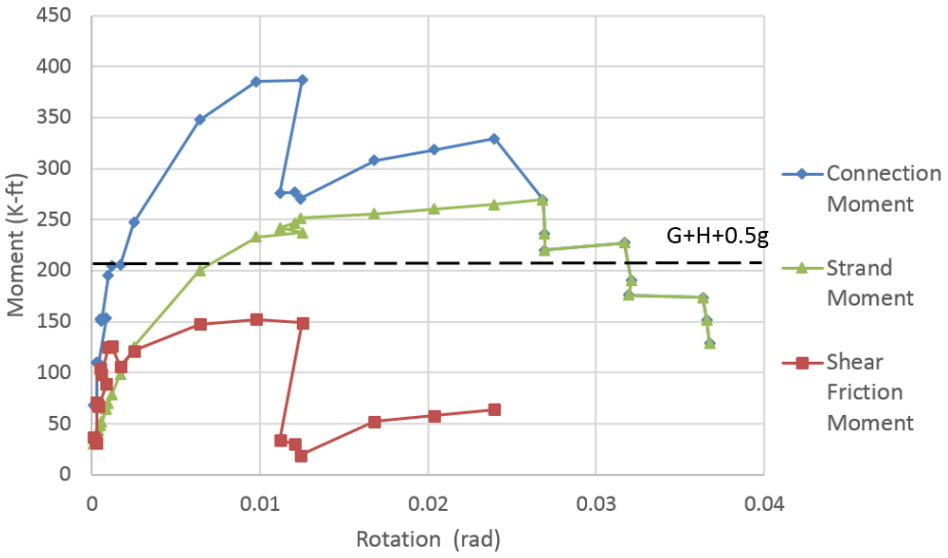

Figure 5-17 *Estimating the Contribution of the Positive Moment Resistance in the ESMS Connection*

The ESMS and the ESLS connections showed comparable behavior in the positive moment direction. The yield of shear friction behavior caused the first connection yielding. The connection reached its ultimate capacity prior to the degradation of the shear friction

behavior. The moment resistance began to degrade beyond the rotation corresponding to ultimate moment capacity, and the residual moment resistance was dependent on the behavior of strands.

CHAPTER 6 DESIGN METHOLODIES

To facilitate the implementation of the connection details investigated in this study, design methodologies that can be adopted in further practice have been developed. Because of the different load-transfer mechanisms that are involved in the negative and positive moment directions, the design methodologies are presented below for each of the two loading directions.

6.1 Negative Moment

As the discussion in Chapter 5, the yield of deck reinforcement caused the first yield of connection. However, the connection still performed in an elastic manner until a significant concrete crushing and spalling took place at the bottom of the girder-to-cap interface. A strength softening of the connection occurred due to this localized failure. As the rotation increased, concrete crushing and spalling formed a void between the bottom of the girder and the bent cap reducing the lever arm for negative moment resistance, which lead to the further strength degradation for the ESMS and ESLS connections. Moreover, the strain of the deck reinforcement was limited in a relatively low level even though it had exceeded the yield value.

The precast bulb-tee girder-to-bent cap connection under negative moments may be evaluated using a sectional analysis of the composite girder-deck cross-section that is present at the girder-to-cap interface. The effect of the dowel bars embedded in the diaphragm is conservatively neglected for the negative moment calculation. For the composite section of the girder-deck assembly, an approximate effective deck width and the corresponding deck reinforcement should be defined as show in *Figure 6-1*. The

effective deck width may be calculated according to the location (i.e., interior vs. exterior) and current Caltrans design practices. Recommendations on moment distribution by Vender Werff and Sritharan (2013) that included test data from previously completed system tests for Caltrans may also be used for this purpose. Material properties for the deck and girder concrete as well as the steel reinforcement should be assigned according to appropriate Caltrans specifications.

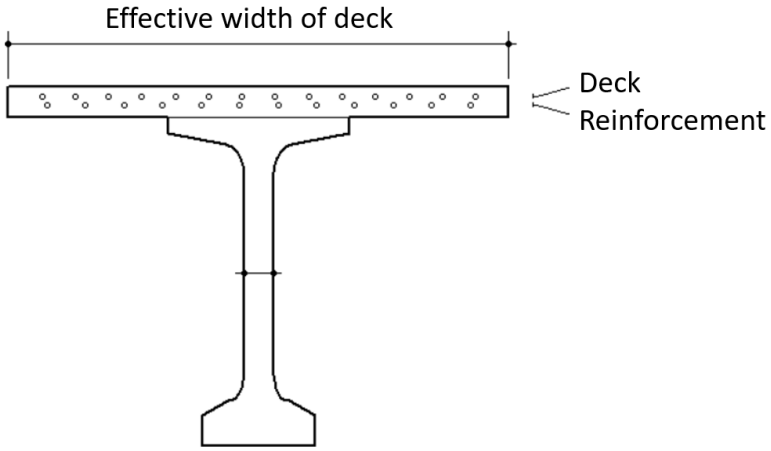

Figure 6-1 *Section of the Precast Bulb-Tee Girder-to-Bent Cap Connection in Negative Moment Direction*

The sectional analysis for the composite cross-section can be performed and a moment-curvature response showing the idealized yield and ultimate moment resistance of the section can be estimated. The corresponding tension force developed in the deck reinforcement can also be easily calculated (*Figure 6-2*).

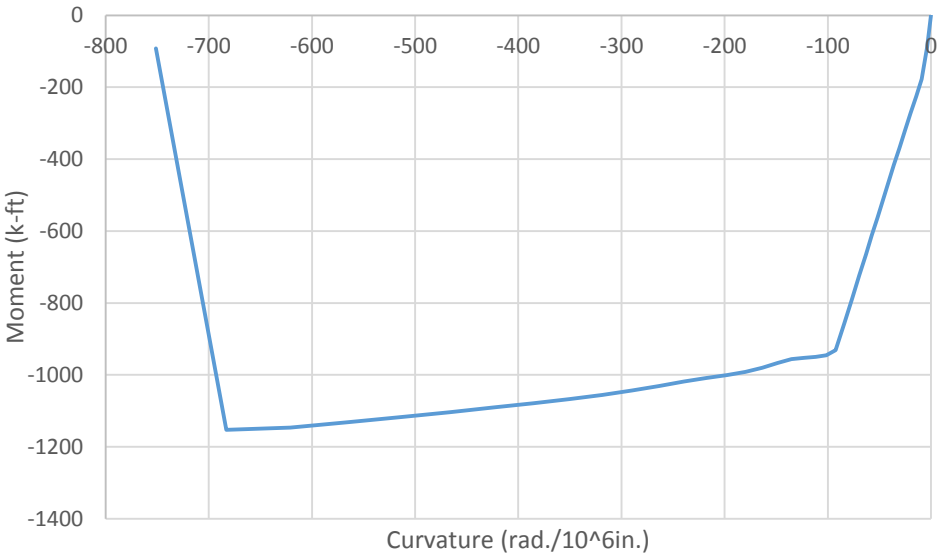

(a) Moment-Curvature Response of the Composite Cross-Section

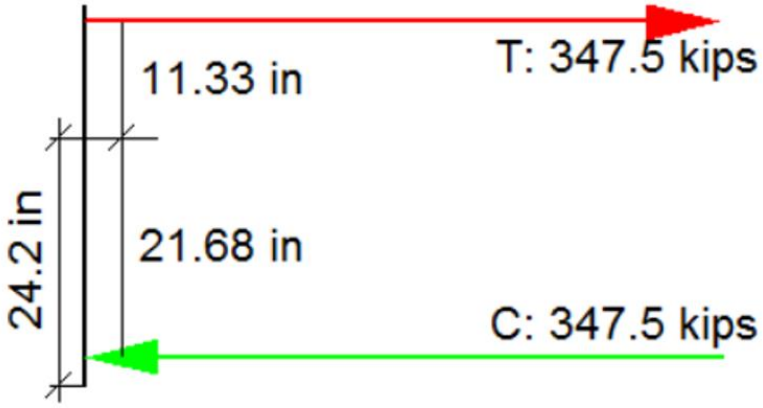

(b) Internal Forces at Idealized Yield Condition

Figure 6-2 *Results of Sectional Analysis*

In addition to the connection moment resistance, the girder rotation corresponding to the applied moment needs to be determined in order to accurately calculate the behavior of the connection. The testing indicated that concrete crushing and spalling at the bottom of the girder-to-cap interface contributed to the majority of rotation under the negative moments by inducing the growing relative distance between the girder end and the bent cap. Unfortunately, concrete crushing is a localized failure and thus the corresponding relative distance is difficult to estimate numerically. Hence, an empirical approach is

followed. *Figure 6-3* shows experimentally measured relative displacement, a good indicator of the amount of the crushed concrete, plotted with the compressive stress which is estimated based on the applied negative moment. Within *Figure 6-3*, the assumptions made were that the compressive stress is uniform at the girder-to-cap interface and that the area of girder below the neutral axis is compressive area. It is indicated from the test data that the point of relative distance occurs by the girder rotating about the neutral axis (N.A.) according to the corresponding applied negative connection moment. For moment values below the connection yield moment, which corresponds to when the deck reinforcement reaches yield stress, the neutral axis may be assumed to be located at the centroid of the girder (*Figure 6-4* (a)). For moments beyond the connection yield moment, the axis of rotation should still be assumed as the girder centroid, but the neutral axis depth ($d_{N.A.}$) should be multiplied by the factor of 0.8 (*Figure 6-4* (b)) since the lever arm for negative moment resistance increases as the applied moments increase.

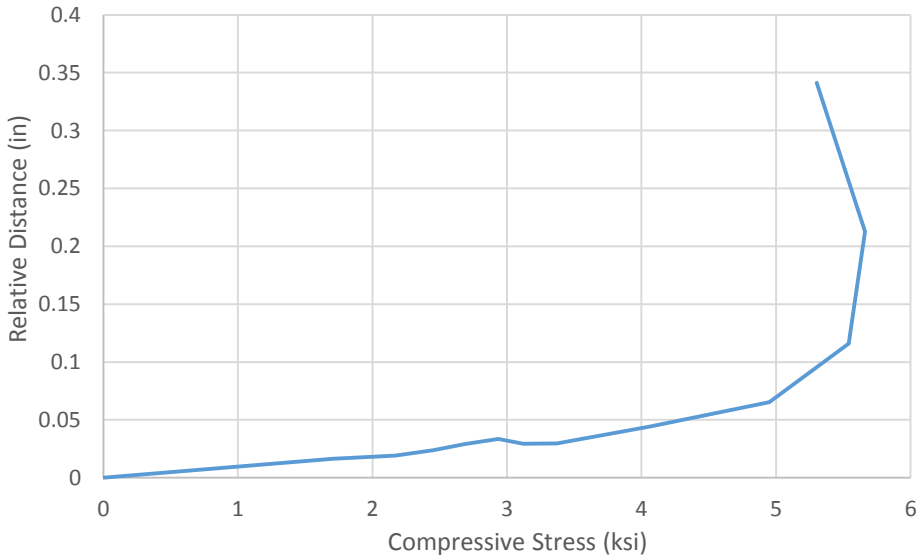

Figure 6-3 *Experimental Measured Relative Distance between Girder End and the Bend Cap*

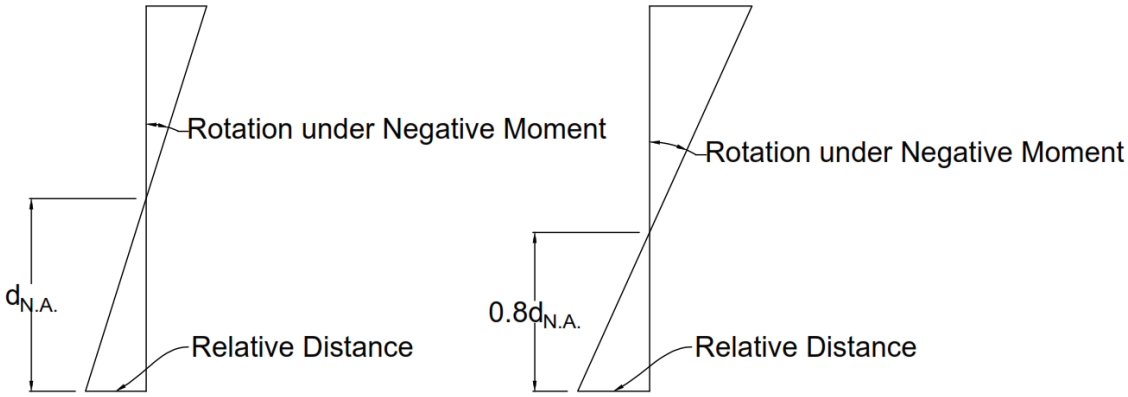

(a) Neutral axis under the moments below the connection yield moment

(b) Neutral axis under the moments beyond the connection yield moment

Figure 6-4 *Assumed Rotation at Girder-to-Bent Cap Connection under Negative Moment*

For any given moment value, the resultant tension force can be obtained from the sectional analysis and is equivalent to the compression force if there is no additional axial force on the girder-to-cap interface. For the design purpose, it may assume that the compressive stress is uniform within the girder-to-cap interface region below the neutral axis. Therefore, *Figure 6-3* then allows a graphical determination of relative distance by using compressive stress resulted from equivalent compression force. The girder rotation (θ) can be then calculated using *Equation (6-1)* or *Equation (6-2)* depending on if the moment is greater than or less than the connection yield moment. Since the rotation of the girder is caused by concrete crushing due to the compressive stress developed under negative moments, it is important to design the deck steel such that the composite section is not compression controlled under the target design demands. If the composite section contains too large an amount of deck reinforcement, a very large tension force will be required in order for the section to yield. If the tension force becomes too large, the corresponding compressive stress will cause significant crushing and subsequent rotation

of the girder. In this case, it is possible that the connection would begin to soften before yielding of the deck reinforcement resulting in a compression controlled section.

$$\theta = \frac{Relative\ Distance}{d_{N.A.}} \tag{6-1}$$

$$\theta = \frac{Relative\ Distance}{0.8d_{N.A.}} \tag{6-2}$$

In summary, by performing the sectional analysis and using *Figure 6-3*, the moment-rotation behavior of the precast bulb-tee girder-to-bent cap can be determined. In order to verify the accuracy of the proposed method, the procedure was used to determine the behavior of the ESMS and ESLS connection. A comparison of the calculated behavior and the experimental results are shown in *Figure 6-5*. Overall, the calculated behavior compares well with experimental measured response envelopes. This confirms that the proposed design methodologies is adequate to determine the behavior of connections with similar geometry and girders with no end block as used in the test units. It is noted that since *Figure 6-3* is determined empirically from test data quantifying localized failure, the same assumption may not be used for other girder type or bulb-tee girders with other end details. For full-scale 7 ft – 5/8 in. depth bulb-tee girders, the recommendations in *Figure 6-3* can be scaled as shown in *Figure 6-6*. For shallow girder, the same correction may be proportioned, with caution.

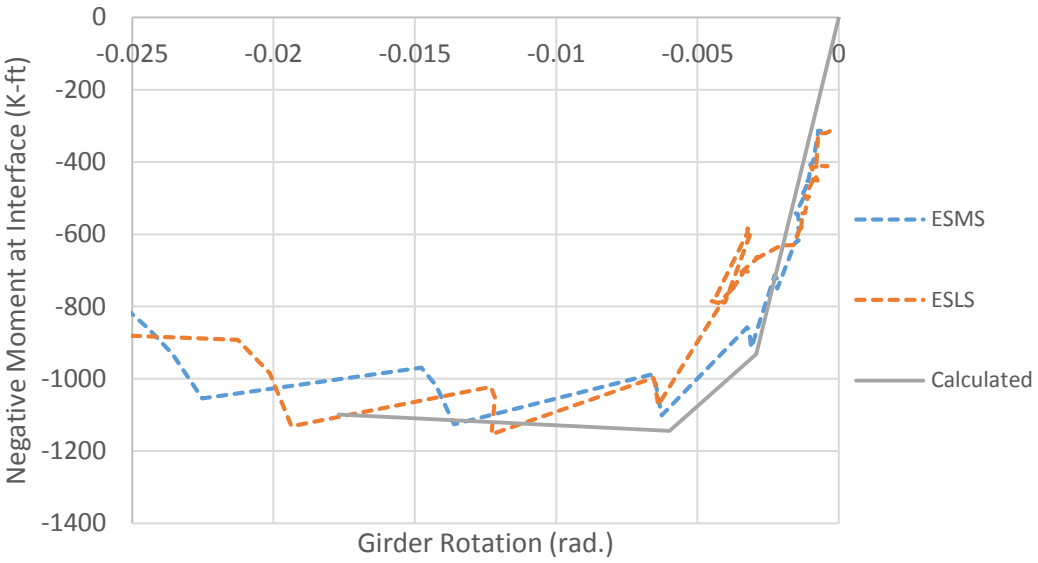

Figure 6-5 *Comparison between the Predicted Behavior and the Experimental Behavior in Negative Moment Direction*

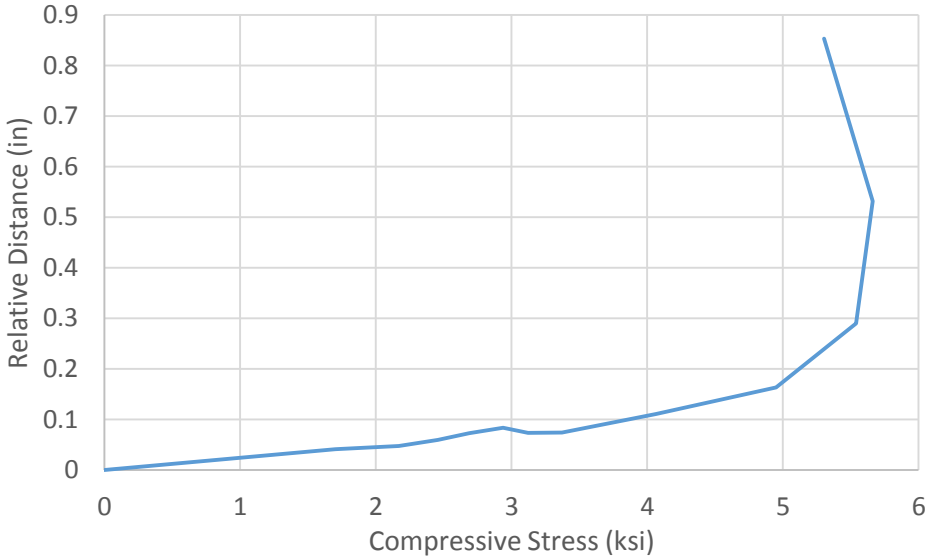

Figure 6-6 *Relative Distance at the Bottom of Girder End under Negative Moment for Full-Scale 7 ft – 5/8 in. Depth Bulb-Tee Girders*

6.2 Positive Moment

For positive moment, the experimental investigations indicted that the dowel bars embedded in the diaphragm and the extended girder strands contributed to resist the applied moment simultaneously. The shear friction behavior developed at the interface between

the girder and the surrounding diaphragm concrete provides the moment resistance by restraining the pull out of the embedded girder end as shown in *Figure 6-7*; meanwhile, the extended girder strands anchored into the cap provide tension continuity for additional positive moment resistance. These two mechanisms may be modeled separately and then combined to determine the total moment resistance of the connection. The following presents the proposed design method for qualifying the connection positive moment behavior.

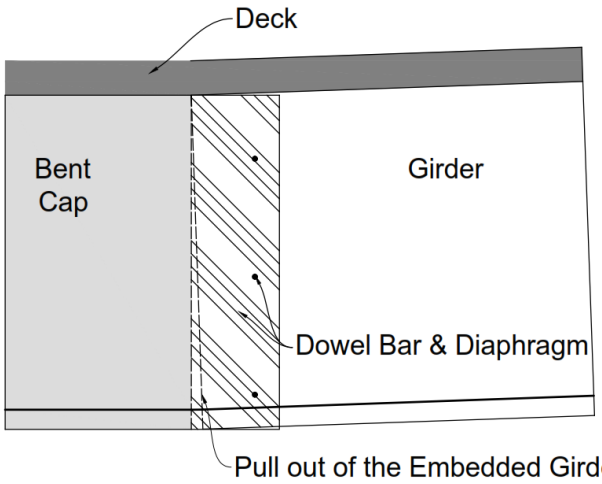

Figure 6-7 *An Illustration Showing Pull out of an Embedded girder into the Diaphragm*

6.2.1 Shear friction behavior

When a precast bulb-tee girder is used in conjunction with cast-in-place bent cap, the girders are erected on the temporary falsework. The dowel bars are then grouted through the girder web, and the diaphragm is cast around the end of the precast girder. As the girder rotates upward under positive moment, the embedded girder end tends to pull out from the diaphragm activating the shear friction mechanism. Shear friction resistance includes two components: cohesion and shear-friction. The cohesion results from shear transferred through the slip plane and contributes by aggregates from diaphragm concrete bearing on the girder and by dowel action. The friction component results from the tension

force developed in the dowel bars, which in turn causes compression on the concrete at the interface. The corresponding shear transfer should be accounted for using an appropriate coefficient of friction. In order to establish an appropriate moment-rotation behavior for the positive moments, the displacement associated with shear friction behavior should be established, and can be used to determine the gap opening at the bottom of the girder and the bent cap as shown in *Figure 6-8*.

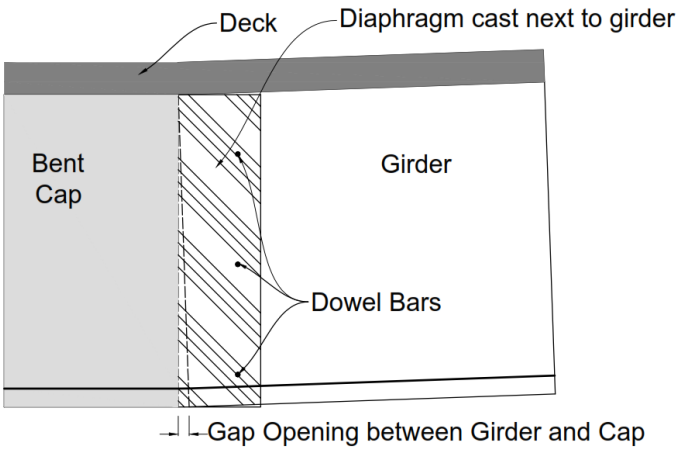

Figure 6-8 *Gap Opening under Positive Moments*

AASHTO LRFD Bridge Design Specifications (AASHTO, 2012) proposes that the resistance due to shear friction as explained above can be estimated as follows:

$$V_{ni} = cA_{cv} + \mu(A_{vf}f_y + P_c) \tag{6-3}$$

The nominal shear resistance (V_{ni}) used in the design shall not be greater than the lesser of:

$$V_{ni} \leq K_1 f'_c A_{cv} \tag{6-4}$$

$$V_{ni} \leq K_2 A_{cv} \tag{6-5}$$

where,

A_{cv} = area of concrete considered to be engaged in interface shear transfer (in.^{2});

A_{vf} = area of reinforcement crossing the shear plane within the area A_{cv} (in.^{2});

c = cohesion factor;

μ = friction factor;

f_y = yield stress of reinforcement (not to exceed 60 ksi for Grade 60 reinforcement);

P_c = permanent net compressive force normal to the shear plane, which is zero for this study;

f'_c = specified 28-day compressive strength of the lowest strength on either side of the interface (ksi);

K_1 = fraction of concrete strength available to resist interface shear; and

K_2 = limiting interface shear resistance.

According to AASHTO, for concrete place against a clean concrete surface, free of laitance, but not intentionally roughened as in case for all girder-to-diaphragm interface in this study:

c = 0.075 ksi;

μ = 0.6;

K_1 = 0.2;

K_2 = 0.8 ksi.

In order to estimate the displacement corresponding to shear friction, experimental observation were used in conjunction with models suggested in the literatures. This resulted in a bi-linear model shown in *Figure 6-9,* which is similar to that suggested by Harries et al. (2012). This model identified the yield and ultimate shear friction resistance for the shear friction behavior, which also corresponds to visible damage at the connection interface. Yielding of the shear friction mechanism usually takes place at displacement values ranging from 0.025 to 0.042 in. for any given interface (Harries et al., 2012). At this yield limit state, a gap would be visible between the bottom of the girder and cap as shown

in *Figure 6-10*. The ultimate shear resistance, approximated to have the same capacity as that at yield, is expected for shear displacement values ranging from 0.25 to 0.3 in. (Kahn and Mitchell, 2002). After the ultimate shear displacement is reached, there is significant strength degradation due to bond failure between the dowel bars and surrounding concrete. The ultimate shear displacement is characterized by damage to concrete due to the girder pulling out adjacent to the girder and spalling of concrete around the dowel bars as shown in *Figure 6-11*. Based on results from the this test, 0.025 in. and 0.27 in. were identified as the yield shear friction displacement and the ultimate shear friction displacement, respectively.

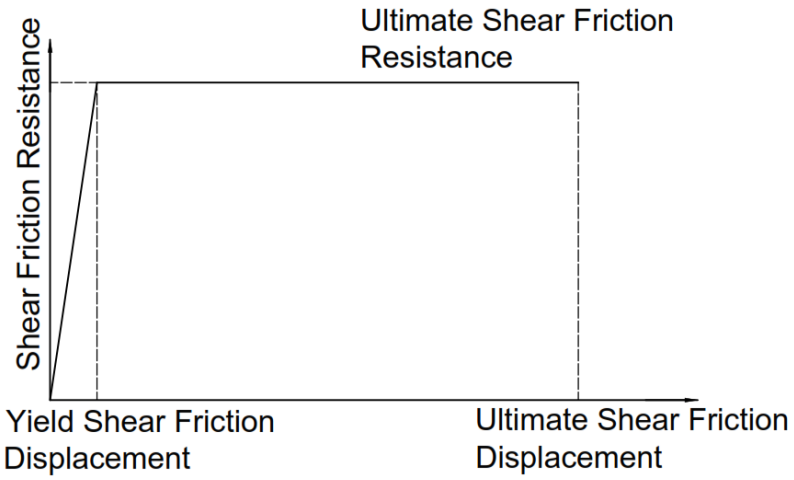

Figure 6-9 *Identified Shear Friction Behavior*

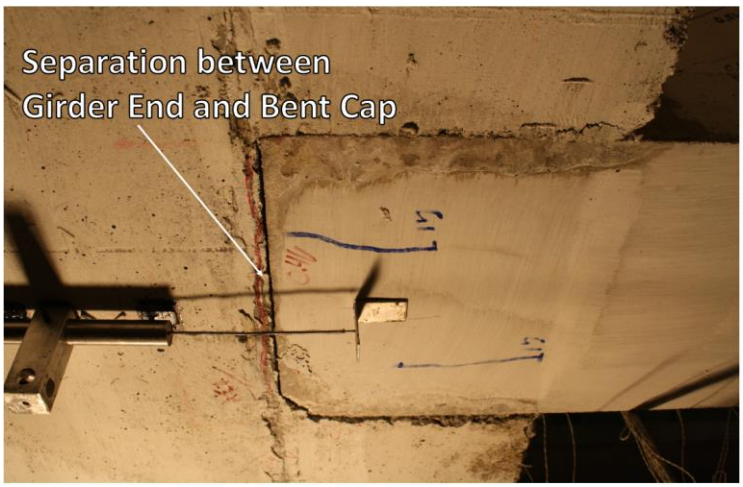

Figure 6-10 *Gap Observed between Girder and Cap*

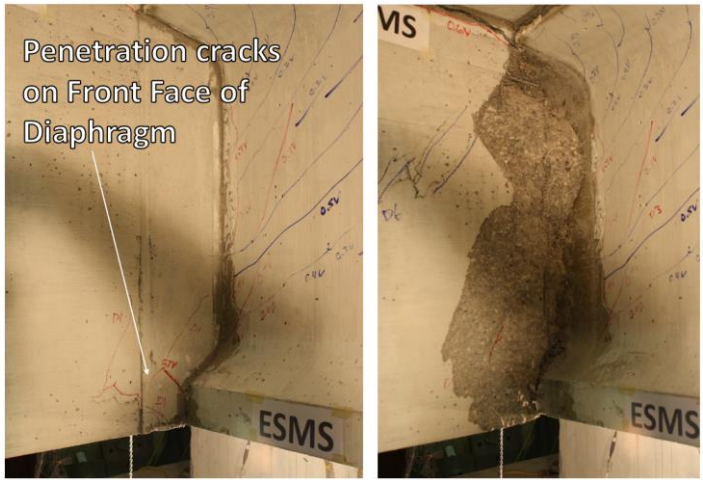

Figure 6-11 *Damage to Concrete due to Girder Pulling out on the Diaphragm Adjacent to the Girder*

The shear resistance provided by shear friction behavior should be calculated at the location of dowel bars as shown in *Figure 6-12* using *Equation (6-3)*. The concept of tributary area is used to define the amount of concrete considered to be engaged for each dowel bars as the force in each bar may be different. However, since the yield shear friction displacement was determined to be a small value (i.e., 0.025 in.), it should be assumed that each dowel bar reaches the ultimate shear resistance simultaneously.

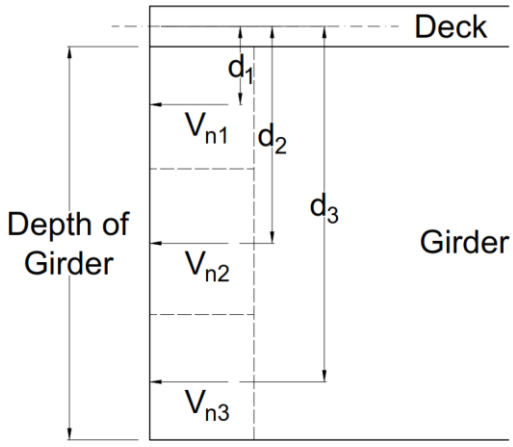

Figure 6-12 *Distance to Dowel Bars for the Positive Moment Resistance Developed between the Diaphragm and Girder*

In a similar manner to the calculations in the negative moment direction, the connection is modeled with the assumption that the shear friction displacement results from rotation of the girder at the interface about the neutral axis. The yield shear friction displacement and ultimate shear friction displacement occurred at the location of the lowest dowel bar. Based on equivalent stress block calculations, the neutral axis for positive moment is located at the top of the girder as shown in *Figure 6-13*.

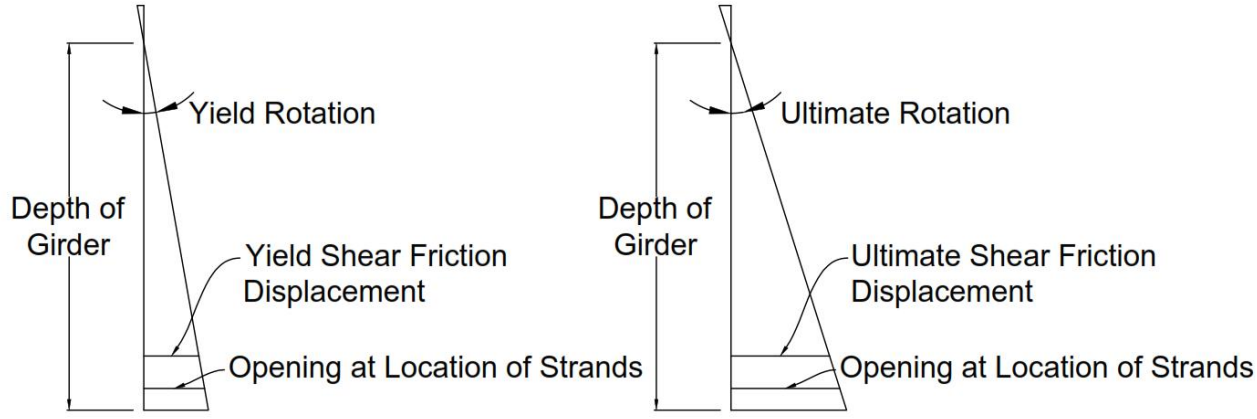

Figure 6-13 *Rotation of Girder-to-Bent Cap Connection in Positive Moment Direction*

Therefore, the moment resistance developed by shear friction behavior should be taken as:

$$M_{s-f} = \sum d_i V_{ni} \tag{6-6}$$

where,

M_{s-f} = moment resistance of shear friction behavior;

d_i = distance from the middle of deck to the dowel bar; and

V_{ni} = nominal shear resistance of the interface plane.

The interface rotation (Θ) shall be calculated as:

$$\theta = \frac{\Delta_{LD}}{d_{LD}} \tag{6-7}$$

where,

Δ_{LD} = shear displacement at the location of the lowest dowel; and

d_{LD} = distance from neutral axis to location of the lowest dowel bar.

6.2.2 Extended girder strands

In addition to the shear friction behavior contributing to the moment resistance, the extended girder strands also contribute to the positive moment resistance. The experimental tests indicated that both the mechanical splice chuck and the anchor chuck with steel plate were able to fully anchor the strands. Anchorage of the strands was validated using the strain gauges mounted to them, which confirmed many of the strands experienced strains approaching yield and in some cases fractured under applied positive moments. However, local strand slip did occur at the connection interface due to the effects of strain penetration and associated debonding. Based on measured data, the strand behavior was characterized to accurately determine moment resistance using corresponding gap opening at the location of strands.

The connection interface is the location where the girder rotation occurs, and is therefore also where the strands experience the highest strain. The strain in the strand decreases in both the girder and cap in proportion to the distance from the interface at a rate that is assumed to be linear as shown in *Figure 6-14 (a)*. The length of strand required for the strand strain to reduce to a value of zero is defined as the strain penetration length. If the strain penetration length reaches the strand anchor as shown in *Figure 6-14 (b)*, the strain will not penetrate beyond the anchorage point. Instead the strain will increase along the anchorage length (l_d) between the interface and strand anchor with the remaining force taken by the end anchor. As mentioned previously, pull-out tests were performed on 3/8 in. and 0.6 in. diameter strands. Results from the pull-out tests showed that the strain reduction along the length can be approximated to $k=$ 0.00022 strain/in. for 3/8 in. diameter strands and 0.0001 strain/in. for 0.6 in. diameter strands. Integration of the strain along the strain penetration length for both the girder and bent cap is equal to the total strand elongation. Note that the same distribution is assumed for the strand along the girder for simplification, this models the debonding expected for the strands at the girder end. Elongation of the strand results in an opening between the girder and the bent cap at the location of strands. In other words, the area of the total strain distribution diagram (for both the girder and bent cap) is equal to the opening of interface at the location of strands.

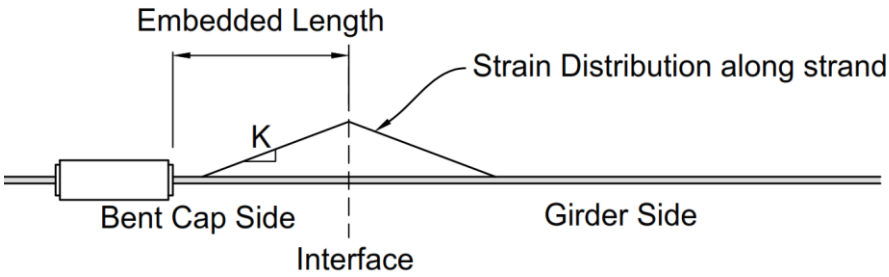

(a)

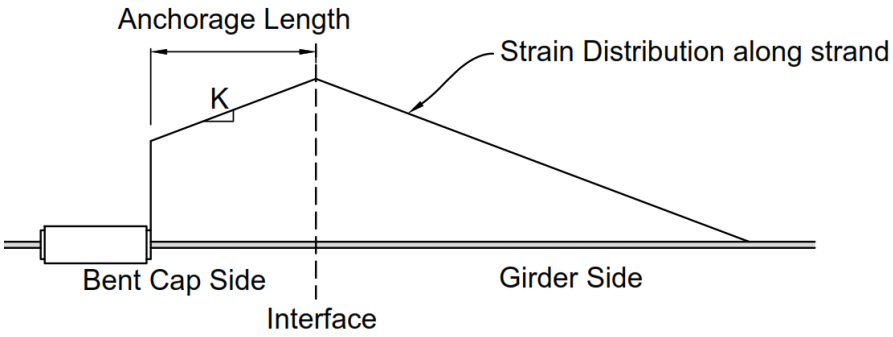

(b)

Figure 6-14 *Strain Distribution along the Strand*

Therefore, for given interface rotation (Θ) the opening, $\Delta_{opening}$, shall be taken as:

$$\Delta_{opening} = \theta d_s \tag{6-8}$$

where,

θ = rotation calculated from dowel bar shear displacement; and

d_s = the depth of strand measured from the neutral axis (neutral axis again assumed to be at the top of the girder).

The strain at interface ($\varepsilon_{interface}$) may be estimated using *Equation (6-9)* if the strain penetration length is less than the anchorage length or *Equation (6-10)* if the calculated strain penetration length is greater than the anchorage length.

$$\varepsilon_{interface} = \sqrt{\Delta_{opengin} k}, \text{ if } \frac{\varepsilon_{interface}}{k} \leq l_d \tag{6-9}$$

$$\varepsilon_{interface} = \sqrt{2} k \sqrt{\frac{\Delta_{opening}}{k} + {l_d}^2} - k l_d, \text{ if } \frac{\varepsilon_{interface}}{k} > l_d \tag{6-10}$$

where:

k = strain distribution factor (Ɛ/in.); and

l_d = anchorage length of the strand embedded in the bent cap (in.).

The stress in the strand can be obtained from the estimated strain using an appropriate stress-strain relationship of the strand. It should be noted that the overestimated stress value may be obtained if a constant elastic modulus (i.e., 28,500 ksi) is used when strain excessed the elastic limit.

The moment resistance developed by the strands shall be taken as:

$$M_s = \sigma_s A'_{ps} N d_{sc} \quad (6\text{-}11)$$

where,

σ_s = stress of strand at interface;

A'_{ps} = nominal area of stand;

N = number of strands extended from precast girder; and

d_{sc} = distance from strands to the moment compression force.

The behaviors of the shear friction associated with the dowel bars embedded in the diaphragm and the extended girder strands were modeled independently. However, the overall positive moment connection behavior should be estimated by combining the two mechanisms as the estimated displacement at the interface based on experimental date which reflected both mechanisms acting simultaneously. As shown, the contribution of shear friction is calculated first and the resulting rotation can then be used to calculate the additional moment resistance provided by the extended strands. The yield condition of the connection should be approximated as the yield point of the shear friction. The ultimate moment capacity of the connection should be designed to occur before the shear friction displacement exceeds the ultimate value of 0.27 in.. However, it is recommended that for the estimated positive moment demand, the connection should be designed to remain

elastic. The suggested models are to establish the characteristic so that its expected performance can be estimated when moment demand exceeds that which is anticipated.

For verification the proposed design methodologies, the behavior of two of the bulb-tee connection was established as shown in *Figure 6-15*. Overall, the calculated behavior compared well to the measured behavior of the experimental tested connections.

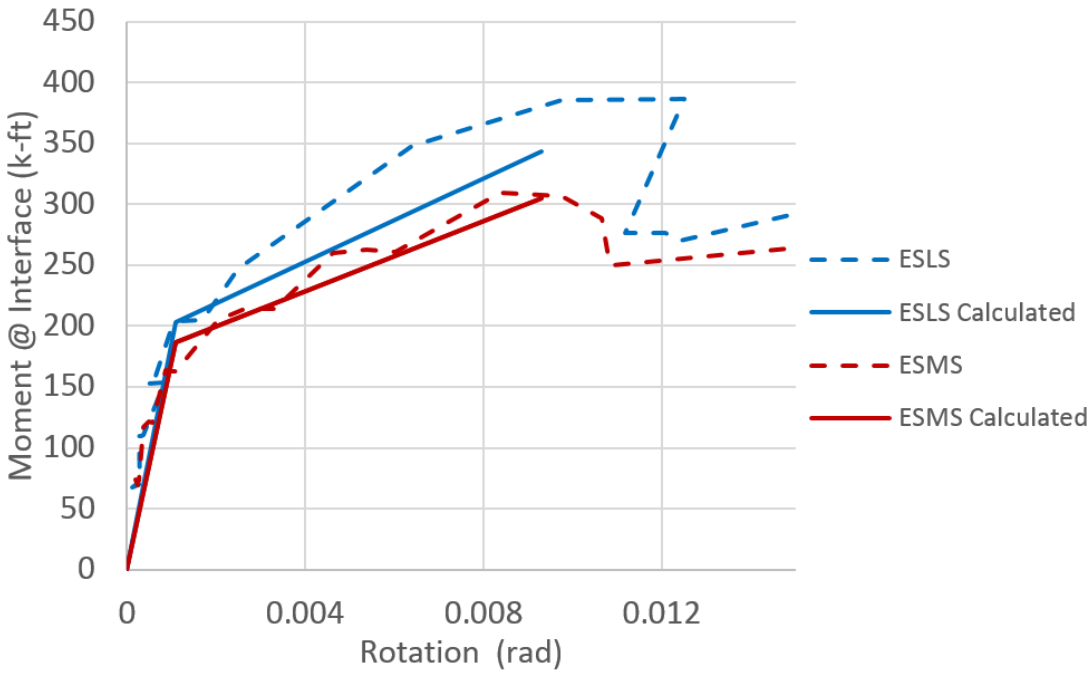

Figure 6-15 *Comparison between the Predicted Behavior and the Experimental Behavior in Positive Moment Direction*

A difference in ultimate moment capacity was observed between the connections as shown in *Figure 6-15*. It is important to note that the ultimate moment of the ESLS connection occurred during a quick overloading process which resulted in a somewhat larger ultimate moment than would occur under the specified cyclic loading protocol. The ESMS connection was expected to exhibit a comparable ultimate moment capacity with the ESLS connection due to the similar connection details. However, the unraveling of strands caused the effective area of the strands to be decreased by use of the factor 0.78 as

discussed previously. The decrease in strand effective area resulted in a moment decrease of 47.5 k-ft, and the difference between the expected moment of 352 k-ft and the observed moment of 307 k-ft is 45 k-ft. Therefore it is reasonable to state that the strength decrease of the ESMS connection was due to the unraveling of the extended girder strands.

CHAPTER 7 CONCLUSIONS AND RECOMMENDATIONS

7.1 Overview

The goal of the research presented herein is to improve understanding of the seismic design of precast bulb-tee girder-to-bent cap connections to ABC. The work included establishing new positive moment connection details, and performing experimental and analytical verifications for the capacity of the proposed details.

A moment resisting girder-to-bent cap connection allows formation of plastic hinges at the top and bottom of the column. This connection should also withstand the effects of vertical seismic acceleration, which has also given consideration herein. The current design practice, as outlined in Caltrans' Seismic Design Criteria, assumes that a precast girder-to-cap connection may degrade under a severe seismic event and should be designed as a pinned connection, decreasing the appeal for using precast girders in seismic regions.

Two particular details providing the opportunity to utilize precast girders in moderate-to-high seismic regions were proposed in this study. In the positive moment direction, a moment resisting connection was developed with unstressed strands extended from the girder and dowel bars grouted through the web of the girder and embedded into the diaphragm. Deck reinforcement over the connection region developed the resistance for the negative moment.

The suitability of proposed seismic connection details was verified using the large-scale experimental tests and analytical investigation. Test results confirmed that the proposed connections can indeed provide adequate continuity between precast girders and

a bent cap under gravity and seismic loads including vertical accelerations represented by 0.5g. Using the test results, a design methodology has been established so that the new proposed connections can be used in seismic design practice.

7.2 Summary of Experimental Test Results

7.2.1 ESMS connection

The ESMS connection was designed with strand splice chucks that connected strands, extending from girders placed on either side of the bent cap and the dowel bars grouted through the web of the girder ends and embedded in the diaphragm adjacent to the bent cap. The ESMS connection had sufficient capacity to resist shear and moment demands expected under combined gravity, horizontal seismic load and vertical acceleration effects due to 0.5g. The ESMS connection reached a maximum positive moment resistance of 300 kip-ft, which can sufficiently resist a demand due to the gravity load, horizontal seismic load, and 0.7g vertical acceleration. The ESMS connection also reached a maximum negative moment resistance of -1124 k-ft, which is equivalent to a demand beyond 1.75g of vertical acceleration effects in addition to the gravity and horizontal seismic effects. The connection remained elastic up to the negative and positive moment demands corresponding to the column overstrength moment expected from horizontal seismic loading and 0.4g vertical acceleration effects. Moreover, the ESMS connection exhibited considerable ductility when it experienced high displacement cycles. Failure of the ESMS connection eventually occurred due to significant spalling of diaphragm and bent cap concrete, which was caused by applying a large displacement at the girder end. During displacement cycles in the negative moment direction, concrete spalled at the bottom of the girder-to-cap interface that caused an upward shift of the

compressive region, subsequent shortening of the negative moment lever arm. Under positive moments, spalling of the diaphragm concrete adjacent to the sides of the girder significantly weakened the shear friction mechanism, allowing the girder to pull out.

7.2.2 ESLS connection

The ESLS connection was similar to the ESMS connection that except it utilized lap splices for the extended strands to provide a positive moment continuity. The ESLS connection also performed well and exhibited sufficient moment resistance for the shear and moment demands corresponding to the gravity, horizontal seismic and 0.5g vertical acceleration effects, and remained essentially elastic. This connection provided a maximum positive moment of 387 k-ft (which is equivalent to demand representing the gravity load, horizontal seismic load, and 0.95g vertical acceleration) and a maximum negative moment of -1158 k-ft (which is equivalent to a demand beyond 1.75g of vertical acceleration in addition to the gravity and horizontal seismic effects). The ESLS connection exhibited inelastic behavior when moment demands resulting from vertical accelerations of 0.5g and 1.0g were applied in the positive and negative moment directions, respectively. Failure in the ESLS connection occurred in a similar manner to the ESMS connection during high displacement cycles with loads corresponding to vertical acceleration effects beyond 0.5g. In the negative moment direction, crushing at the bottom of the girder-to-cap interface again resulted in a reduced lever arm reducing the connection moment resistance. In the positive moment direction, the girder pull out and loss of shear friction caused high strains in the extended strands, ultimately leading to fracture of the strands.

In comparison, the ESLS connection reached the maximum negative resistance of -1158 k-ft, which is very close to the previously tested ESMS connection (maximum

negative moment of -1124 k-ft for the ESMS connection). The maximum positive moment of ESLS connection was 87 k-ft higher than the ESMS detail due to the unraveling that occurred to the extended girder strands in the ESMS connection.

7.3 Conclusions

Based on the completed experimental and analytical investigations on the ESMS and ESLS connections, the following conclusions have been drawn:

- Both the ESMS and ESLS connections exhibited satisfactory experimental performance. These connections remained elastic for the expected seismic demand which included the effects of vertical acceleration due to 0.5g. When subjected to vertical displacement cycles, both of them exhibited additional moment resistance and considerable ductility.
- The continuous reinforcement in the deck over the connection region between the precast girder and bent cap is adequate for resisting negative moments. The crushing and spalling of concrete at the girder-to-bent cap interface eventually caused the strength degradation in the negative moment direction, which is due to the large compressive force acting on the bottom of the bent cap and girder.
- Polypropylene fibers as used in the bent cap according to the recommendations from Caltrans controlled cracking in the bent cap and deck under negative moment. However, the fiber concrete did not prevent crushing and spalling of concrete at the bottom of the bent cap to girder interface.
- Both the unstressed strands and dowel bars embedded in the diaphragm contributed to the positive moment resistance. The shear friction mechanism involving the dowel bars dictated the initial stiffness of the connection as well as a large portion

of the corresponding moment resistance until the connection reached the yield limit state. Beyond yielding of connection, the strands began to contribute significantly to the moment resistance. The connection continued to gain strength until the degradation of the shear friction mechanism occurred.

- The “U” shaped confinement steel, which is added to fit alongside the girder web and between the top and bottom girder flanges, confined the diaphragm concrete surrounding the dowel bars and prevented concrete spalling on the front face of the diaphragm under the positive moment representing the gravity load, horizontal seismic load and vertical acceleration due to 0.5g.

7.4 Design Recommendations

Based on the success of the ESMS and ESLS connection development and investigation, it is clear that these connections are viable and structural sufficient connections. The following recommendations are made to facilitate the use of these two connections in design practice.

- For negative moment resistance, the connections are recommended to be designed as a composite section with the cast-in-place bridge deck. The amount of the deck reinforcement should be appropriately designed so that the composite section does not fail in a compression controlled manner.
- Polypropylene fibers as used in the test unit (BASF M100 micro fiber added at 0.5 lbs. per cubic yard and BASF MAC MATRIC macro fibers added at 3.0 lbs. per cubic yard) controlled cracking on the deck and diaphragm surrounding the girder end, which may be appear to use in the bent cap.

- In order to provide sufficient resistance in the positive moment direction, the amount of the dowel bars and the extended girder stands should be determined based on the design methodology described in Section 6.2.
- When the strands are cut loose from the bulkheads of the stressing bed, the release of prestressing strands may unravel the extended portion, which can be prevented by placing a small diameter pipe around the strands.
- The extended strands must be anchored in the bent cap to provide a reliable tension transfer mechanism. The experimental studies have demonstrated that strand splice chuck and strand chuck consisting of a bearing plate, a barrel anchor, and wedges provide sufficient anchorage to fully develop the strength of the strands.
- Additional diaphragm stirrups ("U" shaped confinement steel) are recommended to be detailed to fit alongside the girder web and between the top and bottom girder flanges to confine the concrete surrounding the dowel bars and prevent spalling on the front face of diaphragm.
- Embedment of steel angles at the bottom corners of the girder and bent cap as shown in *Figure 7-1* could prevent spalling of cover concrete in this region due to opening and closing of gap at the connection interface.

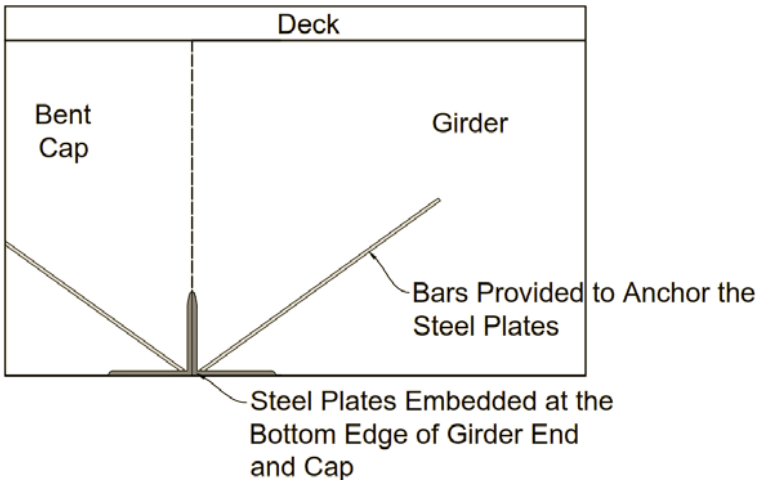

Figure 7-1 *Location of Steel Angles in Girder and Bent Cap*

7.5 Future Research

The test results indicate that concrete spalling and crushing cause bottom of the connection failure under negative moments, and this region may be reinforced to prevent this local failure. Steel angles as shown in *Figure 7-1* were recommended. It is recommended to conduct further research to validate the performance of this detail. Furthermore, it is noted that shear friction mechanism induces considerable positive moment resistance. However, the mechanism of shear friction is complex, and thus it would be useful to investigate the shear friction behavior within connection of precast components in details.

REFERENCES

AASHTO. (2012). *LRFD Bridge Design Specifications.* Washigton, D.C.: American Association of State Highway and Transportation Officials.

ACI 408 Committee. (2003). *Bond and Development of Straight Reinforcing Bars in Tension (ACI 408R-03).* Detroit, Michigan: American Concrete Institute.

ACI Committee, American Concrete Insitute, & International Organization for Standardization. (2011). *Building Code Requirements for Structural Concrete (ACI 318-11) and Commentary.* American Concrete Institute.

Ali, M. A., & White, R. N. (1999). Enhanced Contact Model for Shear Friction of Normal and High-strength Concrete. *ACI Structural Journal, Vol. 96, No. 3*, 348-360.

ASCE. (2014). *Bridges*. Retrieved from Report Card for America's Infrastructure: http://www.infrastructurereportcard.org/a/#p/bridges/overview

Caltrans. (2011, April 14). I-215/I-10 Separation LT (Widen). California.

Caltrans. (2012). Precast-Prestressed Concrete Girders. In *Bridge Design Aids.* Sacamento, CA.

Caltrans. (2013). *Caltrans Seismic Design Criteria.* Sacamento, CA: California Department of Tansportation.

Chen, W. F., & Duan, L. (2003). *Bridge Engineering: Seismic Design.* CRC Press.

Culmo, M. P. (2009). *Connection Details for Prefabricated Bridge Elements and Systems (FHWA-IF-09-010).* Washington, D.C.: Federal Highway Administration.

Eligehausen, R., Popov, E., & Bertero, V. (1983). *Local Bond Stress-slip Relationships of Deformed Bars under Generalized Excitations (Report No. UCB/EERC-83/23).* Berkeley, CA: Earthquake Engineering Research Center, University of California.

Freyermuth, C. L. (1969). Design of Continuous Highway Bridges with Precast, Prestressed Concrete Girders. *PCI Journal, V. 14, No. 2*, 14-39.

Harries, K. A., Zeno, G., & Shahrooz, B. (2012). Toward An Imporved Understanding of Shear-Friction Behavior. *ACI Structural Journal, Vol. 109, No. 6*, 835-844.

Harris, H. G., & Sabnis, G. M. (2010). *Structural Modeling and Experimental Techniques.* CRC Press.

Hason, N. W. (1960). Precast-Prestressed Concrete Bridges 2: Horizontal Shear Connections. *Journal of PCA Research and Development Laboratories, Vol. 2, No. 2*, 38-58.

Herceg, D. E. (1976). *Handbook of Measurement and Control - an Authoritative Treatise on the Theory and Application of the LVDT, rev. ed.* Pennsauken, NJ: Schaevitz Engineering.

Khan, M. (2014). *Accelerated Bridge Construction: Best Practices and Techniques.* Waltham, MA: Butterworth-Heinemann.

Liang, X., & Sritharan, S. (2014). An Investigation of Bond-slip Behavior of Reinforcing Steel Subjected to Inelastic Strains. *Tenth U.S. National Conference on Earthquake Engineering.* Anchorage, Alaska.

Liang, X., & Sritharan, S. (2015). Use of Unstressed Strands for Design of Connections between Precast Concrete Members.

Ma, Z., Huo, X., Tadros, M. K., & Baisha, M. (1998). Restraint Moments in Precast/Prestressed Concrete Continuous Bridges. *PCI Journal, Vol. 43, No. 6*, 40-56.

MacGregor, J. G., Wight, J. K., Teng, S., & Irawan, P. (1997). *Reinforced Concrete: Mechanics and Design (Vol. 3).* Upper Saddle River, NJ: Prentice Hall.

Marsh, M. L., Wernli, M., Garrett, B. E., Stanton, J. F., Eberhard, M. O., & Weinert, M. D. (2011). *Application of Accelerated Bridge Construction Connection in Moderate-to-High Seismic Regions (NCHRP Report 698).* Washington, D.C.: Transportation Research Board.

Mattock, A. H. (1974). Shear Transfer in Concrete Having Reinforcement at an Angle to the Shear Plane. *ACI Special Publication, Vol. 42*, 17-42.

Mattock, A. H., & Kaar, P. H. (1960). Precast-Prestressed Concrete Bridges 3: Further Tests of Continuous Girders. *Journal of the PCA Research and Development Laboratories, Vol. 2, No. 3*, 51-78.

Mattock, A. H., & Kaar, P. H. (1961). Precast-Prestressed Concrete Bridges 4: Shear Tests of Continuous Girders. *Journal of the PCA Research and Development Laboratories, Vol. 3, No. 1*, 19-46.

McDonagh, M. D., & Hinkley, K. B. (2003). Resolving Restraint Moments: Designing for Continuity in Precast Prestressed Concrete Girder Bridges. *PCI Journal, 48(4),* 104-119.

Miller, R. A., Castrodale, R., Mirmiran, A., & Hastak, M. (2004). *Connection of Simple-spen Precast Concrete Girders for Continuity (NCHRP Report 519).* Washington, D.C.: Transportation Research Board.

Mirmiran, A., Kulkarni, S., Castrodale, R., Miller, R., & Hastak, M. (2001). Nonlinear Continuity Analysis of Precast, Prestressed Concrete Girders with Cast-in-place Decks and Diaphragms. *PCI Journal, 46(5).*

Oesterle, R. G., Glikin, J. D., & Larson, S. C. (1989). *Design of Precast Prestressed Bridge Girders Made Continous (NCHRP Report 322).* Washington, D.C.: Transportation Research Board.

Paulsen, R. J., Harwood, D. W., Graham, J. L., & Glennon, J. C. (1978). Status of Traffic Safety in Highway Construction Zones. *Transportation Research Record (693).*

Priestly, M. J., Seible, F., & Calvi, M. (1996). *Seismic Design and Retrofit of Bridges.* New York: John Wiley & Sons.

Restrepo, J. I., Tobolski, M. J., & Matsumoto, E. E. (2011). *Development of A Precast Bent Cap System for Seismic Regions (NCHRP Report 681).* Washington, D.C.: Transportation Research Board.

Salmon, J. R. (1974). *End Connections of Pretensioned I-Beam Bridges (FHWA-RD-77-14 Final Rpt.).* Washington, D.C.: Federal Highway Administration.

Salmons, J. R., & McCrate, T. E. (1977). Bond Characteristics of Untensioned Prestressing Strand. *PCI Journal, Vol. 22, No. 1*, 52-65.

Snyder, R., Vander Werff, J., Thiemann, Z., & Sritharan, S. (2011). *Seismic Performance of An I-girder to Inverted-T Bent Cap Connection.* Sacramento, CA: California Department of Transportation.

Tadros, M. K., Ghali, A., & Bilger, W. H. (1977). Time-dependent Analysis of Composite Frames. *Journal of the Structural Division, Vol. 103, No. 4*, 871-884.

Tang, B. (2013). Accelerated Bridge Construction. In W. F. Chen, & L. Duan, *Bridge Engineering Handbook* (pp. 175-206). Boca Raton, FL: CRC Press.

Thiemann, Z. (2010). *Pretest 3-D finite element analysis of the girder-to-cap beam connection of an inverted-tee cap beam designed for seismic loadings.* Ames, IA: Iowa State University.

US Department of Labor. (2014). *Census of Fatal Occupational Injuries.* Retrieved from Bureau of Labor Statistics: http://www.bls.gov/iif/oshfat1.htm

Valluvan, R., Kreger, M. E., & Jirsa, J. O. (1999). Evaluation of ACI 318-95 Shear-friction Provisions. *ACI Structural Journal, Vol. 96, No. 4*, 473-481.

Vander Werff, J., & Sritharan, S. (2015). *Girder Load Distribution for Seismic Design of Integral Bridges.* ASCE Journal of Bridge Engineering. 20(1), 04014055-1-11.

Vander Werff, J., Peggar, R., Cheng, Z., & Sritharan, S. (2015). *Seismic Performance of Precast Girder-to-Cap Connections for Accelerated Bridge Construction of Integral Bridges.* Sacramento, CA: California Department of Transportation.

Weisbrod, G., Vary, D., & Treyz, G. (2003). Measuring Economic Costs of Urban Traffic Congestion to Business. *Transportation Research Record: Journal of the Transportation Research Board, 1839(1)*, 98-106.

Zhao, J., & Sritharan, S. (2007). *Modeling of Strain Penetration Effects in Fiber-based Analysis of Reinforced Concrete Structures.* 134-141: ACI Structural Journal, Vol. 104, No. 2.

APPENDX A

TEST UNIT DRAWINGS

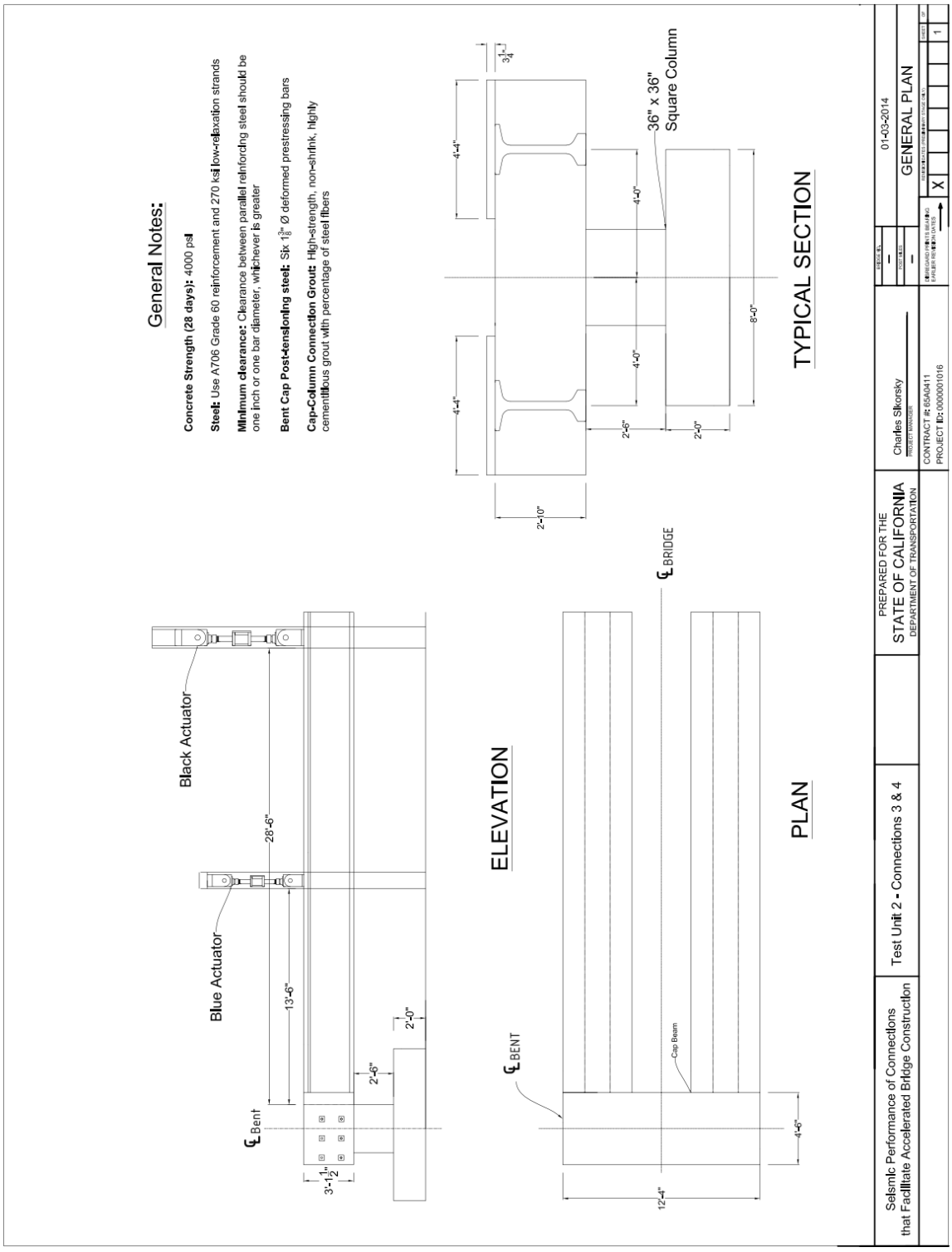

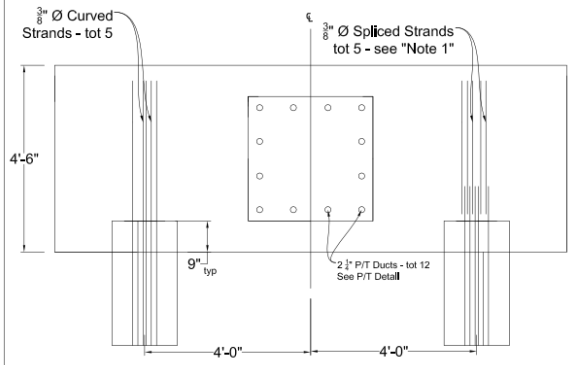

CONNECTION REGION PLAN

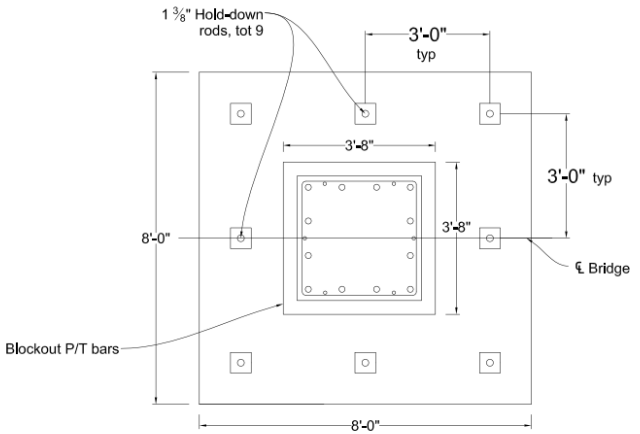

FOOTING PLAN

Test Unit Requirements:

Cast-In-Place (CIP) Footing - 1

Square 36" CIP Column - 1

Pre-cast Bulb-Tee Girder - 2

Bridge Deck and Cap Beam are CIP

Notes:
1. All strands anchored as indicated in strand chuck anchorage detail in "CONNECTION DETAILS"

2. See "CONNECTION DETAILS" for cross-sectional details B-B to D-D

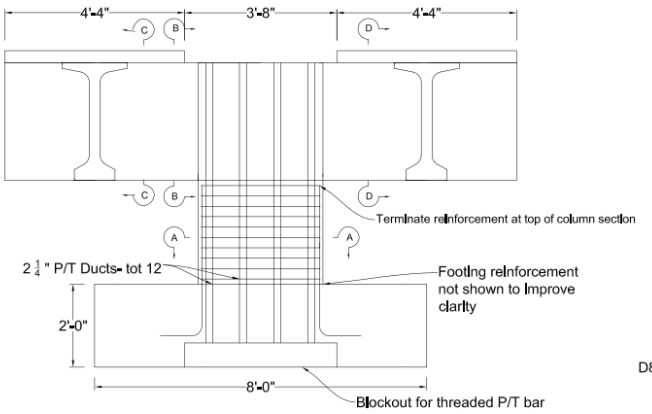

CONNECTION REGION ELEVATION

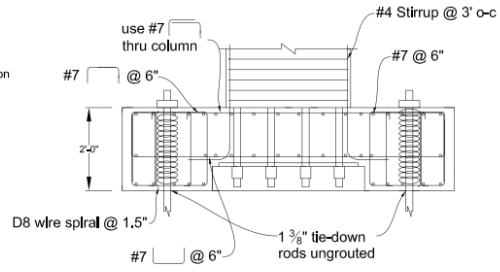

FOOTING ELEVATION

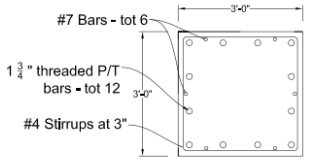

Section A-A

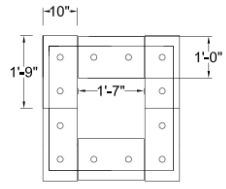

P/T Bars are anchored by 1" steel plates and P/T nuts

P/T DETAIL

Seismic Performance of Connections that Facilitate Accelerated Bridge Construction	Test Unit 2 - Connections 3 & 4		PREPARED FOR THE STATE OF CALIFORNIA DEPARTMENT OF TRANSPORTATION	Charles Sikorsky PROJECT MANAGER	BRIDGE NO. — POST MILES —	01-03-2014 BENT LAYOUT
				CONTRACT #: 65A0411 PROJECT ID: 0000001016	DISREGARD PRINTS BEARING EARLIER REVISION DATES →	REVISION DATES (PRELIMINARY STAGE ONLY) X — SHEET 2 OF

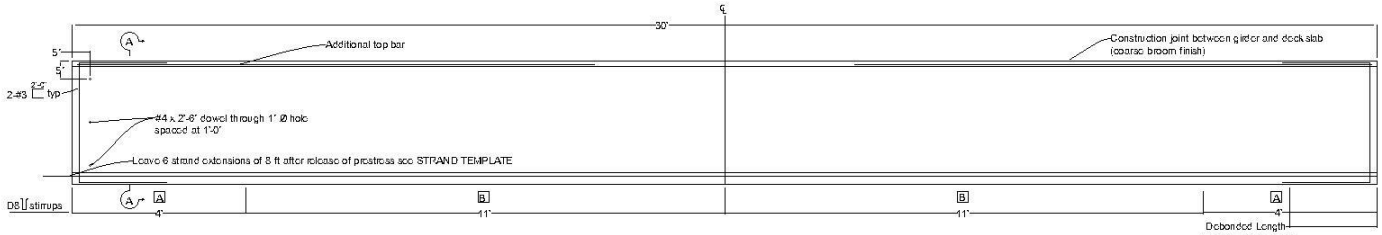

GIRDER ELEVATION

Location	A	B
Stirrup Spacing	D8 @ 2"	D8 @ 4"

PRESTRESSING NOTES

Concrete strength: **f'c** = 5.5 ksi at the time of initial stressing
f'c = 7.0 ksi at 28 days
Pjack = 207 kips (total jacking force)

Notes:
1. Girder ends to be cast such that a level surface is provided at bearing pads

2. After release of prestress, leave 8 ft of strand extending from end of girder with dowel bar holes.

3. All prestressed strands are $\frac{1}{2}$" Ø and continuously bonded unless otherwise noted

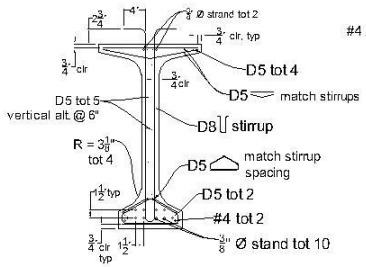

TYPICAL GIRDER SECTION

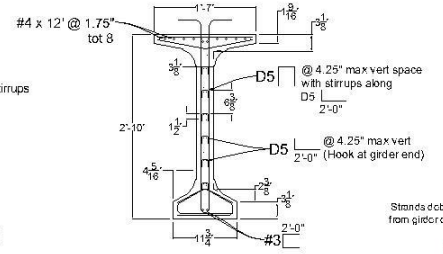

SECTION A-A

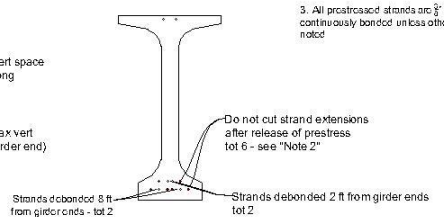

*Denotes extended strand location - tot 6

STRAND TEMPLATE & DEBONDING PATTERN

Seismic Performance of Connections that Facilitate Accelerated Bridge Construction	Test Unit 2 - Connections 3 & 4		PREPARED FOR THE STATE OF CALIFORNIA DEPARTMENT OF TRANSPORTATION	Charles Sikorsky PROJECT MANAGER	01-03-2014
				CONTRACT #: 65A0411 PROJECT ID: 0000001016	GIRDER LAYOUT

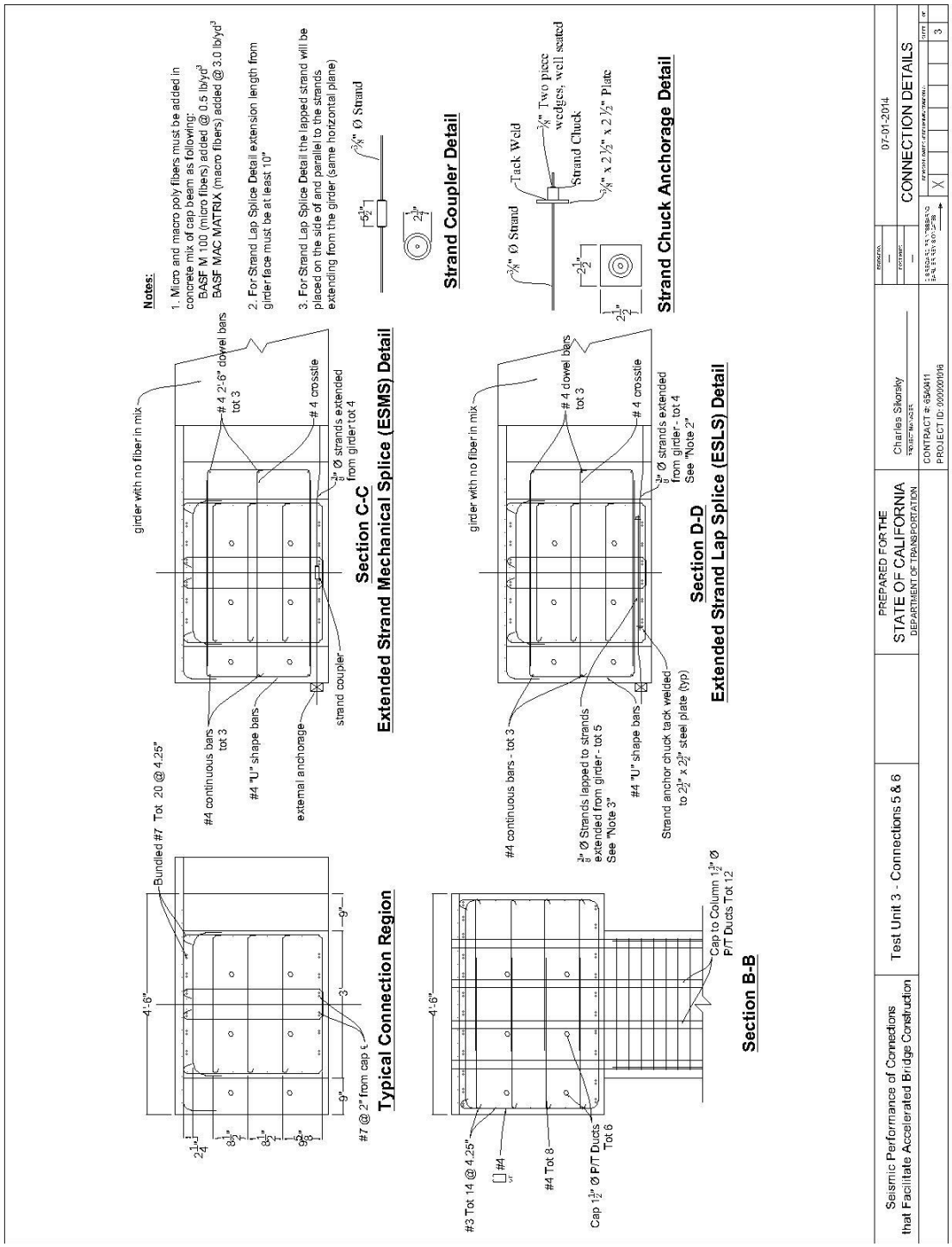
Notes:
1. Micro and macro poly fibers must be added in concrete mix of cap beam as following:
BASF M 100 (micro fibers) added @ 0.5 lb/yd³
BASF MAC MATRIX (macro fibers) added @ 3.0 lb/yd³
2. For Strand Lap Splice Detail extension length from girder face must be at least 10"
3. For Strand Lap Splice Detail the lapped strand will be placed on the side of and parallel to the strands extending from the girder (same horizontal plane)
girder with no fiber in mix
4 2'-8" dowel bars tot 3
4 crosstie
#4 continuous bars tot 3
#4 "U" shape bars
external anchorage
strand coupler
Ø strands extended from girder tot 4
Section C-C
Extended Strand Mechanical Splice (ESMS) Detail
Bundled #7 Tot 20 @ 4.25"
4'-6"
#7 @ 2" from cap ℄
Typical Connection Region
3/4" Ø Strand
Strand Coupler Detail
3/4" Ø Strand
Tack Weld
3/4" Two piece wedges, well seated
Strand Chuck
3/4" x 2 1/2" x 2 1/2" Plate
Strand Chuck Anchorage Detail
#4 continuous bars - tot 3
Ø Strands lapped to strands extended from girder - tot 5 See "Note 3"
Strand anchor chuck tack welded to 2 1/2" x 2 1/2" steel plate (typ)
Ø strands extended from girder - tot 4 See "Note 2"
Section D-D
Extended Strand Lap Splice (ESLS) Detail
#3 Tot 14 @ 4.25"
#4 Tot 8
Cap 1 1/2" Ø P/T Ducts Tot 6
Cap to Column 1 3/4" Ø P/T Ducts Tot 12
Section B-B
Seismic Performance of Connections that Facilitate Accelerated Bridge Construction
Test Unit 3 - Connections 5 & 6
PREPARED FOR THE STATE OF CALIFORNIA DEPARTMENT OF TRANSPORTATION
Charles Sikorsky
CONTRACT #: 65A0411
PROJECT ID: 0000200106
07-01-2014
CONNECTION DETAILS

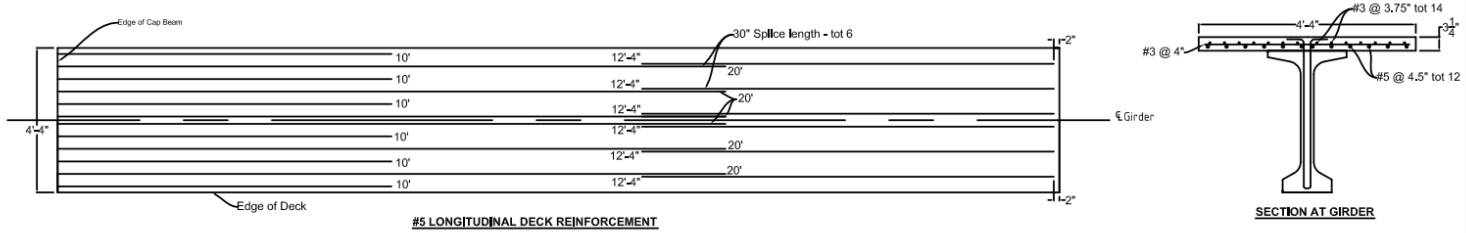

#5 LONGITUDINAL DECK REINFORCEMENT

Notes:
Numbers at the end of the bars indicate length of bars

SECTION AT GIRDER

Seismic Performance of Connections that Facilitate Accelerated Bridge Construction	Test Unit 2 - Connections 3 & 4		PREPARED FOR THE STATE OF CALIFORNIA DEPARTMENT OF TRANSPORTATION	Charles Sikorsky PROJECT MANAGER	BRIDGE NO. — / POST MILES —	01-03-2014 DECK DETAILS
				CONTRACT #: 65A0411 PROJECT ID: 0000001016	DISREGARD PRINTS BEARING EARLIER REVISION DATES →	REVISION DATES (PRELIMINARY STAGE ONLY): X — SHEET 5 OF

APPENDX B

LOADING PROTOCOL

Force Controlled Cycles

	Blue Actuator (K)	Black Actuator (K)	Moment (K-ft)	Shear (K)
G	7.9	-8.2	-37.7	10.7
	25.7	-15.3	-75.7	21.4
	43.3	-22.3	-113.8	32
	61.1	-29.4	-151.7	42.7
G±0.25H	60.9	-27.9	-191.8	44
	61.2	-30.6	-118.9	41.6
	60.9	-27.9	-191.8	44
	61.2	-30.6	-118.9	41.6
	60.9	-27.9	-191.8	44
	61.2	-30.6	-118.9	41.6
G±0.5H	60.8	-26.4	-233.2	45.4
	61.3	-31.8	-86	40.5
	60.8	-26.4	-233.2	45.4
	61.3	-31.8	-86	40.5
	60.8	-26.4	-233.2	45.4
	61.3	-31.8	-86	40.5
G±0.75H	60.6	-24.9	-273.2	46.7
	61.4	-33	-53.2	39.4
	60.6	-24.9	-273.2	46.7
	61.4	-33	-53.2	39.4
	60.6	-24.9	-273.2	46.7
	61.4	-33	-53.2	39.4
G±H	60.6	-23.5	-313.1	48.1
	61.5	-34.2	-20.3	38.3
	60.6	-23.5	-313.1	48.1
	61.5	-34.2	-20.3	38.3
	60.6	-23.5	-313.1	48.1
	61.5	-34.2	-20.3	38.3
G±H±0.1G	65.7	-24.4	-356.3	52.3
	56.2	-33.2	22.7	34
	65.7	-24.4	-356.3	52.3
	56.2	-33.2	22.7	34
	65.7	-24.4	-356.3	52.3
	56.2	-33.2	22.7	34
G±H±0.2G	71.1	-25.4	-400.7	56.7
	51.1	-32.2	63.1	29.9

	71.1	-25.4	-400.7	56.7
	51.1	-32.2	63.1	29.9
	71.1	-25.4	-400.7	56.7
	51.1	-32.2	63.1	29.9
G±H±0.3G	76.4	-26.5	-440.9	60.9
	45.7	-31.2	107.5	25.5
	76.4	-26.5	-440.9	60.9
	45.7	-31.2	107.5	25.5
	76.4	-26.5	-440.9	60.9
	45.7	-31.2	107.5	25.5
G±H±0.4G	81.7	-27.5	-484	65.2
	40.4	30.2	150.5	21.2
	81.7	-27.5	-484	65.2
	40.4	30.2	150.5	21.2
	81.7	-27.5	-484	65.2
	40.4	30.2	150.5	21.2
G±H±0.5G	86.8	-28.4	-527.2	69.4
	35.3	-29.3	193.7	17
	86.8	-28.4	-527.2	69.4
	35.3	-29.3	193.7	17
	86.8	-28.4	-527.2	69.4
	35.3	-29.3	193.7	17
Post-tensioning the longitudinal PT Bars through the Bent Cap				
G±H±0.6G	92.2	-29.4	-571.6	73.8
	30	-28.2	233.9	12.8
	92.2	-29.4	-571.6	73.8
	30	-28.2	233.9	12.8
	92.2	-29.4	-571.6	73.8
	30	-28.2	233.9	12.8
G±H±0.7G	97.5	-30.5	-611.8	78
	24.6	-27.2	278.3	8.4
	97.5	-30.5	-611.8	78
	24.6	-27.2	278.3	8.4
	97.5	-30.5	-611.8	78
End of Force Control				

Displacement Controlled Cycles

	Blue Actuator (K)	**Black Actuator (in.)**
	20	-1
	-10	0.5
	30	-1.5
	-15	-0.75
D -2/1	40	-2
	-22	1
	40	-2
	-22	1
	40	-2
	-22	1
D -3/1.5	40	-3
	-22	1.5
	40	-3
	-22	1.5
	40	-3
	-22	1.5
D -4/2	40	-4
	-22	2
	40	-4
	-22	2
	40	-4
	-22	2
D -6/3	40	-6
	-22	3
	40	-6
	-22	3
	40	-6
	-22	3
D -9/4.5	40	-9
	-22	4.5
	40	-9
	-22	4.5
	40	-9
	-22	4.5
D -12/6 A	40	-12
	-22	6
	40	-12
	-22	6
	40	-12
	-22	6
D -12/6 B	50	-12

	-22	6
	60	-12
	-22	6
	70	-12
	-22	6
D -14/7.5	70	-14
	-22	7.5
	70	-14
	-22	7.5
	70	-14
	-22	7.5
D -14/9	-22	9
	70	-14
	-22	9
	70	-14
	-22	9
D -14/10	-22	10
	70	-14
	-22	10
	70	-14
	-22	10
	70	-14
End of Test		